

TAURI TAMPUU

Synthetic Aperture Radar Interferometry
as a tool for monitoring
the dynamics of peatland surface



TAURI TAMPUU

Synthetic Aperture Radar Interferometry
as a tool for monitoring
the dynamics of peatland surface



UNIVERSITY OF TARTU

Press

Department of Geography, Institute of Ecology and Earth Sciences, Faculty of Science and Technology, University of Tartu, Estonia

Dissertation has been accepted for the commencement of the degree of *Doctor philosophiae* in physical geography at the University of Tartu on June 6, 2022 by the Scientific Council of the Institute of Ecology and Earth Sciences, University of Tartu.

Supervisors: Associate Prof. Ain Kull
Institute of Ecology and Earth Sciences
University of Tartu
Estonia

Assistant Prof. Jaan Praks
Department of Electronics and Nanoengineering
Aalto University
Finland

Senior Researcher Rivo Uiboupin
Department of Marine Systems
Tallinn University of Technology
Estonia

Opponent: Prof. Ramon F. Hanssen
Department of Geoscience and Remote Sensing
Delft University of Technology
The Netherlands

Commencement: Auditorium 127, Oecologicum, Liivi 2, Tartu, on August 23, 2022 at 12:15.

Publication of this dissertation is granted by the Institute of Ecology and Earth Sciences, University of Tartu.

ISSN 1406-1295
ISBN 978-9949-03-911-1 (print)
ISBN 978-9949-03-912-8 (pdf)

Copyright: Tauri Tampuu, 2022

University of Tartu Press
www.tyk.ee

TABLE OF CONTENTS

LIST OF ORIGINAL PUBLICATIONS	7
LIST OF ABBREVIATIONS	8
1. INTRODUCTION	9
2. MATERIALS AND METHODS	14
2.1. Study sites	14
2.1.1. Natural and drainage affected bogs	14
2.1.2. Peat extraction areas in bogs	16
2.2. In situ data for validation of SAR measurements	17
2.2.1. Bog water table data	17
2.2.2. Peat extraction data	18
2.2.3. Bog surface levelling data	18
2.3. Meteorological and land cover data	19
2.4. SAR data	20
2.5. InSAR processing	21
2.5.1. Formation of InSAR coherence time series	26
2.5.2. Calculation of backscatter intensity	27
2.5.3. Computation of DInSAR deformation phase time series	28
2.5.4. Computation of DS InSAR deformation phase time series	29
2.6. Data analysis	30
3. RESULTS	32
3.1. InSAR coherence for assessment of bog surface dynamics	32
3.1.1. Assessment of peatland water table based on single master DInSAR coherence	32
3.1.2. Detection of physical changes in peat surface structure based on short temporal baseline DInSAR coherence	34
3.2. Recording precipitation events with SAR backscatter intensity	40
3.3. Assessment of bog breathing with InSAR phase	41
3.3.1. Method based on single master DInSAR phase	41
3.3.2. Method based on DS InSAR phase time series	42
3.3.3. Method based on short temporal baseline DInSAR phase	44
3.4. Temporal dynamics and magnitude of bog breathing	46
4. DISCUSSION	49
4.1. Changes in peatland water table reflected in InSAR coherence	49
4.2. Changes in peat surface structure reflected in InSAR coherence	51
4.3. Precipitation events reflected in InSAR coherence	52
4.4. Peatland surface motions reflected in InSAR phase time series rela- tive to a common reference date	53
4.4.1. Surface motions in single master DInSAR phase	53
4.4.2. Surface motions in DS InSAR phase time series	54

4.5. Peatland surface motions reflected in InSAR phase changes between consecutive acquisitions.....	54
4.5.1. Surface motions in DS InSAR phase time series converted to changes between consecutive acquisitions	54
4.5.2. Surface motions in short temporal baseline DInSAR phase	55
4.6. Problem of phase ambiguity in C-band InSAR.....	56
5. CONCLUSIONS	60
REFERENCES	62
SUMMARY	75
SUMMARY IN ESTONIAN	77
ACKNOWLEDGEMENTS	80
PUBLICATIONS	81
CURRICULUM VITAE	159
ELULOOKIRJELDUS	161

LIST OF ORIGINAL PUBLICATIONS

This thesis is based on the following publications, which are referred to in the text by Roman numerals:

- I **Tampuu, T.**, Praks, J., Uiboupin, R., Kull, A. (2020) Long term interferometric temporal coherence and DInSAR phase in Northern Peatlands. *Remote Sensing*, 12(10), 1566. DOI: 10.3390/rs12101566
- II **Tampuu, T.**, Praks, J., Kull, A. (2020) Insar Coherence for Monitoring Water Table Fluctuations in Northern Peatlands. In: *2020 IEEE International Geoscience and Remote Sensing Symposium IGARSS*. 26 Sept–2 Oct 2020. Waikoloa, US. 4738–4741. DOI: 10.1109/IGARSS39084.2020.9323709
- III **Tampuu, T.**, Praks, J., Kull, A., Uiboupin, R., Tamm, T., Voormansik, K. (2021) Detecting peat extraction related activity with multi-temporal Sentinel-1 InSAR coherence time series. *International Journal of Applied Earth Observation and Geoinformation*, 98, 102309. DOI: 10.1016/j.jag.2021.102309
- IV **Tampuu, T.**, Praks, J., De Zan, F., Kohv, M., Kull, A. (202X) Could bog breathing be measured by Synthetic Aperture Radar? – The relationship between differential interferometric phase and ground measurements. *Mires and Peat*. Submitted manuscript.
- V **Tampuu, T.**, De Zan, F., Shau, R., Praks, J., Kohv, M., Kull, A. (202X) Can Bog Breathing Be Measured by Synthetic Aperture Radar Interferometry. In: *2022 IEEE International Geoscience and Remote Sensing Symposium IGARSS*. 17–2 July. Kuala Lumpur, Malaysia. Accepted manuscript.

Author’s contribution to the articles denoted by: ‘*’ a minor contribution, ‘**’ a moderate contribution, ‘***’ a major contribution.

	Articles				
	I	II	III	IV	V
Original idea	**	***	*	***	***
Study design	**	**	**	***	***
Data processing and analysis	**	***	***	***	***
Interpretation of the results	**	***	***	***	***
Writing the manuscript	***	***	***	***	***

LIST OF ABBREVIATIONS

ALOS	Advanced Land Observing Satellite
APSYS	Advanced Pixel System Intermittent Small Baseline Subset
C-band	Conventional Wavelength Band
DEM	Digital Elevation Model
DInSAR	Differential Synthetic Aperture Radar Interferometry
DS	Distributed Scatterer
EMI	Eigendecomposition-based Maximum-likelihood-estimator of Interferometric phase
Envisat	Environmental Satellite
ERS	European Remote Sensing (satellite)
ESD	Enhanced Spectral Diversity
InSAR	Synthetic Aperture Radar Interferometry
IQR	Interquartile Range
ISBAS	Intermittent Small Baseline Subset
IW	Interferometric Wide swath mode
L-band	Long Wavelength Band
LOS	Line of Sight
PS	Persistent Scatterers
r_s	Spearman's Rank Correlation Coefficient
RON	Relative Orbit Number
RMSE	Root Mean Squared Error
S1	Sentinel-1
S1A	Sentinel-1A
S1B	Sentinel-1B
SAR	Synthetic Aperture Radar
SD	Standard Deviation
SLC	Single Look Complex
SNAP	The Sentinel Application Platform
SBAS	Small Baseline Subset
SRTM	Shuttle Radar Topography Mission
StaMPS	Stanford Method for Persistent Scatterers
TOPS	Terrain Observation with Progressive Scan
VH	Vertical–Horizontal Polarisation
VV	Vertical–Vertical Polarisation
WT	Water Table
u_{LOS}	LOS Projected to Vertical Direction (u denotes Up component)
$ \gamma $	Magnitude of Interferometric Coherence (Coherence Magnitude)
γ	Complex Correlation Coefficient (Interferometric Coherence)
σ^0	Backscatter Coefficient (Backscatter Intensity)
δ	Differential Interferometric Phase (Phase Difference)

1. INTRODUCTION

The role of peatlands in Earth's climate has been long recognised (Gorham 1991; Turetsky et al. 2015) and the fate of the peatlands will probably determine whether the mankind is able to tackle climate change (Leifeld et al. 2019; Gewin 2020; Witze 2020). Peat is a soil layer consisting of incompletely decayed plant material which has accumulated in place in wet condition (Clymo et al. 1998; Montanarella et al. 2006) and has formed a store of sequestered carbon (Gorham 1991; Clymo et al. 1998; Yu 2012). Any vegetated or non-vegetated area with the naturally accumulated peat layer of a minimum peat depth of 30 cm at the surface is called peatland (Joosten & Clarke 2002). Mires, sometimes referred to as natural peatlands, are peatlands where peat is currently being formed (Joosten & Clarke 2002; Krüger et al. 2015). Peatlands cover ~3% of the Earth's land surface (Gorham 1991; Xu et al. 2018) but constitute 21% (Leifeld & Menichetti 2018) to 30% (Gorham 1991) of the global soil carbon. Peatland soils contain nearly as much carbon as a half of what is currently in the atmosphere (Limpens et al. 2008). A major portion of peatlands is located in mid- and high latitudes of the Northern Hemisphere (Frolking et al. 2011; Xu et al. 2018; Melton et al. 2022), containing large stocks of organic carbon (Nichols & Peteet 2019; Hugelius et al. 2020). There is no clarity in whether individual peatlands nowadays in response to changing climate are growing or contracting in size (Gorham 1991; Dise 2009).

Peatlands are significant in regard to climate change because peatlands may switch from being a net carbon sink to an emitter of greenhouse gases. The delicate carbon balance of peatlands (Gorham 1991; Dise 2009; Yu 2012; Webster et al. 2018) is controlled by the peatland water table (WT) (Silvola et al. 1996; Limpens et al. 2008; Ojanen et al. 2010; Huang et al. 2021) as peat moisture content and its spatio-temporal variability determine greenhouse gas emissions (Ojanen et al. 2010; Frolking et al. 2011; Beyer & Höper 2015; Veber 2021). Bogs are among the most widespread types of peatlands (Ingram 1982; Moore 2002). The raised bog is ombrogenous, i.e. it receives its water solely from precipitation in contrast to other possible sources like ground water and surface water flow (Moore 2002). According to a widely accepted model the peat deposit of a raised bog consists of two distinct layers (Clymo et al. 1998; Moore 2002; Holden & Burt 2003; Howie & Hebda 2018). Acrotelm stretches from the surface to the depth to which the WT sinks in dry summers, i.e. acrotelm is the peat layer that is exposed to periodic aeration. Catotelm below it is constantly waterlogged (Clymo et al. 1998; Holden & Burt 2003). While the lower laying catotelm consists of humified compacted peat, the upper uncompacted porous acrotelm is where the majority of biological activity and exchange of matter and energy occurs (Ingram 1982; Moore 2002; Holden & Burt 2003). Waterlogged conditions with resultant oxygen deficiency decrease the rate of decay of dead organic material and support accumulation of peat (Clymo et al. 1998; Joosten & Clarke 2002; Drösler et al. 2008). A lowered WT leads to increased aerobic respiration in a thicker acrotelm and consequently to faster peat mineralisation rates (Silvola et al. 1996; Drösler et al. 2008). Draining turns peatlands into a net source of greenhouse gases (Gorham 1991; Frolking et al.

2011; Veber 2021). Also, active and abandoned peat extraction sites are persistent greenhouse gas emitters (Waddington et al. 2009; Salm et al. 2012; Mustamo et al. 2016). Peatland conservation and restoration are therefore critical in global climate change mitigation (Leifeld & Menichetti 2018; Harris et al. 2022).

High WT is critical for functioning of natural bogs also because the dominant species there are *Sphagnum* mosses. The *Sphagnum*, being non-vascular (i.e. having no root system), depends on the water supply from the capillary rise to satisfy its transpiration demand for photosynthesis (Schouwenaars 1993; Strack & Price 2009). In raised bogs the moisture content of the surface peat is mainly explained by the distance to the WT through capillary rise (Lindholm & Markkula 1984; Brandyk et al. 1986; Strack & Price 2009). When the WT is low rainfall has also an impact on the surface moisture (Lindholm & Markkula 1984; Strack & Price 2009), whereas the lower the level the stronger the impact. That dependency of peat moisture on precipitation may apply to natural sites after a prolonged dry period but is common in drained mires (Lindholm & Markkula 1984).

A traditional measure of peat wetness is the water table in a dip-well (Kellner & Halldin 2002). Although WT depth can indeed be measured in situ at low costs with dip-wells (Bechtold et al. 2018), continuous homogeneous coverage over large or inaccessible peatland areas is only feasible by remote sensing instruments (Jones et al. 2009; Lees et al. 2018). The most commonly used remote sensing data in peatland studies have been optical, collected by passive multispectral (and hyperspectral) instruments (Czapiewski & Szumińska 2022), covering the electromagnetic spectrum from visible to infrared (Lees et al. 2018; Minasny et al. 2019). The optical and thermal data benefit from detection of spectral properties of the vegetation (Sadeghi et al. 2017; Burdun 2020; Chasmer et al. 2020b), which is assumed to reflect root zone soil moisture (Sadeghi et al. 2017) as the composition of vegetation in peatlands reflects the WT depth (Laine et al. 1995; Veber 2021). A limitation to using thermal data is its coarse spatial resolution (1 km for Moderate Resolution Imaging Spectroradiometer MODIS) (Burdun et al. 2019), making using it ineffective (Jones et al. 2009; Bourgeau-Chavez et al. 2018) in regard to heterogeneity and often small size of peatlands (Merchant et al. 2017; Bourgeau-Chavez et al. 2018). The main limitation of optical sensors is the inability to penetrate cloud cover, abundant in the regions where peatlands occur (Jones et al. 2009; Bourgeau-Chavez et al. 2018; Lees et al. 2018; Mahdavi et al. 2018; Poggio et al. 2019; Mirmazloumi et al. 2021; Czapiewski & Szumińska 2022).

As a significant advantage over optical sensors, passive and active microwave sensors penetrate through clouds and operate indifferently day and night (Minasny et al. 2019; Liang et al. 2020). Also, microwave remote sensing has potential for a direct measurement of soil moisture (Liang et al. 2020) due to sensitivity to the target's dielectric constant which is high for water and low for dry soil (Ulaby et al. 1996; Liang et al. 2020). The 40–50 km resolution of passive microwave missions SMOS (Soil Moisture and Ocean Salinity) and SMAP (Soil Moisture Active Passive) equipped with radiometers is by far too coarse (Minasny et al. 2019; Bechtold et al. 2020; Burdun 2020). Consequently, their use in peatlands has been negligible (Czapiewski & Szumińska 2022).

The most common active microwave imaging instrument is side-looking Synthetic Aperture Radar (SAR) (Minasny et al. 2019; Liang et al. 2020). The sensor emits high energy microwave pulses and records the returning echoes in the same antenna (Moreira et al. 2013; Minasny et al. 2019). While the instrument moves along its flight path a sequence of returning echoes are combined to simulate a very long virtual aperture, taking advantage of the along-track motion of the physical antenna (Moreira et al. 2013). The SAR system measures the amplitude and the phase of the backscatter of the transmitted electromagnetic signal (Moreira et al. 2013). As the amplitude depends on physical (surface geometry, roughness) and electrical properties (dielectric permittivity) of the sensed object in conjunction with the local incidence angle of the SAR beam, the phase measurement contains additionally the information about the distance from the sensor to the object (Jones et al. 2009; Moreira et al. 2013).

SAR is not just an all-weather instrument, it can penetrate vegetation (Liang et al. 2020; Chasmer et al. 2020b). Currently operational satellite SAR systems use microwaves of wavelength of approximately either 3 cm (X-band), 6 cm (C-band), or 24 cm (L-band) (Ferretti et al. 2007; Milodowski et al. 2020). The longer the wavelength, the better the penetration capability (Li & Chen 2005; Moreira et al. 2013; Liang et al. 2020). The SAR backscatter intensity appears to be often perceived as the most promising tool for remotely sensing soil moisture conditions in peatlands and more generally in wetlands (Czapiewski & Szumińska 2022; Chasmer et al. 2020a; Chasmer et al. 2020b). L-band (or long band), being less affected by vegetation and surface roughness, has been the choice of preference for surface soil moisture retrieval (Liang et al. 2020). For example Torbick et al. (2012) using L-band estimated peatland WT depth in a Swedish mire. Owing to its ability to penetrate forest canopy, L-band has also been preferred in wetland mapping (Li & Chen 2005; Mahdavi et al. 2018) and surface subsidence studies in tropical peatlands (Zhou et al. 2019; Hoyt et al. 2020; Umarhadi et al. 2021a; Umarhadi et al. 2021b). Nevertheless, the imagery from Advanced Land Observing Satellite-2 (ALOS-2) is sparse and sporadic, hindering its applicability.

Owing to its continuous coverage, short revisit time and free-of-charge data availability the satellite Sentinel-1, operating in the C-band (conventional band) at a ~ 5.6 cm wavelength, is the used-most radar in peatland research (Czapiewski & Szumińska 2022). C-band backscatter has shown sensitivity to soil moisture in treeless temperate and boreal wetlands of low biomass (Li & Chen 2005; Kasischke et al. 2009; Bourgeau-Chavez et al. 2017; Bechtold et al. 2018; Asmuß et al. 2019; Zwieback & Berg 2019). Problematically, the developed models thus far have not been cross validated (i.e. model testing on the independent data set to ensure the model is able to predict soil moisture also at new locations or in other times) (Millard & Richardson 2018). The cross validated estimates by Millard and Richardson (2018) in the open fen and open bog were promising though their in situ soil moisture data for validation was from the same summer and from the same area. One has to remember that all the backscatter amplitude based solutions are incidence angle dependent. The backscatter of the same target is different depending on whether it is sensed in near range or far range of the swath, i.e. at

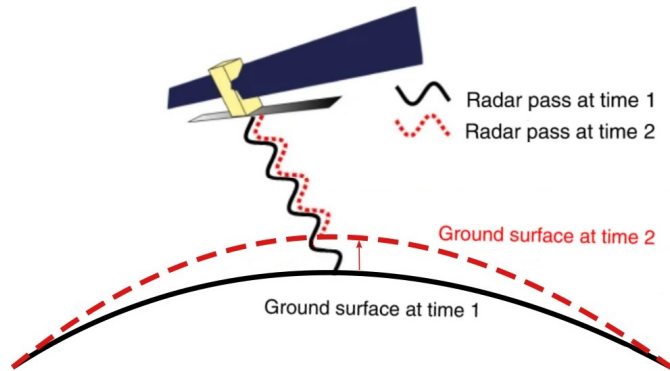


Figure 1: An orbiting SAR satellite senses the land surface at two different times (times 1 and 2). The recorded phase difference between the return signals can be used to estimate the change in surface height that has occurred between these two passes. Adapted from Biggs and Wright (2020).

low or higher incidence angle (Merchant et al. 2017; Bechtold et al. 2018; Mahdavi et al. 2018). That noticeably hinders interpretation and reproducibility (Wagner et al. 2007; Jones et al. 2009; Bauer-Marschallinger et al. 2021).

The incidence angle dependency of the radar can be overcome if instead of amplitude the phase part of the backscattered signal is used in SAR interferometry (InSAR). In InSAR two phase images are combined and the phase difference between the two images is calculated (Bamler & Hartl 1998). Exploiting the phase difference between images from the same orbital position at different times, the interferometric phase becomes a sensitive measure of the distance difference between the sensor and the target (Bamler & Hartl 1998) which translates into surface deformation as shown in Fig. 1). InSAR has been proven in quantifying surface displacements at a millimetre scale (Ferretti et al. 2001; Ferretti et al. 2007; Crosetto et al. 2016; Osmanoglu et al. 2016; Biggs & Wright 2020). The influence of the incidence angle on InSAR products is only limited to lowering the signal-to-noise ratio (SNR) as increasing local incidence angles cause a decrease in the backscattered power (Bamler & Hartl 1998; Ferretti et al. 2007; Moreira et al. 2013). For example a lake, being a smooth flat surface, mirrors the signal away from the sensor (Bamler & Hartl 1998; Ferretti et al. 2007) and decorrelates at any temporal baseline (i.e. time interval) due to low SNR (Moreira et al. 2013).

InSAR phase becomes relevant in measuring the peatland water table (i.e. peat wetness) via the phenomenon known as bog breathing. The sponge-like nature of *Sphagnum* makes peat to adsorb water and trap gases (Dise 2009). Owing to elastic properties of the peat in acrotelm, the peat mass expands and contracts in response to its water content causing the bog surface rise and fall following the water table – this surface oscillation is often referred to as bog (or mire) breathing, (Roulet 1991; Kellner & Halldin 2002; Dise 2009; Howie & Hebda 2018). Bog breathing increases the resilience of the bog to perturbations (Dise 2009) but also provides a proxy to estimate the peatland WT (Howie & Hebda 2018). Only a

few studies have estimated InSAR phase in northern peatlands whereas the ground levelling data for validation has been absent in most cases (Cigna & Sowter 2017; Alshammari et al. 2018). This dissertation aims to fill that knowledge gap by providing InSAR deformation estimates in raised bogs validated with the ground levelling measurements.

A co-product of InSAR phase processing (resulting in formation of InSAR phase image called interferogram) is the InSAR coherence image which describes local phase stability (Ferretti et al. 2007) and is seen as the quality measure of an interferogram (Bamler & Hartl 1998; Moreira et al. 2013). However, the InSAR coherence can also be used as an independent metric in coherent change detection (Preiss et al. 2006). While coherence has been shown to reflect soil humidity in bare agricultural fields (De Zan et al. 2014) and in the desert (Scott et al. 2017), in wetlands coherence has been employed only for delineation of flooding (Zhang et al. 2015; J.-W. Kim et al. 2017) and peatland classification (Ramsey, III E. et al. 2006; S.-W. Kim et al. 2013; Brisco et al. 2017). A few studies have been concerned with classification in northern mires (Millard et al. 2020; Amani et al. 2021; Mohammadimanesh et al. 2018a; Mohammadimanesh et al. 2018b). To fill that knowledge gap this dissertation aims to investigate the InSAR coherence response to water table changes in raised bogs and to peat harvesting related works in peat extraction sites, validated with the ground truth.

While the effect of vegetation is the greatest obstacle to reliable surface soil moisture assessment with the C-band SAR (Bourgeau-Chavez et al. 2013; Millard & Richardson 2018; Liang et al. 2020) raised bogs are mainly open dominated by *Sphagnum* mosses with only sparse shrubs and trees in the vegetation cover (Lindholm & Markkula 1984; Schouwenaars 1993; Clymo et al. 1995). Therefore, bogs promising minimal vegetation effects along with spatio-temporally dynamic moisture conditions could make an interesting test site for SAR (Millard & Richardson 2018). In regard to that, the general aim of this dissertation is stretching the limits of SAR interferometry method while improving peatland monitoring.

The dissertation is based on the hypotheses: 1) InSAR coherence responds to the peat humidity and this signal could be useful in quantification of peatland water table (**Publications I and II**), 2) InSAR coherence can be used to monitor peat production, allowing at a minimum discrimination of the active production area in known production sites (**Publication III**), 3) InSAR phase is able to measure bog breathing at least in less dynamic areas where peat is compacted and less elastic (**Publications IV and V**). The specific objective is to answer based on the validation from comparison with the ground truth data the following questions about the applicability of space-born C-band InSAR:

- 1) Is the long temporal baseline InSAR coherence response to the water table change in the raised bog detectable?
- 2) Is there a quantifiable short temporal baseline InSAR coherence response to the peat surface alteration caused by the milled peat harvesting related activity in peat production sites?
- 3) Is the InSAR phase a reliable measure of bog breathing in open bogs?

2. MATERIALS AND METHODS

The studies discussed in this dissertation concern the raised bog in Estonia whereas 4 study sites are in natural open bogs and 3 in areas converted to peat production sites. The SAR imagery over the study sites from the European Union's Copernicus programme's Sentinel-1 (S1) satellite mission from the years 2016–2019 were used to calculate the time series of interferometric coherence, interferometric phase and backscatter intensity. An overview of the selected study sites, the SAR imagery, the in situ measurements, the processing techniques and the methods of how the ground truth data was used in validation of the SAR results is provided in detail to guide the reader through the dissertation without the need to turn to the original publications for clarity.

2.1. Study sites

The raised bogs in Estonia are characteristic for the northern raised bogs (Moore & Bellamy 1974; Moore 2002; Päivänen & Hånell 2012). The northern peatlands, bogs included, can be found north of approximately 40°N latitude in North America and 50°N in Eurasia (Tarnocai & Stolbovoy 2006) while most of these peatlands belong to the cool temperate zone between latitudes 50°–70°N (Moore 2002). The domed shaped open bogs are dominated by *Sphagnum* mosses. The dominant ridge-hollow-hummock ecotope is characterised by a thick peat layer and a few pools. *Pinus sylvestris* trees (up to 5 m) dominate the ridge-pool ecotope at the central part of the bogs and the marginal areas of the bogs. The bogs are surrounded by the bog forest (tree height 15–20 m) or forest (Paal 2004; Paal & Leibak 2011).

The ice- and snow-free growing period lasts from May to October in Estonia. The snowmelt occurs in April and causes the yearly maximum peatland water table. Thereafter the WT decreases rapidly in next months, propelled by high discharges and evapotranspiration. Usually in July or August the WT reaches its minimum. In autumn hindered evapotranspiration and increased precipitation make the pore water to recharge and raise the WT. The bog surface freezes and a snow cover is formed in November or December. Monthly precipitation is at the minimum in winter and spring and at the maximum in summer and autumn. The maximum distance between any two among our study sites is 70 km.

2.1.1. Natural and drainage affected bogs

The raised bogs in natural or close to natural condition were studied in **Publications I, II, IV and V**. The entire Endla mire complex (58.88°N, 26.18°E) is concerned in **Publications I** while Kanamatsi bog was selected to study InSAR surface deformations. Only Linnusaare bog and Männikjärve bog from the Endla mire complex are concerned in **Publication II**. Umbusi bog (58.57°N, 26.18°E) is studied in **Publications IV and V** and Laukasoo bog (58.43°N, 27.00°E) in **Publication IV**. The thickness of peat in the Endla mire complex is 3–6 meters

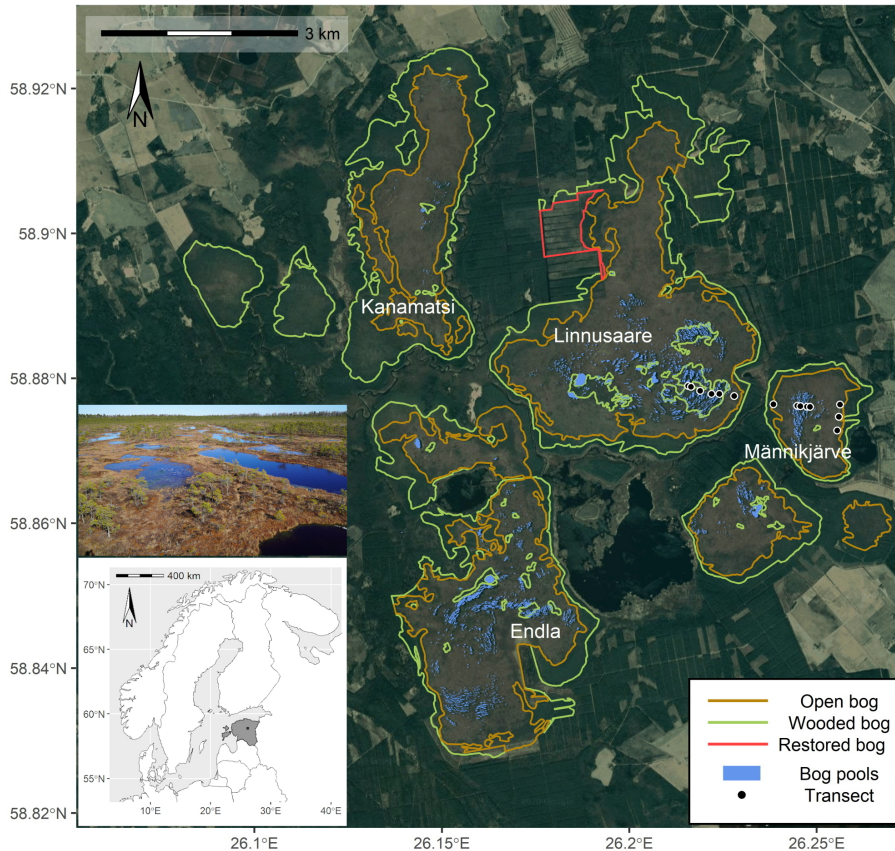


Figure 2: The bogs in the Endla mire complex. The hydrological monitoring transect of gauges and wells at Linnusaare and Männikjärve bogs are marked with black dots. The following land cover types are differentiated: open bog (tree height <1.3 m or canopy cover <0.3), wooded bog (tree height 1.3–10 m and canopy cover >0.3), restored bog and bog pools (pool area >100 m²). The ridge-pool ecotope from the central part of Männikjärve bog is displayed in a photograph. Source: **Publication I** Figure 1.

(occasionally over 7 m) and at our study transects in Umbusi bog and Laukasoo bog ~8 m and ~5 m respectively. The bogs in the Endla mire complex are surrounded by the network of drainage ditches for forestry (Fig. 2). In Umbusi bog (Fig. 3a) and Laukasoo bog (Fig. 3b) the natural bog area borders active milled peat production fields. The border is formed by a deep entire peat layer penetrating main drainage ditch. The production fields lie many metres lower compared to the open bog area and the side of the ditch forms a vertical a few meters high bank. Parallel to the main drainage ditch at a distance of 40 m from it inside the bog, a secondary drainage ditch (~0.5 m deep) runs which cuts through acrotelm. As a direct effect of drainage, the bog area between the ditches is sparsely wooded (*Pinus sylvestris*).

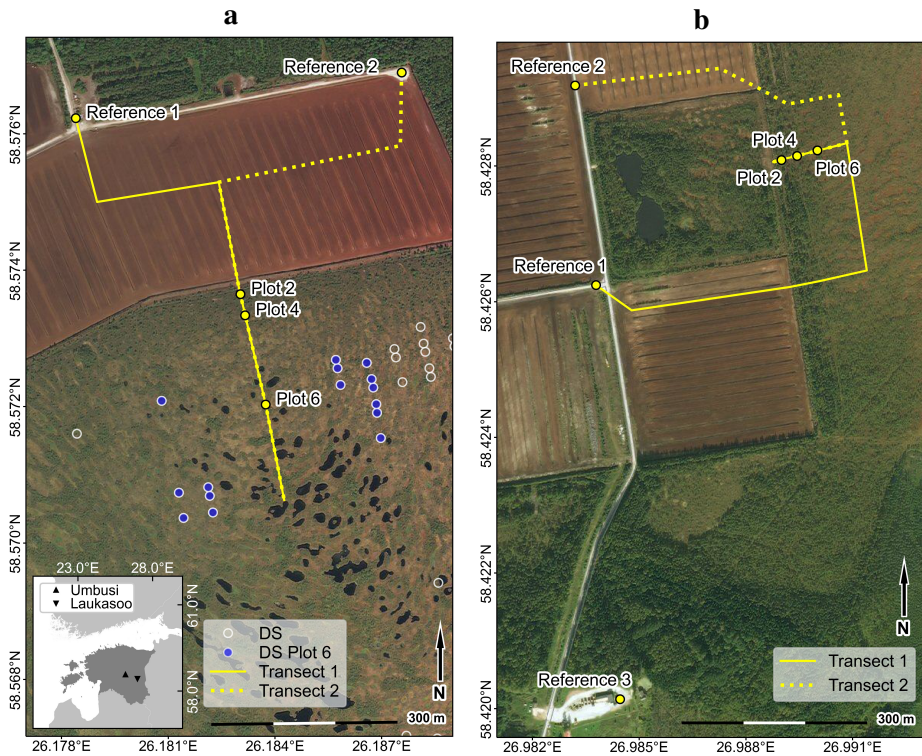


Figure 3: Natural bog and milled peat production fields in Umbusi (a) and Laukasoo (b) raised bogs. Virtual transects stretch from the reference points to the levelling plots in the open bog. In Umbusi (a) all InSAR distributed scatters (DS) in the scene are shown and the DS locations used in validation with the levelling data from the plot 6 are indicated (DS Plot 6). Based on: **Publication IV** Figure 1.

2.1.2. Peat extraction areas in bogs

In **Publication III** the effects of peat extraction were studied in Sangla (58.33°N, 26.25°E), Soosaare (58.57°N, 25.88°E) and Tässi bogs (58.54°N, 25.85°E) where milled peat is produced (Fig. 4). Tässi bog has been entirely converted to a peat production site whereas considerable parts of Soosaare and Sangla bogs are also in drainage affected status and in more distant areas in natural or close to natural condition, similarly to Umbusi (**Publication IV** and **V**) and Laukasoo bogs (**Publication IV**). Near the Sangla site abandoned former peat production fields are found. A peat production site is divided into production blocks by the road network. A production block consists of several production fields separated by drainage ditches after every 20 m (Sundh et al. 2000; Eesti Turbaliit 2022). The smallest production block in our study occupies 8.3 ha (300×275 m) and the largest 25.3 ha (315×800 m).

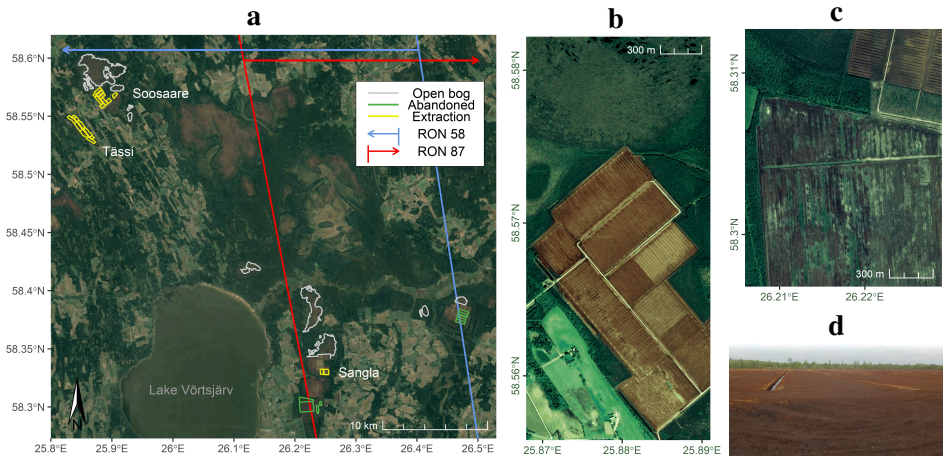


Figure 4: Sangla, Soosaare and Tassi peat production sites and the approximate coverage of the Sentinel-1 relative orbits denoted by their relative orbit number (RON). RON 87 covers the eastern and RON 58 the western side of the scene (both indicated with a line and an arrow), RON 160 covers the entire scene and is not displayed (a). Polygons denote the peat production blocks where we have the in situ records about active peat extraction, abandoned areas and the open bog (a). The areal images cover production blocks and the natural open bog in Soosaare bog (b) and production blocks (upper right corner of the image) and an abandoned area in Sangla bog (c). Peat production fields in Sangla bog are seen in the photograph (d). Based on: **Publication III** Figure 1.

2.2. In situ data for validation of SAR measurements

In all of our studies (**Publications I–V**) the in situ measurements were used to validate the SAR results. However, the in situ measurements have not been specifically designed for SAR validation. Thus, our approach suffers a common disadvantage – the question of representativeness of an in situ point measurement if a SAR pixel has much coarser ground resolution (Alshammari et al. 2018; Marshall et al. 2022), i.e. $2.7\text{--}3.5\text{ m} \times 22.5\text{--}22.7\text{ m}$ in the case of Sentinel-1 (Bourbigot et al. 2016). Nevertheless, the time series of continuous ground levelling from Umbusi bog and Laukasoo bog in 2016 have a value per se. Not only the field of peatland InSAR is characterised by the absence of ground levelling data for validation (Cigna & Sowter 2017; Alshammari et al. 2018) but the bog breathing itself as a phenomenon has not been exhaustively studied and understood (Fritz 2006; Fritz et al. 2008; Morton & Heinemeyer 2019).

2.2.1. Bog water table data

In the Endla mire complex the bog water table is monitored on daily bases automatically along a hydrological monitoring transects of staff gauges in bog pools and sampling wells, stretching from Männikjärve bog to Linnusaare bog (**Publications I and II**). The Tooma Mire Station, part of the Estonian Environment Agency, is responsible for the data collection and distribution. WT data are

presented as daily averages. The sampling wells and staff gauges are anchored in the mineral ground beneath the peat layer. WT is defined relative to the absolute surface height, corresponding to the average surface of the ecotope around the sampling well (Estonian Environment Agency 2022a). We considered exclusively the wells and staff gauges located in the area classified as open or wooded bog. The snow- and ice-free periods in Oct 2016–Nov 2019 were included in the research.

2.2.2. Peat extraction data

The milled peat in the Sangla, Soosaare and Tässä peat production sites (**Publication III**) is produced by the Haku method or by the pneumatic extraction technique (Tissari et al. 2006). The peat production cycle consists of three stages: milling, drying and harvesting. The upper layer of peat is milled to the depth of 10–20 mm. The milled peat is left in the field to dry in the wind and sun until the humidity content has dropped to ~40% (Cleary et al. 2005; Eesti Turbaliit 2022). Drying takes 2–3 days, during what the peat is turned 1–3 times to ensure faster and more even drying. If it happens to rain the process has to be repeated. Harvesting is performed and the harvested peat is stockpiled at the end of the fields until utilisation (Sundh et al. 2000; Eesti Turbaliit 2022). 10–15 such cycles are performed during one production (harvest) season dependent on the weather and the peat conditions (Eesti Turbaliit 2022). The peat production period in the region lasts usually from May to August, seldom from April to October, with the peak time of harvesting in June and July (Pakere & Blumberga 2017; Eesti Turbaliit 2022). Routine field maintenance works are performed usually outside of the peat production period or seldom during the season (Graf et al. 2012).

The in situ validation datasets originate from the peat producers of the particular sites and are based on their internal reporting procedures. The datasets are given in a day precision for the peat production season of 2018. The Sangla record covers two of the peat production blocks of the site and contains a full list of milled peat production cycle related works (milling, turning, harvesting) from 8 May to 27 July. The Soosaare and Tässä records cover the entire peat production blocks (8 in each site) from 11 May to 3 August. The records contain the harvesting events but give also the areal extent of the harvest making it possible to detect when a block was sometimes harvested only partly. The datasets do not contain any record of the maintenance works which are not directly connected to the peat production cycle, e.g. field profiling to enhance surface runoff or maintenance of drainage ditches, complicating interpretation of the SAR data.

2.2.3. Bog surface levelling data

In **Publications IV** and **V** seasonal bog surface height changes were studied in Umbusi bog and Laukasoo bog (50 km apart) where the automatic surface levelling devices recorded the distance from the device to the ground from the end of April to the end of October, 2016 (from the snow-melt to the snowfall). The devices were

attached to a T-shaped metal bar which penetrates the peat layer and is anchored in the underlying stable mineral ground. At the plot 6 two devices were used. One recorded at the hollow and the other at the hummock nanotope with the distance between the devices 2 m. At the plots 2 and 4 a single device was used. The levelling data were collected at an hourly interval. The three ground levelling plots form a transect stretching from the main drainage ditch towards the undisturbed interior of the bog. The plot 2 is located 15 m from the ditch and has a significant tree cover as a direct impact of being severely drainage affected. The plot 4 is located ~50 m from the ditch in Umbusi bog and ~40 m in Laukasoo bog. The plot is still significantly influenced by drainage and represents the lawn nanotope in Umbusi bog and the hollow nanotope in Laukasoo bog. The plot 6 is 200 m from the ditch in Umbusi bog and 75 m in Laukasoo bog. The plot 6 is in nearly natural condition with a functional acrotelmic layer and experiences only weak influence of drainage. We consider the plot 6 to be a natural reference as a simplification.

2.3. Meteorological and land cover data

The meteorological and land cover data were used in comparing the InSAR results and the in situ measurements in an accurate and meaningful way. We used the meteorological data in all **Publications I–V** and the land cover data in **Publications I–III**. The meteorological data were provided by the Estonian Environment Agency (2022b). The summarised daily precipitation data were used in all **Publications**. The air temperatures measured at a 3-hour interval were used in **Publication I**. We employed the measurements from 6 p.m. local time which were the closest to the SAR acquisition time. In **Publications I, II, IV** and **V** the data from the Tooma meteorological station were used. The station is located 1 km south-east of Männikjärve bog in the Endla mire complex, 35 km north of Umbusi bog and 65 km north-west of Laukasoo bog. Regarding the peat production sites (**Publication III**) the precipitation data from the Tartu-Tõravere station (14 km south-east of Sangla) were used at the Sangla site. At the Soosaare and Tässä sites the rainfall estimate was calculated as an average of the three closest meteorological stations (Viljandi, Türi and Jõgeva) forming a triangle around the sites (25 km south-west, 38 km north-west and 35 km north-east of the sites, respectively).

The SAR results – coherence in **Publications I–III** and backscatter intensity in **Publication III** – were masked based on the land cover (**Publications I–III**) and the peat production blocks defined by the producers (**Publication III**). The land cover classification was based on the Estonian Topographic Database (Estonian Land Board 2021). Peatlands are defined as areas with peat depth >30 cm. The following land cover classes were differentiated: open bog (tree height <1.3 m or canopy cover <0.3), wooded bog (tree height 1.3–10 m and canopy cover >0.3), restored open bog, bog pools (pool area >100 m²) and abandoned cutaway bog (abandoned peat production area). The polygons were buffered 50 m inside in **Publication II** and 70 m in **Publication III** to avoid signal contamination between neighbouring land cover classes. In **Publication I** buffering was not applied.

2.4. SAR data

The SAR data in this dissertation were collected by the European Union's Copernicus programme's Sentinel-1 (S1) satellite mission employing a constellation of two identical satellites (A and B units) in the shared sun-synchronous orbit. The satellites Sentinel-1A (S1A) and Sentinel-1B (S1B) both use ~ 5.6 cm wavelength microwaves (C-band) for imaging. S1 was the preference in this study as each satellite returns to the exact same orbital position in every 12 days, whereas the combined revisit cycle of the two satellites is 6 days only. That allows forming continuous dense image time series over the test sites. S1 images are free of charge and supported by the free analysis software SNAP in accordance with the overall objective of the mission to provide C-band SAR data for operational applications and services globally (Torres et al. 2012).

Interferometric Wide swath mode (IW) Single Look Complex (SLC) dual-polarisation data products from Sentinel-1 satellite obtained from ascending orbits are used in all **Publications I–V**. The image acquisition time is around 4 p.m. UTC (Coordinated Universal Time) which corresponds to 7 p.m. EEST (Eastern European Summer Time) – the local summer time. Our research only concerns the snow- and ice-free period of the year after the snow-melt in April until the surface freeze and a snow cover formation in December. In 2016 (**Publications IV and V**) we are limited by the unavailability of continuous Sentinel-1A data before 1 July and Sentinel-1B before 29 September. In all **Publications** vertical transmit–vertical receive (co-polarisation VV) data are employed. In **Publication III** additionally vertical transmit–horizontal receive (cross-polarisation VH) is used. Cross-polarisation channel is strongly sensitive to vegetation resulting in strong backscatter from vegetated areas while bare surfaces reflect the SAR signal away from the sensor resulting in low backscatter. Co-polarisation backscattering in contrast is significantly influenced by the soil properties, i.e. its physical structure and moisture content (Pampaloni et al. 1997; Millard 2016; Bousbih et al. 2017). A polarisation channel in the IW acquisition mode contains 3 SLC images, one image per sub-swath. The pixel spacing is 2.3×14.1 m and the spatial resolution 2.7×22.5 , 3.1×22.7 and 3.5×22.6 m in range and azimuth direction, from lowest to highest incidence angle (Bourbigot et al. 2016).

The number of S1 acquisitions by orbital geometries indicated by the relative orbit number (RON), the study period and also the InSAR processing method along with the main product used in **Publications I–V** are shown in Table 1. In **Publication I** the imagery covers the Endla mire complex (13×13 km²) in 2017–2018 and in **Publication II** Linnusaare and Männikjärve bogs in the Endla mire complex in 2016–2019. In **Publication III** the total area of around 40×40 km² is covered containing active and abandoned peat extraction sites and raised bogs in Sangla, Soosaare and Täsäsi bogs in 2018. There are 3 consecutive days with an image per day from 3 orbital geometries after every 4 days, given the 6-day repeat visit for an orbit. Acquisitions for 26 July and 19 August (RON 58) are missing (resulting in four missing image pairs). The DInSAR processing in **Publications IV and V** covers 2016. The Distributed Scatterer (DS) time-series processing in

Table 1: The SAR data from the Sentinel-1 (S1) satellite (A and B units) used in the publications included in this dissertation. Viewing geometries referred by their relative orbit numbers (RON) and the number of acquisitions (Acq.) are shown. The data were used in conventional DInSAR processing or in a hybrid PS/DS time-series processing technique with DS phases being estimated with the EMI algorithm (Ansari et al. 2018).

Publication	Satellite	RON	Acq.	Study period	Method	Product
I	S1A	160	18	24 Oct 2017–18 Dec 2018	DInSAR	γ/δ
II	S1A	160	63	29 Oct 2016–19 Nov 2019	DInSAR	γ
III	S1A/B	58	29	3 May–31 Oct 2018	DInSAR*	γ
		87	30			
		160	31			
IV	S1A/B	160	14	1 July–29 Oct 2016	DInSAR*	δ
V	S1A/B	160	206	9 Nov 2014–28 June 2020	DS (EMI)	δ
		160	14	1 July–29 Oct 2016	DInSAR*	

* Computed over the consecutive short temporal baselines (differently from Publications I and II where single masters were used)

Publication V covers 2014–2020. The two study areas – the segments of Umbusi bog and Laukasoo bog in **Publication IV** both occupy less than $2 \times 2 \text{ km}^2$. In **Publication V** the study area covers $8 \times 8 \text{ km}^2$ containing Umbusi bog and the mineral land north of it.

2.5. InSAR processing

SAR interferometric processing was selected as the main tool in this dissertation as it allows resolving changes in the target occurring between two SAR acquisitions, including subtle height changes and potentially changes in the moisture content. The orbits in the Sentinel-1 radar mission are deliberately designed for the change detection. The sensor revisits the exact same position in orbit every 12 or just 6 days if both of the twin satellites are available allowing the same viewing geometry over the target (Torres et al. 2012; Geudtner et al. 2018). The two main products of InSAR processing – phase and coherence – were calculated as time series over our test sites in order to analyse based on the ground truth whether the measurements traditionally gathered in situ could be replaced by the space-born data. InSAR phase is directly related to relative surface deformations and coherence is the measure of similarity between the images describing systematic nature of the change. In this study temporal baselines, i.e. time separation between the SAR images forming an InSAR image pair, are categorized into two time scale classes: short temporal baselines (days) and long temporal baselines (weeks to months).

Each pixel of a digital SLC SAR image is a complex number that contains amplitude and phase information of the transmitted electromagnetic signal backscattered

from the corresponding resolution cell projected on the ground (Ferretti et al. 2007). When two phase images are combined in SAR interferometry, an interferogram is formed (Bamler & Hartl 1998). The SAR interferogram is generated by cross-multiplying, pixel by pixel, the first SAR image with the complex conjugate of the second (Ferretti et al. 2007). The phase (InSAR phase) of the resultant interferogram is the phase difference between those two images (Bamler & Hartl 1998; Ferretti et al. 2007). If the images are from the same viewing geometry but from different times (the approach called differential InSAR, shortly DInSAR), the phase difference indicates a change of the target during the time between the two acquisitions (Ferretti et al. 2007). Assuming that the scattering properties such as change in dielectric properties caused by changed moisture content or propagation properties remain the same in both images and therefore do not give rise to the phase changes, the InSAR phase becomes a sensitive measure of the distance difference between the sensor and the object, translating into surface deformations in the case of DInSAR (Bamler & Hartl 1998). A co-product of InSAR phase processing (interferogram formation) is InSAR coherence. Coherence is a quality measure of an interferogram and allows to judge the reliability of the local InSAR phase estimate (Bamler & Hartl 1998; Moreira et al. 2013).

Interferometric coherence (Zebker & Villasenor 1992) – a common term to refer to the magnitude of the complex correlation coefficient γ (Bamler & Hartl 1998; Preiss et al. 2006) – is a normalised measure of the local similarity in amplitude and phase between two SAR acquisitions forming a complex cross-correlated InSAR image pair (Preiss et al. 2006; Scott et al. 2017). Coherence is estimated for every image pixel over a small moving averaging window (Ferretti et al. 2007). Local coherence, ranging from 0 to 1, is high when the relative position and physical properties of the scatterers within the averaging window are similar in both images. The more manifested the random changes are between the two acquisitions, the lower the coherence is (Tamm et al. 2016; Scott et al. 2017). The surface deformations in the natural terrain are expected to be spatially continuous, thus the consequent InSAR phase field has to be also continuous (Bamler & Hartl 1998; Ferretti et al. 2007). Therefore, if the only change in the target between two acquisitions has been caused by the surface movement, it results in a locally coherent phase shift in the same direction as the motion. The coherence is high and the quality of interferogram is good, showing a continuous phase field with clear interferometric patterns. But if the random changes dominate instead of systematic changes such as what are produced by surface deformation, random phase shifts cause coherence loss, i.e. temporal decorrelation. The interferogram does not display a continuous phase field, indicating that the reliable deformation phase has not been preserved (J.G. Liu & Mason 2009) and deformation estimation is impossible (Ferretti et al. 2007). Formation of a good and a bad interferogram is illustrated in Fig. 5 with a simplified example of terrain surface displacements. An interferogram and the associated InSAR coherence image from Umbusi bog are given in Fig. 6. Coherence can also be used as a metric on its own (Bamler & Hartl 1998; Preiss et al. 2006; Moreira et al. 2013) as it provides information about the properties of the scatterer (Bamler & Hartl 1998).

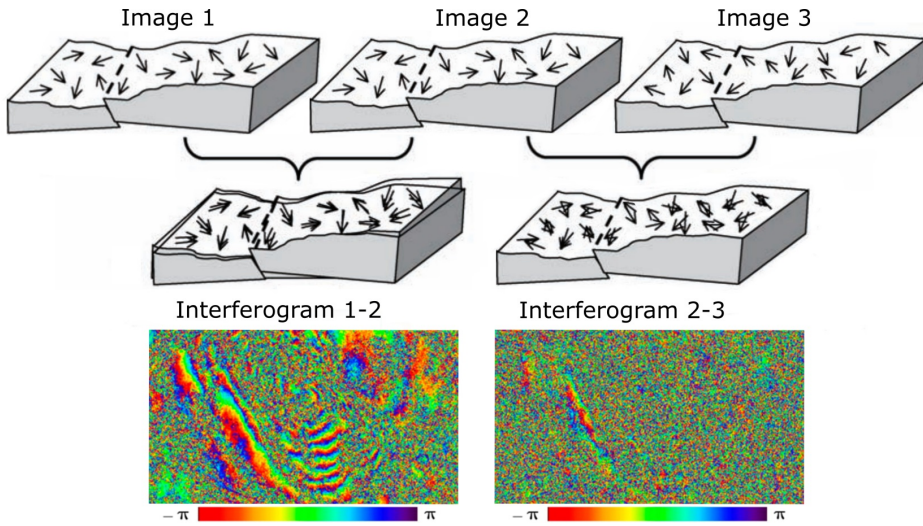


Figure 5: The effects of terrain deformation along a fault and random surface changes on interferograms. Three SAR phase images (Images 1–3) have been obtained over the same terrain from three satellite passes at different times. The small arrows in the images represent the phase angles of the backscattered SAR signals from the terrain surface. The uniform surface movements along a fault (marked with a dashed line) between the Images 1 and 2 cause a coherent phase shift in the same direction as the motion. The coherence is high and the quality of Interferogram 1-2 is good. A continuous phase fields with recognisable interferometric patterns are visible and have recorded the terrain deformation. But between the Images 2 and 3 instead of uniform movements random surface changes have occurred which result in random phase shifts. Each small arrow in the Image 3 has randomly changed its orientation in regard to the arrows in the Image 2. The random phase shifts cause coherence loss. Interferogram 2-3 is noisy and does not display any continuous phase field where phase could be reliably estimated. The block scheme is adapted from J.G. Liu and Mason (2009) and the interferograms (for illustrative purposes) are from Pepe and Calò (2017).

In a differential interferogram the relative surface height change (deformation) between two SAR images is recorded in the way that it is wrapped in 2π radian phase cycles. In InSAR the amount of height change that leads to a 2π change in interferometric phase is called height of ambiguity (Bamler & Hartl 1998; Rosen et al. 2000; Ferretti et al. 2007). In the case of zero-baseline differential InSAR, a 2π phase cycle corresponds to half of the SAR wavelength as the signal has to make a round trip between the sensor and the target. The surface elevation change along the radar line of sight (LOS) direction corresponding to a phase cycle could thus be called the displacement height of ambiguity (referred to as height of ambiguity in this dissertation). LOS changes larger than the height of ambiguity need ambiguity resolution, commonly referred to as phase unwrapping. Phase unwrapping is addition of the correct integer multiple of 2π to the InSAR phase to reconstruct the true altitude difference, assuming the true phase gradient is continuous because the surface of natural terrain is elastic and the 2π phase discontinuities visible

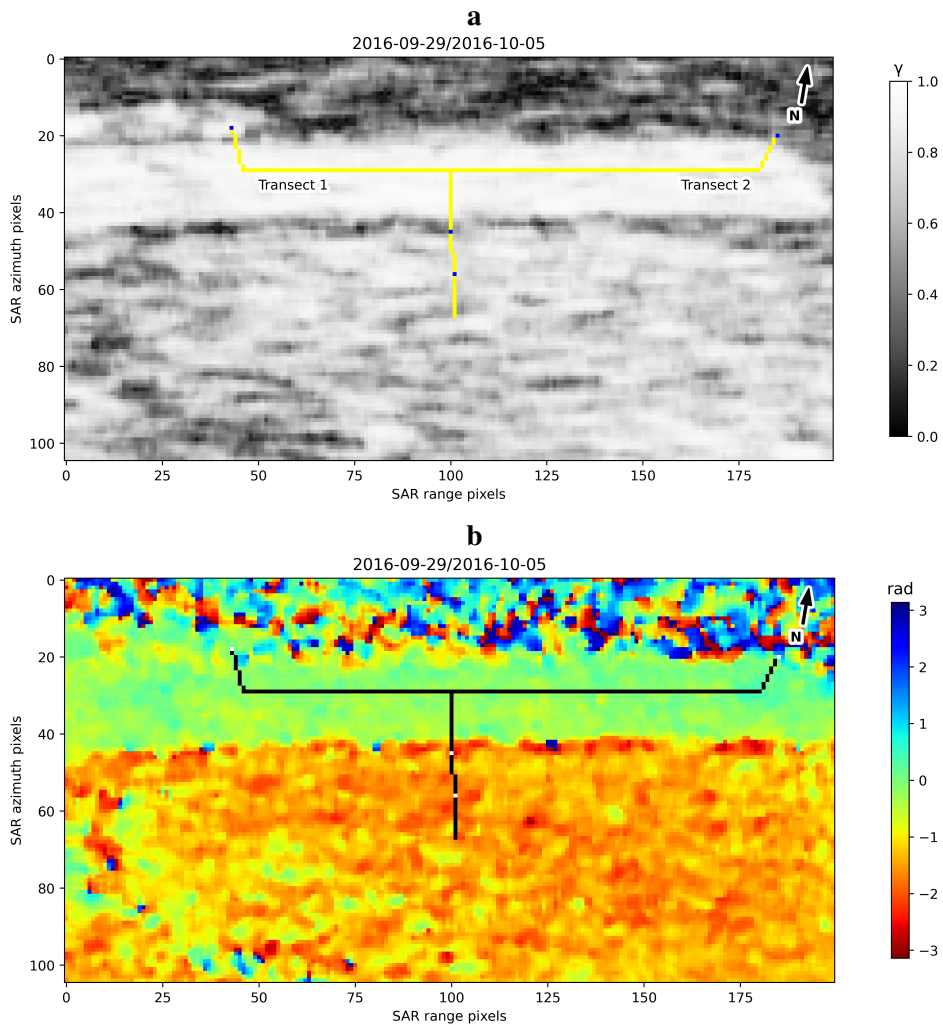


Figure 6: InSAR coherence γ (a) and phase (b) images in radar coordinates over the test site in Umbusi bog for the image pair 29 Sept–5 Oct 2016. Notice the phase in radians without using π . The areal image of the scene in the geographic coordinates is shown in Fig. 3a. Source: **Publication IV** Figures 4 a, b.

in the interferogram are not caused by real abrupt shifts of the observed surface (Bamler & Hartl 1998; Ferretti et al. 2007). Unwrapping in natural landscapes can be very complicated because the presence of the low coherence areas causes discontinuities in the phase field and leads to phase unreliability (Zhou 2013; Alshammari et al. 2018). When solved incorrectly unwrapping leads to wrong deformation estimates. Therefore, the deformations smaller than the height of ambiguity are intrinsically less error-prone. Reduction of the temporal baseline between the two acquisitions constituting an interferogram is the simplest way to account for smaller magnitudes in peatland surface deformation (Alshammari

et al. 2018), as done in **Publications IV** and **V**. Given the non-rigidity of the peat matrix and its dynamic response to the WT level (Kellner & Halldin 2002), longer time periods allow developing larger elevation changes (Marshall et al. 2022).

Another way to reduce the need for unwrapping is to work within a single height of ambiguity and avoid phase discontinuities by rotating the InSAR phase (confined between $\pm 1\pi$) as done in **Publications I, IV** and **V**. If the stable area where no deformation occurs is simply set to corresponds to 0π radian in an interferogram (which would be a natural choice), it means that the unambiguous change can be found confined to the phase changes not larger than $\pm 1\pi$, i.e. a quarter of the radar wavelength which is ~ 1.4 cm in the case of a ~ 5.6 cm wavelength of S1 (Novellino et al. 2017; Esch et al. 2019). All deformations beyond that limit ($\pm 1\pi$) need phase unwrapping. Nevertheless, the phase value of the reference point from the stable area can be arbitrarily set at whichever value in the phase cycle. If there is confidence about the direction of the deformation, it would be reasonable to set the value of the reference level at the either end of the phase cycle which allows measuring unambiguous changes either from 0 to -2π or from 0 to $+2\pi$ on demand. It means the entire range of the height of ambiguity, i.e. a half of the radar wavelength, could then be used unambiguously. In the case of the bog the direction of the deformation cannot be known without prior knowledge but what can be expected is that the direction of the change is locally spatially uniform. The short term bog surface height changes are determined by WT which functions as a hydrological unit (Kellner & Halldin 2002; Paal et al. 2016). The method we applied to determine the direction of the displacement and to choose an appropriate reference phase value contains rotating the ambiguous phase until the best fit for the area of interest in the interferogram is found inside the phase cycle. It means setting the reference level so that after the phase rotation the phase discontinuities seen in the interferogram do not appear in our area of interest but on the periphery and the phase field in that part of the interferogram that is of our interest displays maximally continuous. Thus, occasions of phase shifts from $+1\pi$ to -1π radian or vice versa visible as a fringe in an interferogram (Alshammari et al. 2018) are minimised.

Due to limitations such as temporal decorrelation and atmospheric distortions induced errors (Hu et al. 2014; Crosetto et al. 2016; Gong et al. 2016) the conventional DInSAR method is either limited to the areas of very good coherence (Hu et al. 2014; Alshammari et al. 2018) or nowadays mainly used as basis for InSAR time-series analysis (Hu et al. 2014; Crosetto et al. 2016; Osmanoglu et al. 2016). However, considering that DInSAR method employs only two SAR images at a time, it has potential for relatively easy near-real-time routine monitoring (Hu et al. 2014) while open bogs have been shown to display relatively high coherence (Corr & Rodriguez 1999; Zhou 2013; Alshammari et al. 2018).

InSAR time-series analysis is an umbrella term for advanced DInSAR techniques developed to overcome the limitations of conventional DInSAR (Hu et al. 2014; Gong et al. 2016). Time-series approaches can be broadly categorized into two: methods relying on persistent scatterers (PS) or distributed scatterers (DS) (Gong et al. 2016; Osmanoglu et al. 2016; Ho Tong Minh et al. 2020). In PS

InSAR only the coherent pixels with stable scattering properties over the full image stack are exploited (Ferretti et al. 2001; Osmanoglu et al. 2016) usually leading to low PS density in nonurban landscapes (Crosetto et al. 2016).

In DS InSAR the limit on the stability of the scatterers is relaxed and the DS can undergo coherence loss in the time series (Ansari et al. 2018; Yunjun et al. 2019) because the technique links the interferograms computed as multiple separate data subsets (Berardino et al. 2002; Crosetto et al. 2016). DS pixels are typically selected from multi-master interferograms with small perpendicular baselines (orbital separation) and short temporal baselines to suppress spatio-temporal decorrelation (Berardino et al. 2002; Hu et al. 2014; Gong et al. 2016), multilooked (i.e. averaging adjacent pixels) (Ferretti et al. 2007) to reduce phase noise and selected by a coherence based criterion (coherence threshold) (Berardino et al. 2002; Crosetto et al. 2016). The effect of perpendicular baseline for Sentinel-1 is negligible (Prats-Iraola et al. 2015; Geudtner et al. 2018).

2.5.1. Formation of InSAR coherence time series

Coherence time series were studied in **Publications I–III**. In **Publications I** and **II** the long temporal baseline InSAR coherence images with the time separation from two weeks to approximately six months cover the snow- and ice-free period of a year (growing period; April to November) together with the end of the growing period of the preceding year (end of October, November). **Publication I** covers the year 2018 and **Publication II** covers the years 2017–2019 in three independent stacks. Each image stack was calculated from a common master image (single master). The master image in **Publications I** was chosen to represent the time as close as possible to the maximum water table caused by the snow-melt in spring while not being directly affected by the fully water-saturated peat conditions. In **Publication II** the master images were chosen to be the last acquisitions in May to ensure comparability between and among the individual stacks and with **Publication I**. There were no precipitation on any of the master dates. In **Publication III** coherence was calculated over short temporal baselines forming 6-day InSAR pairs for three orbital geometries over the growing period 2018 accommodating the peat production season (Table 2).

The Sentinel Application Platform (SNAP) containing Sentinel Toolboxes (ESA 2022) was utilised for coherence estimation in all three **Publications I–III**. The processing chain (following Bourbigot et al. 2016 and Yagüe-Martínez et al. 2016) includes the SNAP operators: S1 TOPS Coregistration with ESD, Coherence estimation integrated with topographic phase subtraction and flat-earth phase subtraction, TOPS Deburst and Range-Doppler Terrain Correction. The Shuttle Radar Topography Mission (SRTM) 1 Arc-Second digital elevation model (DEM) and bilinear interpolation were used in coregistration and terrain correction. Estonian Coordinate System of 1997 (EPSG:3301) was used in terrain correction to project the SAR data on the ground, resulting in a square pixel of $\sim 14 \times 14$ m. The details of the size of moving coherence estimation window are given in Table 2. The footprint of the window projected to the ground approximates to

Table 2: Formation of coherence time series resulted from conventional DInSAR processing. In Publications I–III coherence time series were studied. In Publications I, IV and V phase differences were studied. A horizontal line separates the coherence stacks from the phase difference stacks in the table. Publications are denoted (Publ.), given are the number of image pairs (Img.) in a stack, study period, whether the stack was computed from a single master image (the date of the master image displayed) or between consecutive acquisitions (multiple masters) and the temporal baseline in days. The time between consecutive acquisition is shown for the single master stacks as it differs from the temporal baselines. The size of the moving averaging window in SAR slant range pixel coordinates (px) in azimuth and range direction used in coherence estimation (Coh.) and in phase filtering (Flt.) is displayed. For coherence the approximate footprint of the window on the ground is also shown.

Publ.	Img.	Study period	Master	Master img.	Baseline (day)	Coh. (px)	Footpr. (m)	Flt. (px)
I	11	2017–2018	Single ⁽¹⁾	28 May 2018	12–216	3×10	40×40	
	22	2016–2017		21 May 2017	12–204			
II	22	2017–2018	Single ⁽²⁾	28 May 2018	12–216	3×10	40×40	
	22	2018–2019		23 May 2019	12–204			
III	85	2018	Multiple		6	5×19	70×70	
I	11	2018	Single ⁽³⁾	28 May 2018	12–180	3×10	40×40	15×30
IV	13	2016	Multiple		6 or 12	3×10	40×40	3×10
V*	13	2016	Multiple		6 or 12	3×10	40×40	3×10

⁽¹⁾ 24- or 36-day separation (roughly a month) between consecutive SAR acquisitions

⁽²⁾ 12-day separation

⁽³⁾ 12- or 24-day separation

* DS time-series processing in Publication V (subsection 2.5.4) not included in the table

40×40 m in **Publications I** and **II** (following Fielding 2018 and Braun 2021) and to 70×70 m in **Publication III** best addressing the trade-off between the estimation bias towards higher coherence values and the loss of spatial resolution (Touzi et al. 1999; Dahdal 2011; Tamm et al. 2016). Signal-to-noise ratio (SNR) correction was applied only in **Publication III**.

2.5.2. Calculation of backscatter intensity

Backscatter intensity – the dimensionless (m^2/m^2) backscatter coefficient σ^0 (Bamler & Hartl 1998) which is the back-scattering cross-section of a distributed target per unit area (Bourbigot et al. 2016) – was studied in **Publication III**. Backscatter intensity σ^0 is calculated by squaring the backscattering amplitude (Ferretti et al. 2007). We estimated σ^0 utilising the SNAP software. The processing chain (following Bourbigot et al. 2016, Tamm et al. 2016) includes the SNAP operators: Applying Orbit File, Thermal Noise Removal, Calibration and Range-Doppler Terrain Correction.

2.5.3. Computation of DInSAR deformation phase time series

In **Publications I, IV** and **V** the stacks of interferograms cover the growing period of one year. **Publication I** covers the year 2018 in 11 interferograms of long temporal baseline (from two weeks to approximately six months) calculated from a single master. **Publications IV** and **V** cover the year 2016 since 1 July in 13 interferograms of short temporal baseline of 6 or 12 days (Table 2). The interferograms were computed in SARPROZ software (Perissin 2022). The processing (following Perissin 2019) included co-registration and interferogram formation, integrated with topographic phase subtraction using SRTM DEM and flat-earth phase subtraction. The analyses were performed in SAR slant range pixel coordinates. Projection to the ground was not applied to preserve the original phase values and the dimensions of the resolution cell. The size of the moving averaging windows used in coherence estimation and in Modified Goldstein phase filtering (Goldstein & Werner 1998) are shown in Table 2. In **Publication I** after the export from SARPROZ, additional Goldstein filtering was applied on demand in MATLAB programming language (MathWorks 2022) to treat the interferograms of lower coherence. The phase rotation and further analysis of the interferograms were executed in MATLAB (**Publication I**) or in Python programming language (Python Software Foundation 2022) (**Publications IV** and **V**).

Without any ground calibration data, we used a relatively stable area where the displacement was assumed to be zero in all interferograms as a reference for InSAR phase, following the work by L. Liu et al. (2010). The reference point allowed also accounting for the atmospheric effects on the phase as the atmosphere is ought to stay relatively constant over a few kilometres (Webley et al. 2004; Foster et al. 2006; Bekaert et al. 2015). With the phase rotation we aimed at the smoothest deformation field over the open bog area delineated with the land cover mask in **Publication I** or represented by virtual transects drawn on interferograms in **Publications IV** and **V**. In the visual inspection neither fringes were seen in the interferograms nor phase shifts that were not solvable with phase rotation were found along the transects. That indicated unwrapping was not needed as the LOS measurements fitted in a single phase cycle in any of the three **Publications I, IV** and **V**. The virtual transects acting as peat surface deformation profiles were used also in analysing the interferograms.

For analysis purposes a transect was also drawn in **Publication I** along a cross-section of Kanamatsi bog. Kanamatsi bog was the preference of choice due to its high InSAR coherence. While the interior parts of the bogs tended to decorrelate due to the presence of bog pools with consequent advanced tree growth, the concentration of pools is low in the central parts of Kanamatsi bog. To better visualise the seasonal dynamics of the bog surface height we chose an arbitrary point in the central part of Kanamatsi bog on the transect to be visualised as a single point time series. The exact location of the transect and the arbitrary point can be found in **Publication I** Figure 9a. The reference point (ground tie-point) was taken at the margin of the open bog where the peat is shallower and its bulk density higher indicated by advanced tree growth in the vicinity and thus peat

deformations of a smaller magnitude can be assumed. Contrarily, the center of the bog with its thick layer of porous water filled peat of low bulk density and active acrotelm is dynamic, experiencing bog breathing. The deformation values are given in the radar LOS altitude differences in millimeters.

In **Publication IV** the physically established ground levelling transects were virtually extended over the peat production fields until the stable area on the mineral soil or on the compacted organic soil resulting from the peat production. Exceptionally, we did not draw a transect to connect the Laukasoo reference point 3 with the levelling locations because the former was separated from the rest of the scene by the forest (Fig. 3) causing decorrelation. At that reference point the phase rotation from the nearest transect (transect 1) was used. The reference points were taken at causeways and buildings – a road extension and sheds in Umbusi bog and a road section, junction and a building in Laukasoo bog. The distances from the furthest levelling point to the tie-point were 560 m and 960 m respectively in Umbusi bog and in Laukasoo bog. In **Publication V** the virtual transect is confined to overlap with the levelling transect and ends with the main drainage ditch. In **Publications IV** and **V** the LOS altitude differences (in radians) were projected to the vertical direction (u_{LOS} ; in centimeters) using the local incidence angles assuming no horizontal motion in the peat, following the work by Alshammari et al. (2018), Hoyt et al. (2020) and Marshall et al. (2022).

2.5.4. Computation of DS InSAR deformation phase time series

The DS time-series processing in **Publication V** followed the method by Ansari et al. (2018) which is a hybrid PS/DS approach with DS phases being estimated with the Eigendecomposition-based Maximum-likelihood-estimator of Interferometric phase (EMI) algorithm. The time series covers 2014–2020 in Umbusi bog. The tropospheric phase simulated from ERA5 reanalysis data (Hersbach et al. 2022) was removed before the DS calculation step. The estimated phase time series is relative to an arbitrary master. The DS pixel footprint on the ground approximates to a square of a ~ 200 m side. After the DS calculation the year 2016 was extracted for comparison with the available ground levelling data. Only DS points with coherence >0.9 were included. That resulted in 15 DS points in the vicinity of the levelling plot Umbusi 6 hummock, located around the plot at 125–230 m and 150–350 m from the main drainage ditch, belonging to the ridge-hollow-pool ecotope similarly to the plot 6. The median elevation change of these 15 points was found for every date in the time series and referenced to the median of a cluster of 8 stable reference points available ~ 4 km away to further account for the atmospheric effects. The InSAR altitude measurements along the line of sight (LOS) were projected to the vertical direction (u_{LOS}) using the local incidence angle of the plot 6, assuming no horizontal motion in the peat.

2.6. Data analysis

In **Publications I, II** and **III** we used image segmentation approach and aggregated the pixels of InSAR coherence images into polygons (Karl & Maurer 2010) with the aim at representing landscape units or entire sites as discrete regions, following the work by Millard (2016) and Tamm et al. (2016). Segmentation into objects helps to compensate for pixel noise (Millard 2016; Tamm 2018) arisen mainly from speckle (Goldstein et al. 1988) and is advised for target objects larger than an image pixel (Karl & Maurer 2010). There are 46 polygons included in **Publication III**, among them 18 peat production blocks (defined by the producer), 10 polygons from abandoned areas and 18 from the open bog. RON 160 covers all the 46 polygons, RON 58 covers 39 and RON 87 covers 19 polygons (the approximate coverage of orbits is shown in Fig. 4). The land cover classes were the basis of segmentation in natural and abandoned cutaway bogs in **Publications I, II** and **III**. The mean, median, maximum, minimum and standard deviation (SD) of coherence (γ) magnitude and backscatter intensity (σ^0) and additionally VV/VH ratio for coherence were calculated inside each polygon in **Publication III**. The characteristics we found useful in our study were median and SD of γ and median σ^0 . In **Publications IV** and **V** pixel-based comparisons were used. Though, spatial filtering had been applied in the DInSAR processing and multilooking in the DS processing, both to suppress the speckle arisen noise (Goldstein et al. 1988).

In **Publication I** the data preparation was done in Microsoft Excel software (Microsoft Corporation 2022), the statistical analysis concerning InSAR coherence was executed in R software (R Core Team 2022) and concerning InSAR phase in MATLAB software (MathWorks 2022). In **Publications II** and **III** the data were analysed in R and in **Publications IV** and **V** in Python software (Python Software Foundation 2022). In **Publications IV** and **V** the outliers were removed from the hourly ground levelling dataset using the Tukey's fence method with a multiplier of 1.5 (Tukey 1977) in a discrete 3-day window. Thereafter, the daily median values were calculated, except the Laukasoo plot 2 where only daily averages were available, to be used in further analysis. The Shapiro–Wilk test (Shapiro & Wilk 1965) was used to analyse data distribution and the Spearman's rank-order correlation (r_s) (Spearman 1987) was applied to estimate correlation between not normally distributed time series in **Publications I, II, IV** and **V**. In **Publications I** and **III** the Mann–Whitney U test (Mann & Whitney 1947; Hart 2001; McDonald 2014) was used to compare samples, following the Benjamini–Hochberg (BH) procedure (Benjamini & Hochberg 1995). In **Publication III** a nonparametric test was preferred as we could not expect normal data distribution and in addition our datasets were relatively small.

In **Publication III** box-and-whisker plots were used to visualise data. A box marks the interquartile range (IQR), i.e. data points between the 25th and 75th percentile. Whiskers indicate the range of a set of data that is not more than 1.5 times the IQR from the box (R Documentation 2022). Beyond whiskers the outliers are displayed. A notch surrounding the median shows the confidence interval. If the notches of two boxes do not overlap then there is 95% of confidence that their

medians differ, although it should not be regarded as a formal test (Chambers et al. 2018; R Documentation 2022). In **Publications I** and **II** the regression analysis was used to estimate the relationship between variables. Root Mean Squared Error (RMSE) was calculated for non-linear regression models. All the statistics were considered to be statistically significant at p -value < 0.05 .

3. RESULTS

3.1. InSAR coherence for assessment of bog surface dynamics

Interferometric coherence describes local phase stability (Ferretti et al. 2007), i.e. it tells us whether the changes in the target occurred in time have been systematic or random (J.G. Liu & Mason 2009). Contrary to backscatter whose interpretation and reproducibility are hindered by the incidence angle dependency, coherence is almost indifferent to incidence angles and could potentially make a good tool for global non-site-specific usage. However, the coherence response is complex and affected by many factors (Zebker & Villasenor 1992; De Zan & Gamba 2018). In this dissertation it has been studied what information about the bog surface dynamics can be derived from the coherence.

3.1.1. Assessment of peatland water table based on single master DInSAR coherence

Peatland water table dynamics determines the processes affecting greenhouse gas fluxes from the bog but also water retention, peat formation and compaction and acrotelm functioning. InSAR coherence is sensitive to changes in the terrain surface including changes in surface moisture but also to changes in vegetation (Zebker & Villasenor 1992). Open *Sphagnum* dominated raised bogs with minimal effects from vegetation but spatially and temporally dynamic moisture conditions could favour application of radar remote sensing (Millard & Richardson 2018).

Single master InSAR coherence behaviour in the raised bog was studied in **Publications I** and **II**. It is shown in **Publication I** that open bogs sustained coherence over half a year – during the growing period (snow- and ice-free period from April to December 2018) and also over the winter (October 2017–May 2018). The mean coherence in regard to a single master on 28 May 2018 of the open bog area was significantly higher compared to other natural land cover classes (wooded bog, bog pools and forest) (p -value < 0.05). The spatial distribution of the pixels of higher or lower average coherence, the threshold set according to our data while considering the literature (Weydahl 2001; Cigna & Sowter 2017; Braun & Veci 2021) is shown in Fig. 7. The pixels from the open bog displaying higher average coherence (≥ 0.5 ; upper 10th percentile of the open bog pixels) were concentrated to the most homogeneous hummocks dominated ecotope with no hollows or pools in the marginal areas of the open bog. In the central part of the bog higher coherence occurred in the ecotope dominated by hummocks and lawns and the pixels from the areas dominated by hollows and ridges are only occasional. The lowest coherence (≤ 0.25 ; lower 10th percentile of the open bog pixels) occurred in the ridge-hollow-pool ecotope where small water bodies are found and tree growth is supported in central parts of the bog and at the margins of the open bog close to the wooded bog or peatland forests.

The open bog land cover class displayed temporal variance in coherence and a pattern of coherence recovery. Coherence was highest in the spring coinciding

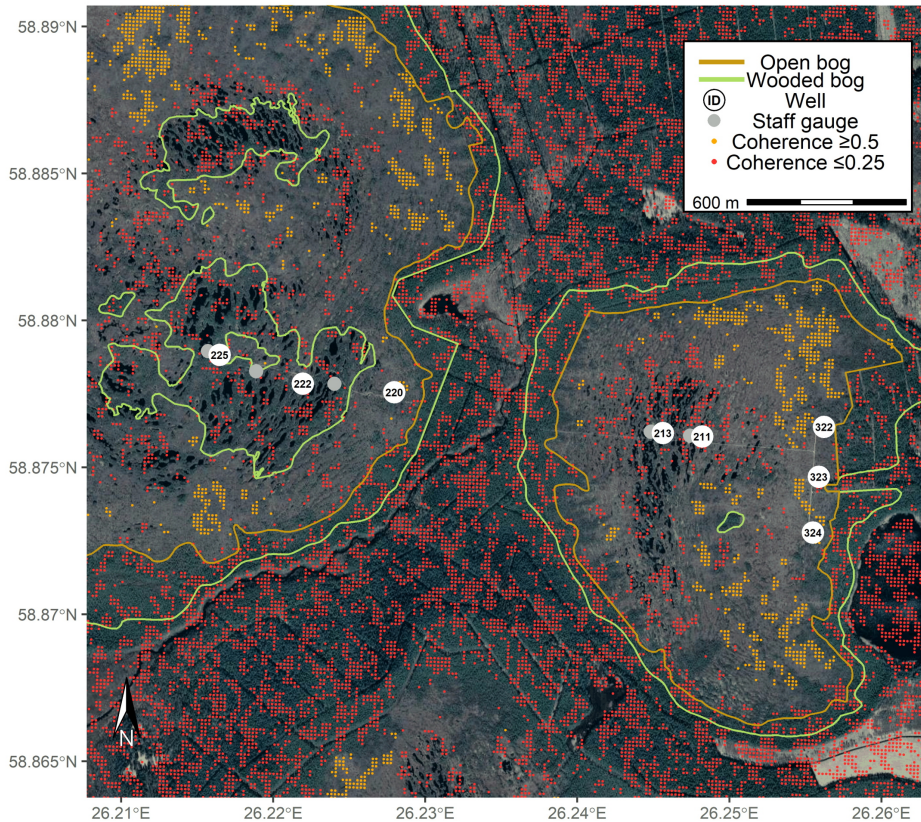


Figure 7: Spatial distribution of SAR image pixels characterised by higher average InSAR coherence or decorrelation. The pixels of intermediate value are not displayed. The hydrological monitoring transect of sampling wells (labeled with the well ID) and staff gauges is shown. Source: **Publication I** Figure 7.

with the shortest temporal baselines. The open bog decorrelated in the summer but became correlated again in the autumn. The other studied land cover classes (wooded bog, bog pools and forest) did not display a recovery in coherence (Fig. 8a). Fig. 8b displays how the lowest mean coherence coincides with the lowest water table in all the sampling wells. The lowest WT in the bog pools measured by staff gauges occurred in August. That lag can partly be explained by the higher evaporation from the open pool surface compared to the evapotranspiration of the vegetated peat surface (Kellner 2001; Kont et al. 2007). Reduced coherence in December can be explained by a snowfall. The absence of recovery pattern at the restored bog site could be attributed to the fact that the restoration process, e.g. damming ditches, was still in progress in 2018 and the WT dynamics was affected by different processes compared to the open bog. Consequently, the restored bog area (Fig. 2) was excluded from further analysis and is not displayed in Fig. 8a.

In **Publication II** we extend the work from **Publication I** and studied the relationship between coherence and WT over the three growing periods (2017,

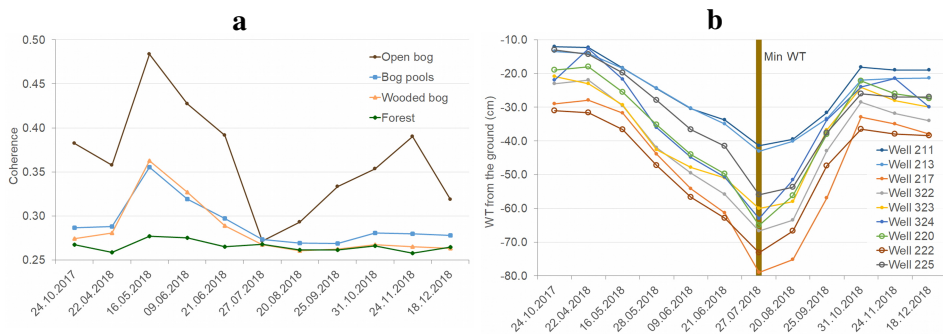


Figure 8: The mean long temporal baseline InSAR coherence from a single master on 28 May 2018 by natural land cover classes (a). The water table (WT) depth from the ground (defined as the average surface height of the ecotope around the sampling well) in sampling wells in the open bog (b). "Min WT" stands for the minimum WT on the dates of the SAR acquisitions. The wells in Männikjärve bog are indicated with small filled circles, in Linnussaare bog with larger hollow circles. Source: **Publication I** Figures 4 and 5a.

2018 and 2019) of different climatological conditions. The relationship was the strongest in 2018 which was characterized by drier-than-normal conditions during the 2018 drought event in Europe (Schuldt et al. 2020) and the largest WT changes. In 2019 (a normal climatological year with the autumn rainier than average) coherence was responsive to the WT until heavy autumn rains. In 2017 which was a wet year, coherence did not respond to the WT (Fig. 9). The relatively weak but statistically significant relationship (p -value < 0.001) could be described by the second degree polynomial regression models with RMSE 0.047 and RMSE 0.098 calculated for the dimensionless coherence magnitude in 2018 and 2019, respectively (Fig. 9 b2, c2). While light rain did not affect the regression considerably, the heavy rainfalls caused decorrelation.

3.1.2. Detection of physical changes in peat surface structure based on short temporal baseline DInSAR coherence

The short temporal baseline (6-day) InSAR coherence was studied in **Publication III**. Median coherence of the polygons (displayed in Fig. 4a) from the different land cover classes (milled peat production sites, abandoned cutaway peatland, open bog with marginal drainage effect) during the peat production season of 2018 (3 May–3 August) are shown in Fig. 10. The coherence magnitude of the peat production blocks in both polarisations (0.19 in VV and 0.17 in VH) was significantly lower (p -value < 0.001) than in the open bog (0.60 in VV; 0.38 in VH) or in the abandoned cutaway bog (0.58 in VV; 0.39 in VH). The open bog and the abandoned cutaway bog behave statistically similarly, i.e. they are inseparable from each other (p -value > 0.05 in both polarisations). The coherence in both polarisations is capable of distinguishing the areas where active peat extraction occurs from abandoned cutaway peatlands or natural bogs. The further analysis is focused on the VV-polarisation which is more sensitive compared to VH.

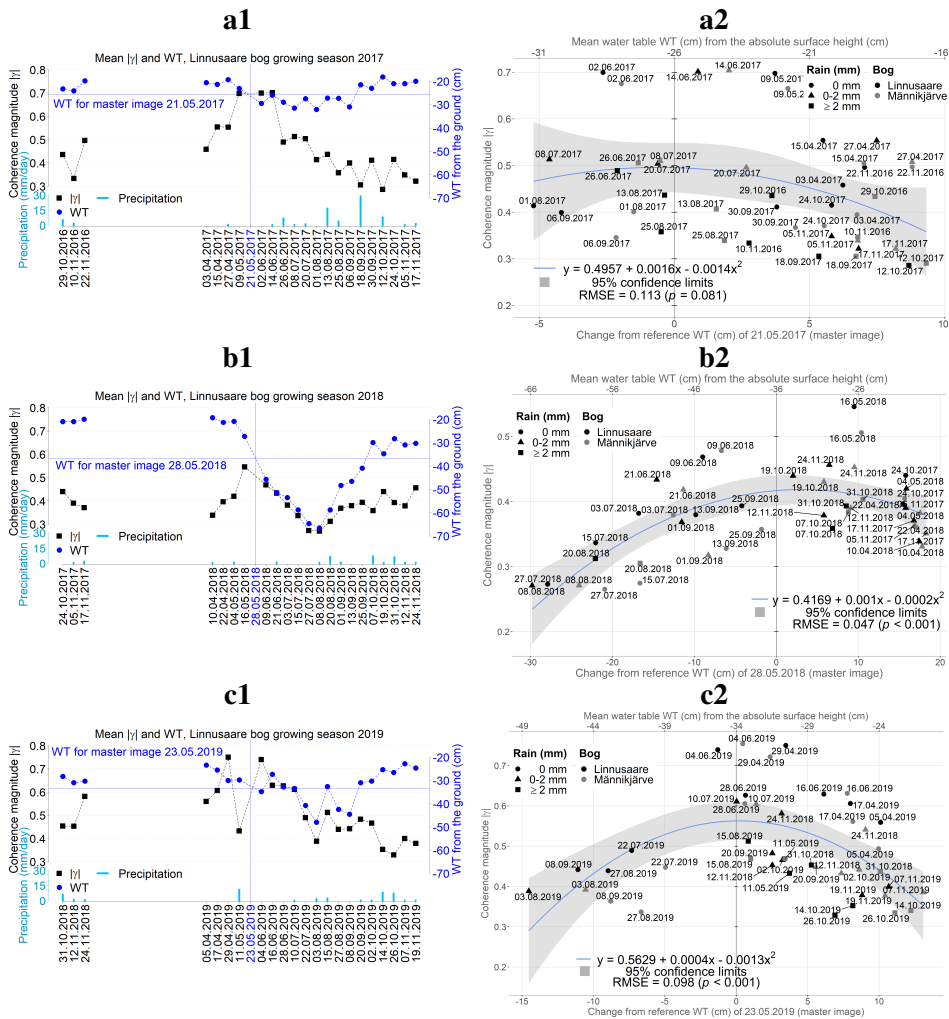


Figure 9: The mean coherence magnitude $|\gamma|$ related to the mean water table (WT) depth over 3 growing periods in the sampling wells, presented as time series (a1, b1, c1) and scatter plots (a2, b2, c2). WT is measured from the ground surface. γ is estimated from a single master on 21, 28 and 23 May, respectively in the stack of 2017 (a1, a2), 2018 (b1, b2) and 2019 (c1, c2). An image pair is indicated by the acquisition date of the slave image. The daily precipitation sum is shown as blue bars. Only the time series from Linnusaare open bog is presented (a1, b1, c1). In the regression the data from both Linnusaare and Männikjärve open bogs are used (a2, b2, c2). The WT change is estimated from the master image. Root Mean Squared Error (RMSE) is calculated for γ . Source: **Publication II** Figures 3 and 4.

In August–October after the peat production season the production area no longer displayed such low coherence magnitudes. Instead, the milled peat production area had VV median coherence of 0.67 and did not differ statistically from the abandoned area (0.71). The open bog (median coherence 0.62) differed from both

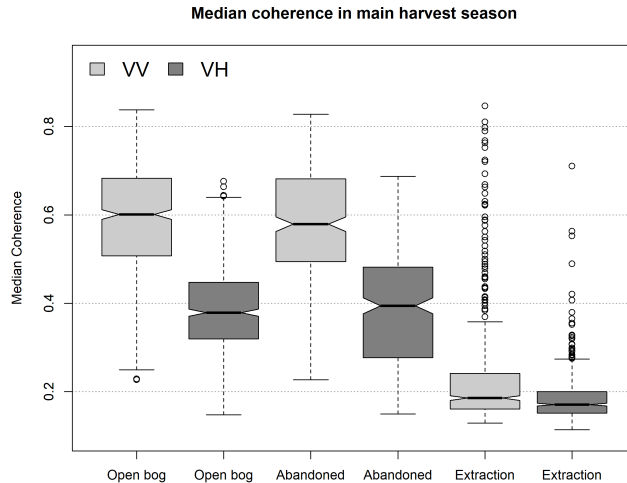


Figure 10: Median coherence (6-day temporal baseline) of the polygons from the differentiated land cover classes (production sites characterised by active peat extraction, abandoned cutaway peatland, open bog) during the peat production season in 2018 at VV and VH polarisations (RONs 58, 160 and 87). Source: **Publication III** Figure 2.

of the previous (p -value < 0.001) having the lowest median and also the lowest dispersion (variability). Dispersion among the peat production blocks was high compared to the other land cover classes due to occasional maintenance works. Any work become improbable in October when the temperature falls, evaporation is low and peat becomes too wet to support heavy machinery. The extraction area displayed VV median coherence of 0.87, the abandoned area 0.80 and the open bog 0.70 in October. All the three differed statistically (p -value < 0.001) whereas the extraction area had the lowest dispersion.

Fig. 11 illustrates the changes in coherence (RON 160) in the production block Sangla 1 compared with the reference polygons from the abandoned cutaway bog and the natural bog. Decorrelation characterised the production block until the image pair 27 July–2 August which marked the known end of the production season. In the period after the season when no in situ data were available, the behaviour of coherence was erratic and it is not known whether decorrelation was caused by maintenance works altering the peat surface (e.g. profiling) or natural phenomena (e.g. heavy rainfall). Clues can be provided via comparison with the reference polygons from known undisturbed sites. In this context the abandoned cutaway bog and the natural bog can serve as proxies for what the production blocks would look like when no works are carried out. Only the extraction site became decorrelated in the image pairs of 20–26 Aug and 13–19 Sept (Fig. 11). That indicates surface altering works. On the contrary, the heavy rain on 20 Aug (18 mm/d) decorrelated all the 3 polygons in the image of 14–20 Aug. Though, the rain of 20 Aug did not decorrelate the open bog and the abandoned cutaway in

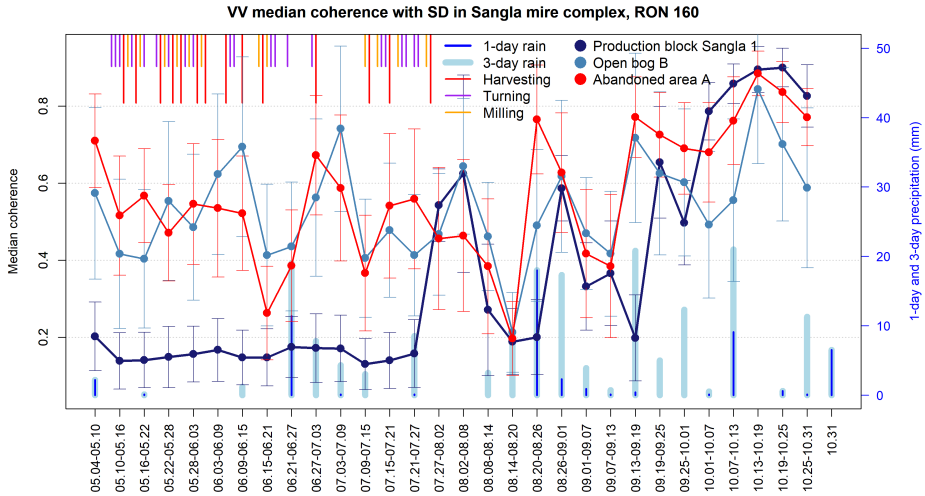


Figure 11: VV coherence median values with the standard deviation of Sangla peat production block 1, abandoned area A and open bog B from one orbital geometry (denoted by its relative orbit number (RON) 160). 1-day and 3-day precipitation sum (bottom) and the recorded works constituting the peat production cycle (top) are shown. Precipitation corresponds to the second date in an image pair. Source: **Publication III** Figure 6.

20–26 Aug as both days were rainy (2.3 mm/d on 26 Aug) and the soil is expected to have been wet on both dates.

Another way to detect peat production related activities is through combining multiple orbital geometries (3 relative orbits in our study) as shown in Fig. 12. While heavy rainfall decorrelates a site only temporarily and the impact of atmospheric disturbances or rainwater on the ground disappears in time, peat extraction or any other surface altering work changes the peat surface irreversibly. Therefore, a sequence of temporally partially overlapping image pairs from different orbits with an offset of few days have all to be decorrelated if the change was permanent. If not all of the image pairs in the sequence are decorrelated the loss of coherence can be attributed to something temporary. If a temporary event like a heavy rainfall has an effect that lasts one day, it affects only that particular image pair that begins or ends on the date of that event. The image pairs from other orbits neither beginning nor ending with that particular date are not affected even though the image pairs cover the period when the event occurred. All the 3 relative orbits were unanimous in recording the peat extraction during the production period (Fig. 12). All the 3 geometries were decorrelated in 8–14, 12–18 and 13–19 Sept (RONs 87, 160 and 58, respectively) showing there was a surface altering work carried out on 13 or 14 Sept which are the overlapping dates of the 3 geometries, in concordance with what we saw in Fig. 11. Contrary, the decorrelation of RON 58 in 24–30 Oct and RON 87 in 2–8 Aug had to be caused by weather as other two geometries stayed coherent. Conclusive interpretation of the low coherence magnitudes between 7–26 Aug were hindered by the missing image from RON 58.

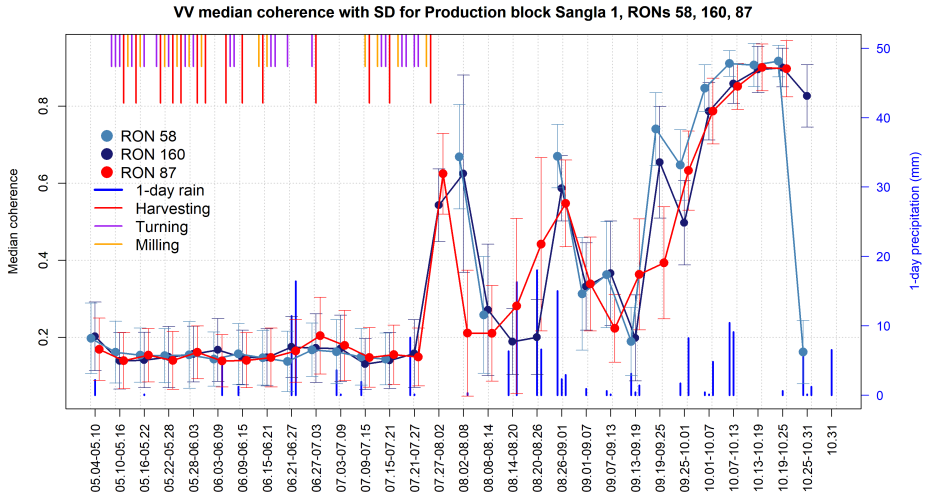


Figure 12: VV coherence median with the standard deviation of Sangla peat production block 1 from 3 geometries (denoted by their relative orbit numbers abbreviated as RON). 1-day precipitation sum (bottom) and the recorded works constituting the peat production cycle (top) are shown. Precipitation corresponds to the second date in an image pair. Source: **Publication III** Figure 7.

Table 3: Characteristics describing the dispersion in the peat extraction intensity classes grouped by the extraction frequency in a peat production block. Each data point shows the VV median coherence of a 6-day acquisition period from the corresponding production block (represented as a polygon) during the production period. VV median coherence values of individual polygons are aggregated into classes (Class) that indicate the number of harvest cycles repeated in a polygon. The number of observations from the corresponding polygons in a class is shown (Count). Median, mean, standard deviation (SD) and interquartile range (IQR) of the coherence values in the class are given. Source: **Publication III** Table 1.

Class	Count	Median	Mean	SD	IQR
16 cycles	225	0.186	0.207	0.075	0.060
11–15 cycles	285	0.183	0.228	0.115	0.093
6–10 cycles	60	0.199	0.318	0.225	0.302
Abandoned cutaway	328	0.579	0.577	0.134	0.187
Open bog	646	0.601	0.594	0.116	0.175

The peat production blocks aggregated into extraction intensity classes according to the production cycles repeated during the production season are given in Table 3. Group "16 cycles" was made of 7 blocks, "11–15 cycles" of 8 and "6–10 cycles" of 3 blocks. Each data point corresponds to the median coherence of the corresponding polygon from a 6-day image pair. All 3 orbital geometries are included. At both polarisations the open bog and the abandoned cutaway peatland

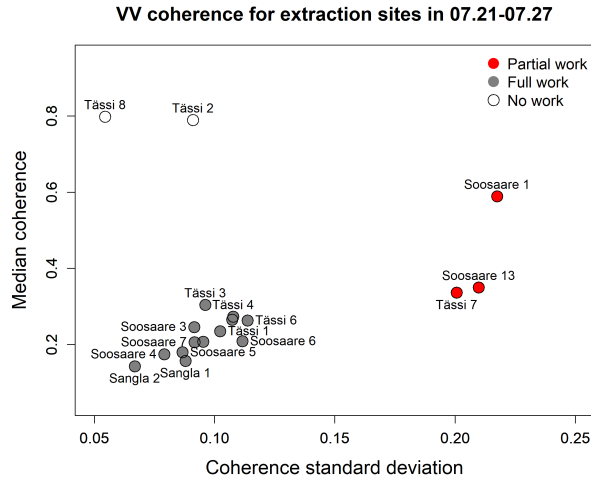


Figure 13: Peat production blocks in the image pair of 21–27 July (2018) from the relative orbit number 160. Gray circles mark full harvest (works that constitute the harvest cycle executed in the whole extent of a block), red partial harvest (works executed in a partial extent of a block) and white no activity, according to the Sangla, Soosaare and Tassi datasets of harvesting events. Source: **Publication III** Figure 8.

were similar to each other but differed from the extraction area (differentiated to extraction intensity classes). The peat extraction intensity classes displayed similar median coherence values and were statistically inseparable according to the Shapiro-Wilk test (p -value < 0.001). However, the increasing dispersion of the coherence magnitude coincided with the decreasing number of production cycles performed. That may provide grounds for assessment of extraction intensity in a peat production block (represented as a polygon) via mean, standard deviation (SD) and interquartile range (IQR) of the coherence values which display pronounced differences at VV. Dispersion in VH polarisation was low.

The peat production blocks were large enough to allow differentiation also inside a block. If some production fields (about 20×300 m) forming a block have not been harvested for some reason, differentiation may help to detect such a partially harvested block. Detection of partially harvested areas is not achievable by using only the median coherence of a polygon (corresponding to a block) but it could be achieved via combining the median with the SD, as given in Fig. 13, showing the image pair of 21–27 July. The in situ records of the harvesting events from Soosaare and Tassi containing the areal measure of harvest confirmed the InSAR characteristics. Also, visual interpretation of coherence images from RON 160 showed sharp straight borders between correlated and decorrelated parts in the polygons (shown in **Publication III** Figure 9).

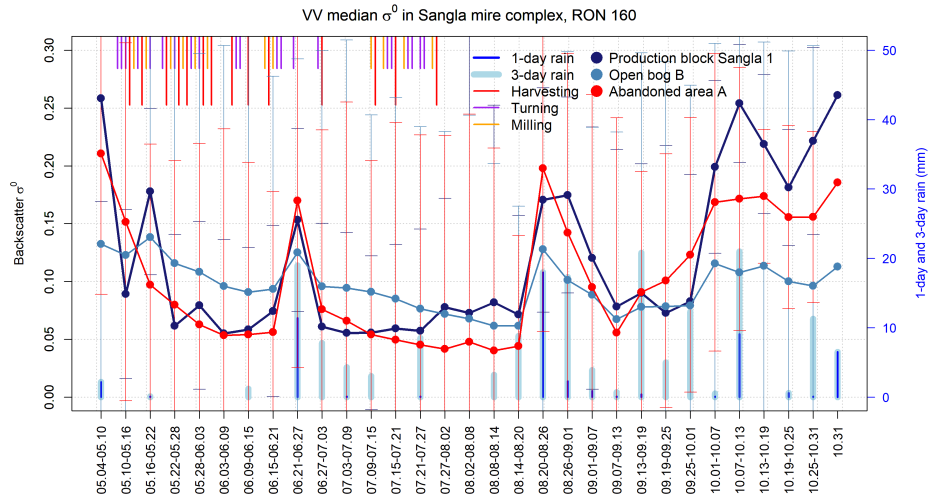


Figure 14: VV backscatter intensity σ^0 median with the standard deviation in Sangla peat production block 1, abandoned area A and open bog B from relative orbit number (RON) 160. 1-day and 3-day precipitation sum (bottom) and the recorded works constituting the peat production cycle (top) are shown. Source: **Publication III** Figure 10.

3.2. Recording precipitation events with SAR backscatter intensity

SAR backscatter intensity σ^0 has been the most commonly used SAR product because it is relatively easy to compute compared to interferometry. Due to its direct sensitivity to moisture content, it has also been often applied in peatland studies. In this dissertation (**Publication III**) backscatter intensity was used to identify precipitation events which could be confused for surface altering works in peat extraction sites due to their similar coherence response.

Not only coherence but also σ^0 was sensitive (statistically significant weak relationship) to harvesting events during the peat production season (shown in **Publication III** Figure 4a). That weak sensitivity, however, was entirely overshadowed by the response σ^0 had to precipitation events, witnessed by distinctive peaks on rainy days, and to soil humidity in all the land cover classes (Fig. 14). The declining trend of σ^0 in summer seen in the open bog and in the abandoned cutaway peatland is related to the decrease in surface humidity. As expected, such a trend did not occur in the area of active peat extraction. In the autumn when the peat is saturated with rainwater σ^0 stays high in all the land cover classes. σ^0 was sensitive to 1-day precipitation sum but insensitive to 3-day sum, indicating that the bare peat surface dries fast and rainwater infiltrates quickly in the vegetated bog. VV and VH polarisation behaved similarly, VH being just ~ 10 times weaker.

In all the viewing geometries more precipitation corresponded to stronger backscatter. The response to 1-day precipitation sum in the peat production blocks is quantified and shown over the growing period in Fig. 15. Days have been aggre-

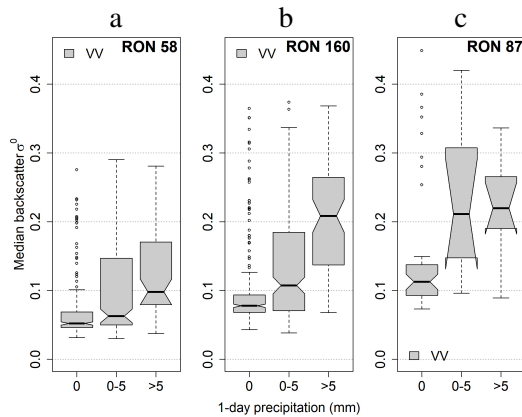


Figure 15: VV σ^0 median in the peat production blocks during the growing period by relative orbit number (RON): 58 (a), 160 (b), 87 (c). 1-day precipitation sum has been grouped as no rain (0), up to 5 mm (0–5) and more than 5 mm (>5). The distinction between the rainfall groups are the most pronounced for RON 160 where the group differed significantly (p -value < 0.001). For RON 87, only "0" and "0–5" differed (p -value < 0.05). Source: **Publication III** Figure 11.

gated into groups according to the amount of rain (0 mm, 0–5 mm and >5 mm). The groups differ significantly (p -value < 0.001) in RONs 160 and 58. In RON 87, only the 0 mm and 0–5 mm groups differ (p -value < 0.05) and the difference between the 0 mm and >5 mm groups is approaching statistical significance (p -value 0.075 and 0.05 in VV and VH, respectively). Given the incidence angle dependency polygons were not directly comparable and quantitative analysis was complicated. σ^0 of similar targets in near and far range is different; analogically, the same target reflects the signal differently when sensed from different orbital geometries.

3.3. Assessment of bog breathing with InSAR phase

Interferometric SAR has become a trusted monitoring tool of Earth's surface movements (Biggs & Wright 2020). InSAR has been shown promising also for measuring long and short term peatland surface deformations, though the studies have mostly not been validated with the ground truth data (Cigna & Sowter 2017; Alshammari et al. 2018). This dissertation demonstrates based on the in situ validation data how InSAR reflects seasonal bog surface oscillations known as bog breathing. Bog breathing follows the peatland water table dynamics and is thus an indicator of the peat water content and the health of the bog.

3.3.1. Method based on single master DInSAR phase

Relatively high InSAR coherence over half a year period (**Publication I**; also shown in subsection 3.1.1) allowed us to apply conventional DInSAR technique

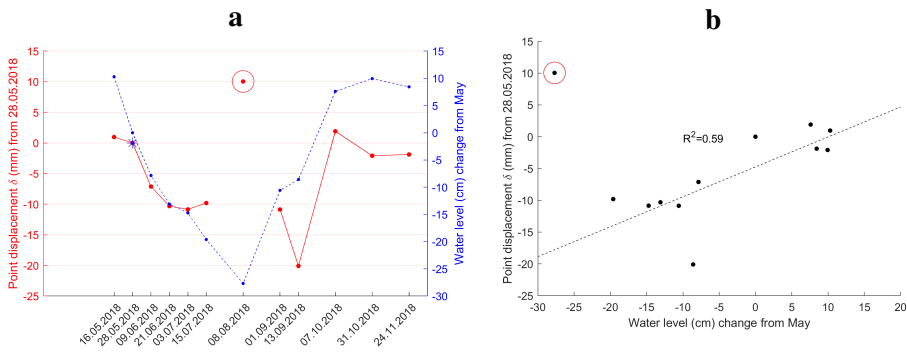


Figure 16: The mean radar line of sight (LOS) displacement δ of an arbitrary virtual point from the central part of Kanamatsi bog from an arbitrary virtual transect compared to the mean water table (WT) change in the sampling wells during the growing period (16 May–24 Nov 2018), presented as a time series (a) and a scatter plot (b). δ (mm) is from a single master on 28 May 2018 and WT change (cm) is given relative to the date of the InSAR master image. The image pair 28 May–8 August is an outlier (denoted with a red circle around the point) due to decorrelation. δ is indicated with a red solid line and the WT with a blue dotted line, a point with spikes marks the master image (a). The linear regression (the outlier not included) is given between δ and WT (b). Source: **Publication I** Figure 10.

(Bamler & Hartl 1998; Hu et al. 2014) in the open bog. Single master long temporal baseline interferograms were calculated in **Publication I**. After applying phase rotation we obtained continuous line of sight (LOS) displacement maps that did not need phase unwrapping in the open bog (the interferograms are presented in **Publication I** Figure 8). Decorrelation affected the areas near bog pools and bog margins where tree growth is supported due to drainage effects.

The radar LOS displacement time series were studied at an arbitrary virtual point in the central part of Kanamatsi bog on the arbitrary virtual transect through comparison with the mean WT change in the sampling wells (Fig. 16). The LOS displacements of the phase center agreed in general with the WT dynamics showing subsidence in the dry summer and uplift in the autumn. The recorded LOS deformation range was up to 3 cm relative to the tie-point. The relationship was described by the linear regression model with $R^2 = 0.59$ after omitting the image of 28 May–8 August as an outlier due to decorrelation. The result is only indicative as it is dependent on the choice of a tie-point, transect placement and the location of the control point.

3.3.2. Method based on DS InSAR phase time series

DS InSAR time-series technique was employed in **Publication V**. Hummocks and ridges are the stable-most micro site elements in the bog, whereas the surface fluctuates at much larger amplitudes at hollows and lawns. Nevertheless, the DS time series that measures the surface displacements with respect to one common

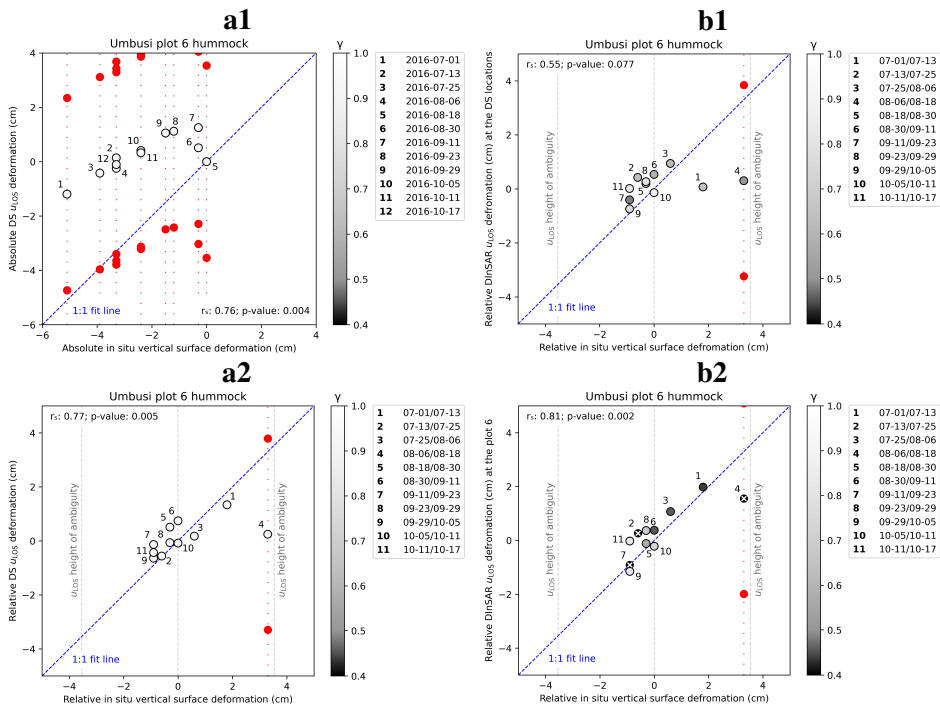


Figure 17: Correlation (r_s) between the in situ surface deformation at the Umbusi plot 6 hummock and the InSAR line of sight deformation projected to vertical dimension (u_{LOS}) in the growing period 2016. Given are: DS time series indicated here as Absolute DS as the time series is referenced to one common master (18 Aug 2016, the SAR acquisition date corresponding to the maximum levelling height, defining the zero level) (a1), deformations corresponding to short temporal baselines extracted from the DS time series indicated here as Relative DS (a2), median short temporal baseline (indicated as Relative) DInSAR deformations at the DS locations (b1) and median short temporal baseline (indicated as Relative) DInSAR deformations at the plot 6 (b2). The DS time series were calculated as the median of the DS points in the vicinity of the plot 6; the median long term average InSAR coherence (γ) is shown (a1, a2). Black points with a white cross (\times) denote γ below the reliability threshold of >0.4 (b1, b2). Red points represent u_{LOS} values if an ambiguous phase is added or subtracted. Notice that the axes of subfigure a1, though shifted, have the same 10 cm extent as the other plots. Source: **Publication V** Figure 2.

master acquisition underestimated the bog surface at the hummock nanotope. In the figure Fig. 17a1 the median InSAR line of sight (LOS) displacements projected to vertical dimension (u_{LOS}) of the DS points located near the Umbusi plot 6 are displayed. The underestimates were often in the magnitude of the u_{LOS} height of ambiguity. It means the presence of unwrapping errors. Despite the underestimation, the DS results followed the trend in the ground levelling data (correlation $r_s = 0.76$, p -value 0.004).

When the temporal baselines were reduced as recommended in Alshammari et al. (2018) to the minimum (12 or 6 days in our case) via converting the DS values

that are referenced to a single master date to short temporal baseline deformations between two consecutive acquisitions, ambiguity resolution was mostly no longer needed as demonstrated in Fig. 17a2. The correlation between the relative in situ surface changes at the plot 6 hummock and the median u_{LOS} DS deformations converted to short temporal baselines was 0.77 (p -value 0.005). The conventional DInSAR technique yielded similar results. Correlating the levelling data with the median DInSAR deformations at the centers of DS point locations (a DS point is averaged over many image pixels) gave $r_s = 0.55$ (p -value 0.077) (Fig. 17b1) and correlating with the DInSAR deformations at the plot 6 gave $r_s = 0.81$ (p -value 0.002) (Fig. 17b2). The DS time series converted to short temporal baselines and DInSAR surface height changes in Umbusi bog are shown in Fig. 18a. The stable reference points used in InSAR processing were located ~ 4 km from the plot 6, meaning reduced capability to compensate for atmospheric effects. Difficulty of finding stable areas on the organic soil is common in mires while the mineral ground and especially bigger buildings are located relatively far away.

3.3.3. Method based on short temporal baseline DInSAR phase

In **Publication IV** conventional DInSAR technique (Bamler & Hartl 1998; Hu et al. 2014) exploiting the shortest available temporal baselines was used. Meaningful deformation results were obtained only if the tie-point was chosen in a built area but not on the causeways. All the tie-points stayed less than 1 km from the levelling points. In Laukasoo bog the reference (a building) was not connected to the levelling plots by a transect and was located at a longer distance than in Umbusi bog (sheds). The plot 2 was decorrelated due to advanced tree growth in both bogs. The plot 4 was affected by the tree growth and experienced relatively large surface fluctuations – larger than at the natural hummock plots (the plots 6). At the plot 4 the correlation (r_s) between the DInSAR u_{LOS} displacements and the levelling data was 0.53 (p -value 0.061) in Umbusi and 0.48 (p -value 0.133) in Laukasoo. The plot 6 hollow had the largest deformation range (Fig. 19) but correlated better with the DInSAR results than the plot 4. At the plots 6 hollow $r_s = 0.85$ (p -value < 0.001) in Umbusi and $r_s = 0.51$ (p -value 0.074) in Laukasoo bog. The plot 6 hummock had the smallest dynamic range and the strongest correlation, $r_s = 0.93$ (p -value < 0.001) in Umbusi and $r_s = 0.82$ (p -value 0.002) in Laukasoo.

The DInSAR and the levelling data agreed the best in the autumn at the 6-day temporal baselines, in contrast to 12 days in the summer. The shorter the temporal baselines, the smaller the deformation amplitudes that needs capturing. In regard to the 6-day baseline, also coherence was the highest in the autumn. At the plot 6 the levelling data were from a hollow and a hummock nanotope 2 meters apart. The DInSAR image pixel containing the signal from both of the micro relief elements correlated better to the dynamics of the hummock (Fig. 18 b, c).

The DInSAR often recorded a false deformation over the peat production fields in the summer (the selected interferograms and deformation profiles are displayed in **Publication IV** and in Tampuu et al. 2021). Production fields in fact are characterised by compacted peat (Pouliot et al. 2011), effective drainage and thus

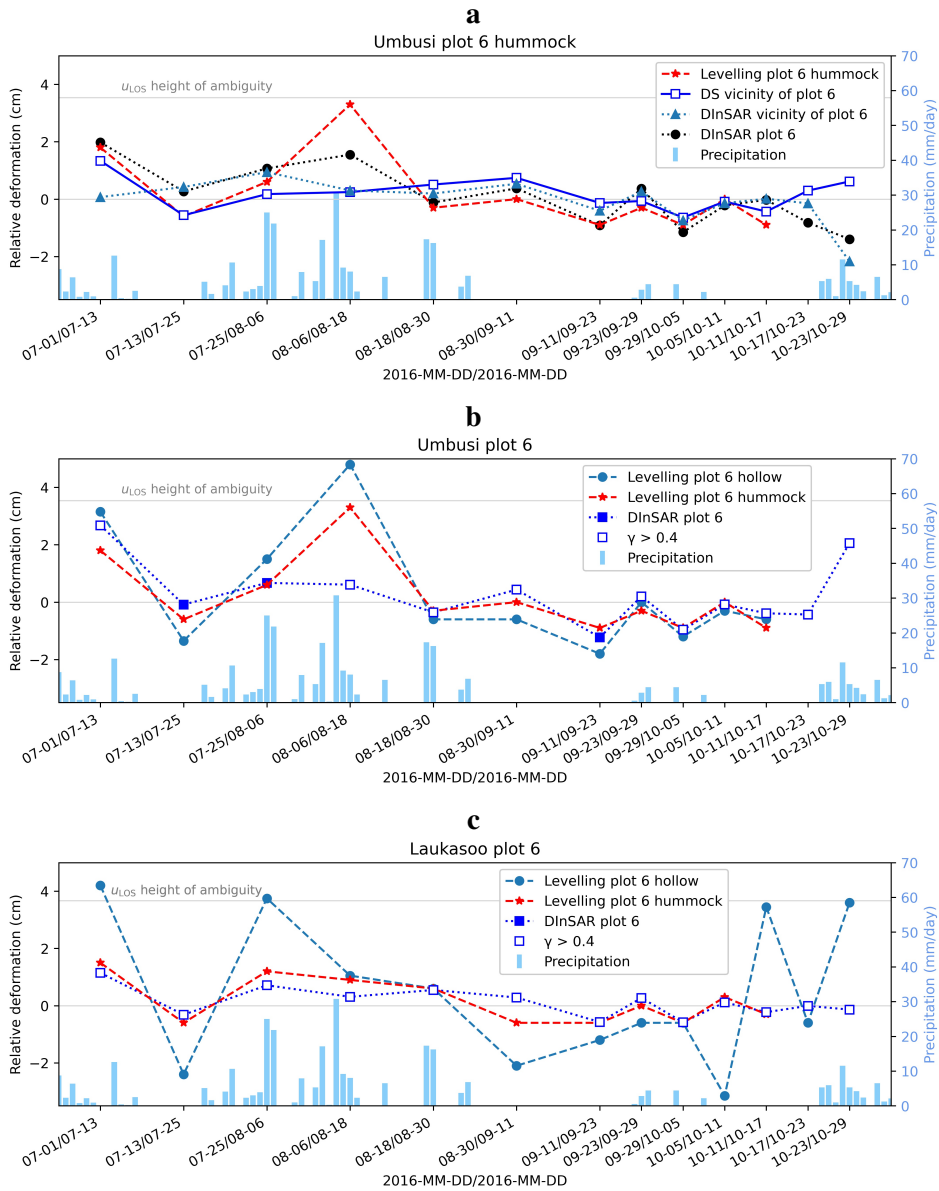


Figure 18: The DS time series converted to short temporal baselines and short temporal baseline DInSAR line of sight deformations projected to vertical direction (u_{LOS}) compared to the relative in situ vertical surface deformations between consecutive SAR acquisition dates at the plots 6 in Umbusi bog (a, b) and Laukasoo bog (c) in the growing period of 2016. The daily precipitation sum corresponds to the second date in the image pair. Coherence threshold $\gamma > 0.4$ indicates reliability of the phase estimate (b, c). Source: adopted from **Publication V** Figure 1; **Publication IV** Figures 7b, 8b.

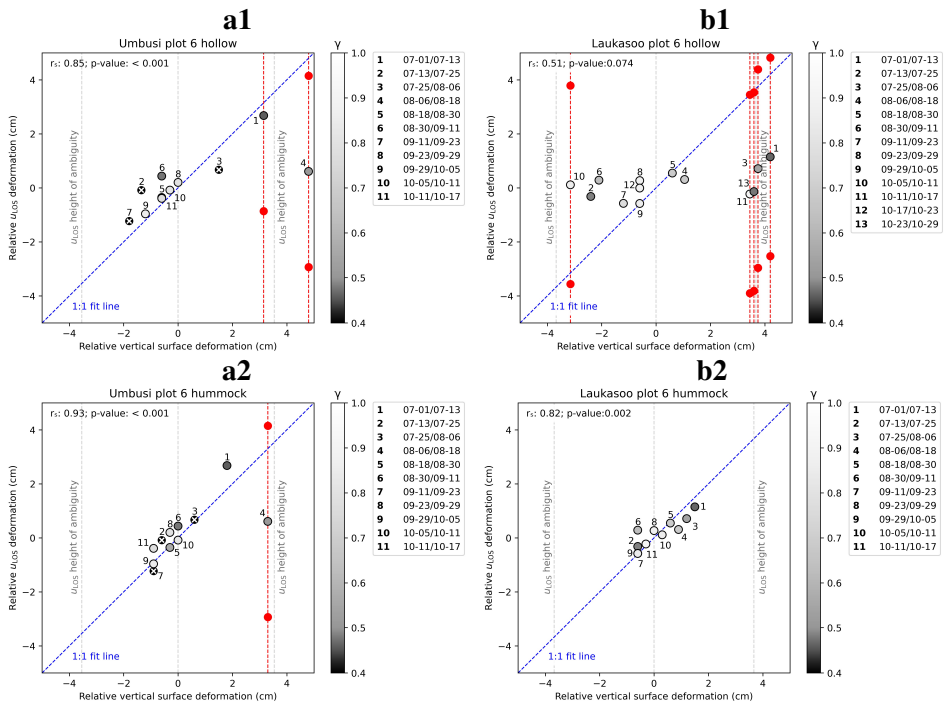


Figure 19: Correlation (r_s) between the relative in situ surface change and the DInSAR line of sight deformation projected to vertical dimension (u_{LOS}) in Umbusi bog (a) and Laukasoo bog (b) in the growing period 2016. Red points represent u_{LOS} values if an ambiguous phase is added or subtracted. Black points with a white cross (×) denote data of DInSAR coherence (γ) below the reliability threshold of >0.4 . Source: **Publication IV** Figures 9 a2, a3, b2, b3.

relative stability. That spurious deformation was also present in the interferograms of good coherence. However, it did not occur in autumn images. In Umbusi bog the transect 1 was referenced to the sheds with median coherence >0.9 and the peat production field retained coherence over most of the study period while displaying often higher coherence than the open bog. Therefore, we do not believe the phenomenon to be due to phase noise.

3.4. Temporal dynamics and magnitude of bog breathing

The phenomenon of bog breathing is well documented, however it has not been exhaustively studied and understood. The lack of understanding of its pace and magnitude has obscured the evaluation whether (e.g. when and where) C-band radar is capable to accurately record short and long term peatland surface changes.

The pace and magnitude of bog breathing from two bogs in Estonia was studied in situ in **Publication IV**. Generalised over all the study plots in the growing period of 2016 (15 April–31 October), the intraseasonal range of deformations

Table 4: The range of the surface oscillation at the study plots in Umbusi bog and Laukasoo bog in the growing period of 2016 (15 Apr–31 Oct). The range of surface deformation and the median distance from the highest surface level of the nanotope during the period are shown. Based on: **Publication IV** Table 1.

Plot	Nanotope	Drainage effect	Range (cm)	Median (cm)
Umbusi plot 2	Haplotelmic	Severe	9.5	−5.4
Laukasoo plot 2	Haplotelmic	Severe	8.0	−3.9
Umbusi plot 4	Lawn	Significant	10.8	−5.7
Laukasoo plot 4	Hollow	Significant	11.6	−3.3
Umbusi plot 6	Hollow	Minor/Intact	12.6	−5.7
Laukasoo plot 6	Hollow	Minor/Intact	14.7	−4.3
Umbusi plot 6	Hummock	Minor/Intact	7.5	−3.3
Laukasoo plot 6	Hummock	Minor/Intact	6.9	−2.2

stayed between 6.9–14.7 cm (Table 4). The hummocks in the natural part of the bog were the most stable nanotopes at the plots studied. The surface of hollows and lawns was much more dynamic both at the plots 6 and the plots 4, whereas the dynamic range was smaller at drainage affected (i.e. disturbed) nanotopes (the plots 4). The hollow and hummock in nearly natural conditions (the plots 6) fluctuated at different magnitudes during most of the summer but harmonised in the autumn. The surface of the severely drainage affected area (the plots 2) do not have microforms per se as acrotelm-catotelm system has degraded to haplotelmic structure. The nanotopes at the plots 2 fluctuated the least temporally and in magnitude.

Even of greater importance than the intra- and interseasonal dynamic range of the deformations, in the context of InSAR, are the magnitude and the pace of relative changes. In a 6-day time period (equal to the revisit cycle of Sentinel-1) the bog surface changed time to time more than the Sentinel-1 LOS height of ambiguity ~ 2.77 cm (Table 5). That happened at all the study plots but the hummock nanotopes of the plots 6 which are in natural or close to natural condition. The highest occurrence of such large surface deformations was recorded at the Laukasoo plot 4 (happened 58 times) which is a significantly drainage affected hollow nanotope. Even in just a 1-day period we recorded several occasions of deformations larger than the S1 height of ambiguity, mainly at the Laukasoo plot 4 (28 occasions). 4 occasions were recorded at the intact hollow at the Laukasoo plot 6. There were 7 occasions at the haplotelmic nanotope in the severely drainage affected zone at the plots 2.

Table 5: The relative (in a 6-day and a 1-day period) bog surface deformations that exceeded the line of sight (LOS) height of ambiguity ~ 2.77 cm of Sentinel-1 in Umbusi bog and in Laukasoo bog in 2016 (28 Apr–7 Oct). The count (N) of such occasions is given. Subsidence (–) and uplift (+) are distinguished. Presented is the median bog surface changed with the range in parenthesis. Source: **Publication IV** Table 2.

		6-day period				
	Plot	N	N–	Subsidence (cm)	N+	Uplift (cm)
Umbusi	Plot 2	7	1	3.0	6	3.3 (3.0...5.0)
	Plot 4	4			4	3.3 (3.0...3.6)
	Plot 6 hollow	7			7	3.5 (3.0...4.1)
	Plot 6 hummock	0				
Laukasoo	Plot 2	10	2	3.7, 3.9	8	3.2 (3.1...4.7)
	Plot 4	58	30	4.7 (3.0...8.6)	28	4.3 (3.0...8.4)
	Plot 6 hollow	19	1	3.2	18	3.6 (3.0...5.9)
	Plot 6 hummock	0				
		1-day period				
	Plot	N	N–	Subsidence (cm)	N+	Uplift (cm)
Umbusi	Plot 2	1	1	2.9		
	Plot 4	0				
	Plot 6 hollow	0				
	Plot 6 hummock	0				
Laukasoo	Plot 2	6	3	4.1 (3.0...4.8)	3	4.3 (2.9...5.1)
	Plot 4	28	13	5.0 (3.2...7.8)	15	4.1 (3.0...6.6)
	Plot 6 hollow	4	1	3.0	3	3.2 (3.0...3.5)
	Plot 6 hummock	0				

4. DISCUSSION

SAR is a promising remote sensing method for peatlands. However, its accuracy and limits have not yet been adequately determined. Partly it is explained by the lack of in situ validation data. In this dissertation SAR results such as backscatter, InSAR coherence and InSAR phase are discussed in the light of the ground truth data, consisting most importantly of peatland water table measurements, surface levelling data and the records of the peat production cycle.

4.1. Changes in peatland water table reflected in InSAR coherence

During the dry periods single master long temporal baseline interferometric coherence was responsive to water table as shown in **Publications I** and **II**. The image pairs where the second image (slave image) was from wet weather conditions when the pores in the upper peat layer are filled with water yielded higher coherence magnitudes than image pairs with the slave image from dry conditions. The recovery of coherence of long temporal baseline (up to 6 months in our case) in natural vegetated landscapes such as we showed for the growing period of 2018 (a drought event in Europe) has not been according to the best of my knowledge known previously. The vegetation cover in bogs has been believed to cause irreversible decorrelation over time (Zhou 2013; Mohammadimanesh et al. 2018a). Flooding status of vegetation has been known to alter the coherence magnitude (Tsyganskaya et al. 2018; Amani et al. 2021; Mohammadimanesh et al. 2018a) and snow cover to cause sudden decorrelation (Brisco et al. 2017; Mohammadimanesh et al. 2018a). Similarly to our results recovery of coherence and the correlated temporal behaviour of moisture and coherence have been shown in bare agricultural fields at airborne L-band (De Zan et al. 2014; Zwieback et al. 2015b) and in the hyperarid desert with little to no vegetation at Sentinel-1A C-band (Scott et al. 2017). Nevertheless, in 2019 that was a normal climatological year with the autumn rainier than average the relationship between WT and coherence was present only in summer. In 2017 that was a wet year coherence was not responsive to the WT.

In **Publication III** we compared the magnitudes of short temporal baseline coherence from three distinct peatland land cover classes of the open bog: 1) large areas characterised by heterogeneity in vegetation and micro relief, 2) small uniform areas extracted based on homogeneity from bigger intact open bog areas, 3) small open bog patches adjacent to the peat production area. While the first two classes behaved similarly and maintained high coherence, the third class tended to decorrelate and was unsuitable as reference area for peat harvesting (consequently, this class was excluded from further analysis). The decorrelation seen in the third class was probably connected to the larger ground WT fluctuations caused by the effects of drainage, in concordance with **Publications I** and **II** where WT affected the long term coherence.

To put the results into context one has to comprehend how precipitation, peatland WT and moisture content of the upper peat layer in the bog are related and how these relationships control the bog surface oscillations (bog breathing). Dry peat moss and dry peat are hydrophobic (Howie & Hebda 2018). Rainwater moistens the growing peat moss only to some extent and evaporates or drains through the peat pores in the upper peat layer without being fixed there and the surface fluctuations therefore rely exclusively on the uniform expansion or shrinkage of the lower lying peat layers. The bog surface moisture remains related to the WT through capillary rise (Lindholm & Markkula 1984; Brandyk et al. 1986; Strack & Price 2009). That dynamics was seen in 2018 and in the summer 2019. Also, when the peat is fully saturated, i.e. when pores are entirely filled with water up to the peatland surface, the excess rainwater simply drains away as the surface flow and all the surface oscillations are solely caused by relatively uniform changes in the WT. Consequently, the magnitudes of relative surface change at the hollow and at the hummock micro sites are the most uniform when the peat is either very dry or fully water saturated. Such harmonisation of the oscillation magnitudes at hollows and hummocks coinciding with peat water saturation characterised the Umbusi plot 6 in the autumn 2016.

In contrast what we saw in the summer 2016, the year 2017 and the autumn 2019 was partially saturated wet peat. Wet peat and wet peat moss are hydrophilic (Holden et al. 2004). When continuous or frequent rain fills pores in peat and cells of peat moss with water, the water-filled pore space becomes a poor conductor of water. AS the infiltration to the deeper peat layers is hindered the water content in the peat moss and in the top-most peat layer increases up to $\sim 90\%$ (Kellner & Lundin 2001; Beamish 2013) independently of the WT. The surface humidity and surface oscillations become directly determined by the amount of precipitation and where the rainwater accumulates on the surface. The amplitudes of surface fluctuations are at the largest in such periods. That was seen in the summer 2016 which was rainier than average. Also, the accumulation of rainwater in hollows causes relatively faster WT rise and higher WT levels there compared to neighbouring ridges and hummocks. Therefore, moisture conditions in the hollows changing from dry to humid and inundated must be the main driver of spatial coherence in the open bog.

InSAR coherence is not influenced solely by the soil moisture. Also the vegetation gives rise to temporal and volumetric decorrelation (Monti-Guarnieri et al. 2020) and ground changes affect the coherence making soil moisture estimation directly from coherence probably impossible (De Zan & Gomba 2018). Coherence magnitude is, however, known to be insensitive to surface displacements as locally spatially uniform height changes induce collectively coherent phase shifting in the surface scatterers (J.G. Liu & Mason 2009; Zwieback et al. 2017). That is crucial for measuring bog breathing with InSAR. Our single master long temporal baseline (up to 6 months) coherence results from open bogs suggest that coherence, nevertheless, could help to characterize seasonal hydrological conditions, distinguish ecotopes and derive information about the WT in dry summers or in the sites with intensive drainage induced high surface and subsurface flow. Long temporal

baseline coherence could also be used in distinguishing the open bog from the wooded bog. Short to medium baseline (days to weeks) coherence has previously been shown useful in wetland classification in northern latitudes (Amani et al. 2021; Mohammadimanesh et al. 2018a) and short temporal baseline coherence change detection has been suggested as aid to wetland monitoring (Brisco et al. 2017; Amani et al. 2021).

4.2. Changes in peat surface structure reflected in InSAR coherence

Over the peat production areas in **Publication III**, we found VV coherence to be more responsive than VH to surface altering works associated with peat extraction which caused decorrelation in both polarisations. It has long been known that cross-polarisation (e.g. VH) is sensitive to volume scattering, i.e. vegetation causes strong backscatter while bare surfaces have low backscatter. Co-polarisation (e.g. VV) is sensitive to surface scattering, being influenced by soil characteristics and soil moisture (Pampaloni et al. 1997; Millard 2016; Bousbih et al. 2017). Decorrelation in peat production areas has to be caused by a combination of the geometric change via physical dislocation of soil fragments of the uppermost layer and changing soil moisture in unknown proportions. These two factors are known from low-biomass areas like agricultural fields (Wegmüller & Werner 1997) and forest clear-cuts (Thiel et al. 2009). Milling, turning and harvesting not only change the peat surface physically but the lower lying peat which becomes exposed is also more humid than the topmost dried peat.

Using InSAR coherence makes possible to distinguish between actively used peat production blocks and the blocks where peat production has stopped for whatever reason. It is also possible to detect the blocks where the production has been carried out only on partial spatial extent. That could be of interest also in other domains wherever polygon-based change detection is used, for example the mowing detection in grasslands where partially mown parcels could cause errors (De Vroey et al. 2021). Furthermore, we demonstrated potential for monitoring peat extraction intensity – potentially beneficial both to the authorities and produces. A monitoring technique that allows distinguishing between active and abandoned peat production areas and discriminating between given areas according to the intensity of use would benefit climate mitigation by pushing for depletion of the production blocks already in use instead of opening new blocks.

Discrimination between the individual stages in the production cycle (milling, turning, harvesting) was not possible. It was not possible to distinguish individual production circles either because Sentinel-1 has a 6-day repeat visit but production cycles last 2–3 days (Sundh et al. 2000; Eesti Turbaliit 2022) and in good weather conditions follow one after another without a pause. However, it would not be possible to assess the volume of the extracted peat even if the areal extent and the count of the cycles were known. Harvesting depth of horticultural and energy peat is different and varies also depending on soil humidity.

The method we have proposed for monitoring peat production is transferable to other kinds of wide-area open-pit mining. For example, there could be a potential use of it in difficult to access oil sands in Canada. Short temporal baseline Sentinel-1 InSAR coherence change detection has been previously used to detect grassland mowing (Tamm et al. 2016; De Vroey et al. 2021; Lobert et al. 2021) and to monitor stages of crop growth and sowing and harvesting events (Pandit et al. 2022). The greatest challenge is seen in changing weather conditions (Askne et al. 1997; Askne et al. 2003), especially in rain (Santoro et al. 2002; Tamm et al. 2016). We have identified three methods how to isolate the decorrelation caused by rainfall via applying multiple orbital geometries, comparison with reference areas or inclusion of backscatter intensity (section 4.3).

4.3. Precipitation events reflected in InSAR coherence

Our results (**Publications I–III**) showed that only heavy rain could cause decorrelation in the open bog, the abandoned cutaway bog and in the peat production area while lighter rain were only of modest importance. The previous findings from forests (Santoro et al. 2002) and grasslands (Tamm et al. 2016) have attributed great importance to rainfall. Why we came to other results can be explained by the radically different nature of organic soils compared to mineral soils (described in section 4.1). Furthermore, the structure of peat whether in the natural bog, in the disturbed peatland or in the milled peat production fields is intrinsically different (Price et al. 2003). Natural peat is porous filled with large pores and with vertically oriented capillaries, remnant of dead plant residues, which enhance infiltration. Disturbed peat is characterised by compaction and reduced pore space which hinders infiltration (Price & Schlotzhauer 1999; Beheim 2006). A milled peat layer exposed on the surface of peat production field is composed of peat fragments whereas natural peat structure is destroyed. Small pores, hydrophobic peat fragments (i.e. when the peat becomes dry) and the sloped profile of the production field all support formation of surface runoff.

It seems that only heavy rain on one of the acquisition dates while the other date is dry can cause decorrelation similar to what surface altering works do. In the context of monitoring peat extraction, we have shown three ways in **Publication III** how to isolate the decorrelation caused by rainfall, which otherwise could induce a false positive. Namely: 1) the more orbital geometries are included, the lesser the risk for false positives, 2) comparison with undisturbed reference areas helps to reduce the risk, 3) including backscatter intensity can detect precipitation events. The rainfall caused decorrelation may, however, obscure preceding works if only one orbital geometry is relied upon.

4.4. Peatland surface motions reflected in InSAR phase time series relative to a common reference date

4.4.1. Surface motions in single master DInSAR phase

We believe that the temporal and spatial consistency in LOS displacement patterns of the InSAR phase over the entire season (with the decorrelated August excluded) and the concordance with the WT dynamics shown in **Publication I** indicates that what we observed was indeed the real bog surface displacement signal. It is natural to mire that the peatland surface elevation follows the WT fluctuations – a phenomenon known as bog breathing (Roulet 1991; Kellner & Halldin 2002; Dise 2009; Howie & Hebda 2018). However, direct dependency of DInSAR phase on changes in soil moisture (Barrett et al. 2013; Zwieback et al. 2015a), independent of any physical deformation (swelling or shrinkage of soil) (Nolan & Fatland 2003; De Zan et al. 2014; Zwieback et al. 2015b), has been shown in agricultural fields. The soil moisture effects have been observed to correspond to up 0.5π of the radar wavelength (i.e. more than 10% of the wavelength) and deserve to be considered in repeat-pass InSAR studies (Zwieback et al. 2015b; Zwieback et al. 2017). A decrease in soil moisture leads to shortening of the optical path travelled by the wave and therefore the backscattering surface has seemingly moved closer to the sensor (Rudant et al. 1997). Such a spurious drying-induced uplift has potential to mask the actual surface subsidence if the displacement is small (Zwieback et al. 2017). The problem is probably minor in mires where larger changes in peat moisture coincide with proportionally larger surface elevation changes (Fritz et al. 2008). Ways for removing moisture contribution from the displacement estimates have been discussed by others (Zwieback et al. 2017; De Zan & Gomba 2018)

The LOS displacement results in the range of up to 3 cm relative to the tie-point in **Publication I** seemed realistic though rather modest in the light of what is known of bog breathing in natural bogs from ground levelling measurements. Bog breathing accounts for 2.6–11 cm according to Fritz (2006). A mean multiyear average of 11.7 cm was reported by Howie and Hebda (2018). We measured 6.9–14.7 cm in **Publication IV**. It was not possible for us to use a tie-point on the mineral ground, which would have been needed to ensure zero displacement at the reference, because the bog margins are commonly wooded (the wooded bog or the forest). The tree cover causes decorrelation and the low coherence in the area is unsuitable for DInSAR. Neither could we have chosen a tie-point further away at any built area because that would have meant a decorrelated region between the tie-point and the area of interest that would have disrupted the continuous phase field. The disrupted phase field would have made it impossible to reconstruct the phase from the tie-point to the area of interest. Therefore, we had to pick a tie-point at the edge of the open bog to ensure the connection via the continuous phase field. That meant the tie-point was located on the natural bog peat which is not stable but simply relatively more stable than the area of interest on the thicker peat. The continuity of the field allowed reconstruction of the phase between the reference and the area of interest but an unknown extent of the bog breathing – equivalent

to the oscillation at the assumed stable tie-point – remained undetected. Another shortcoming of the current study, which is shared with majority of peatland InSAR studies, was the absence of ground levelling data for validation (Cigna & Sowter 2017; Alshammari et al. 2018).

4.4.2. Surface motions in DS InSAR phase time series

The InSAR result in **Publication V**, confirmed with in situ levelling data, showed that the DS time-series approach clearly underestimated the actual elevation changes due to propagation of phase unwrapping errors. We have recently reaffirmed that finding, originated from the ascending RON 160, in the comparison with the descending RON 80 which was also severely biased (Tampuu et al. 2022). Only recently have there been other studies also claiming that the Sentinel-1 C-band InSAR time-series approach is not reliable over peat. These works are Heuff and Hanssen (2020) (pastures on drained peat soils), Conroy et al. (2021) (different soil types) and Umarhadi et al. (2021a) (tropical peatlands). None of them had levelling data for comparison. Marshall et al. (2022) showed based on levelling measurements that S1 InSAR struggled to measure outside an inter-seasonal range of 1–2 cm since the underestimation in the blanket bog was evident. However, they attributed the large deformation magnitude foremost to the summer drought of 2018 (Schuldt et al. 2020) and assumed that exceeding the capacity of S1 to measure the motion is not supposed to occur in normal conditions (Marshall et al. 2022). Alshammari et al. (2018) demonstrated based on limited levelling data the underestimation in a afforested drainage affected peatland (former blanket bog) but remained positive about the potential of the C-band. The occurrence of unwrapping errors was also shown by Zhou (2013) and we warned about the risk for underestimation in **Publication I**.

4.5. Peatland surface motions reflected in InSAR phase changes between consecutive acquisitions

4.5.1. Surface motions in DS InSAR phase time series converted to changes between consecutive acquisitions

Based on our results from a natural ridge-hollow-hummock ecotope in Umbusi bog (**Publication V**) and the work by others (subsection 4.4.2) it has to be concluded that the time-series approaches are unreliable in measuring the magnitude of seasonal and short term vertical peatland surface changes. Nevertheless, ambiguity resolution was in most cases not needed when we converted the single master referenced DS time series into changes between consecutive acquisitions. It means we extracted from the time series the deformation estimates at baselines of 12 or 6 days and the agreement with the levelling data improved remarkably. That indicates the DS time series did contain accurate deformation magnitudes, though accessible only as elevation changes between consecutive acquisitions. Thus, our DS time series estimation failed foremost in referencing the interferograms to a

common date to obtain long temporal baseline deformation values (Pepe & Lanari 2006; Hu et al. 2014; Esch et al. 2019). However, the only extracted short temporal baseline DS image pair, namely 8–18 Aug, that needed unwrapping as indicated by the levelling at the hummock plot also failed. The results indicate C-band InSAR deformation estimates could potentially be reliable in peatlands and bog regions of less dynamic seasonal behavior, in concordance with Marshall et al. (2022).

4.5.2. Surface motions in short temporal baseline DInSAR phase

The aim in **Publication IV** was to tackle the problem of tie-point stability versus the continuity of the phase field (discussed in subsection 4.4.1) and to evaluate the reliability of conventional DInSAR (also as the base for any advanced InSAR technique) over peatland areas. In Umbusi bog and Laukasoo bog the natural open bog is bordered by peat production fields and the tie-points can be chosen at the stable edge of the fields. It means that all the area where we employed InSAR was open except a narrow stripe of sparsely wooded land cover in the vicinity of the main drainage ditch. Relatively good coherence what we often recorded over the peat production fields meant that peat harvesting occurred only seldom (based on the rationale in the section 4.2). Considering the hot and dry weather in 2018 (European drought event) it is reasonable to believe the annual harvest quota had already been reached by the second part of the summer.

Owing to the good coherence of the reference point and relatively good coherence of the peat production fields, we assume that the spurious deformation of the peat production area that we often recorded was not an artefact but had a physical cause. These deformations were often too large to be explained by mere changes in soil moisture. Soil moisture has been shown to account for up to $\sim 10\%$ of the wavelength (Zwieback et al. 2015b; Zwieback et al. 2017). Therefore, we would attribute these spurious deformations to the changing water level in the drainage ditches. The ditches separate peat production fields with a 20-meter interval, resulting in a mixed signal from fields and from ditches in every image pixel over a peat production block.

Our DInSAR results contain unwrapping errors though the elevation profiles along the transects did not display any phase shifts. Therefore, the question arises where the phase shifted so that the shift was not visible. It may be that the phase shift was lost at the vertical side of the main drainage ditch, many metres high. The seasonal surface oscillation in the range of 9.5 cm and large rapid surface changes, occasionally larger than the LOS height of ambiguity of Sentinel-1 in a single day, were present already at the plot 2 which is located mere 15 m from the drainage ditch. The maximum detectable deformation gradient of DInSAR is one fringe per pixel (Massonnet & Feigl 1998; Rosen et al. 2000) whereas coherence and the number of looks play also a role (Jiang et al. 2011). That means the image pixel of Sentinel-1 with spatial resolution of 22 m (Bourbigot et al. 2016) might be per se too large to capture the deformation gradient. Such scenarios can also apply to natural bogs as the raised bogs are domed above the surrounding landscape (Ingram 1982) and sometimes have a steep marginal slope (Couwenberg

& Joosten 2005). Behind the marginal slope, where peat is compacted and peat matrix has lost flexibility, a relatively narrow transitional zone occurs. That narrow zone possesses active acrotelm and is characterised by low peat bulk density and significant seasonal water table fluctuations that are expressed in vertical surface movements. The magnitude of the surface deformations can be many times the height of ambiguity of C-band. Also, the decorrelation caused by the denser tree cover near the ditch could have helped to mask the phase shift. In any case, a slope in the phase values near the location of the ditch was common for the DInSAR deformation profiles along the transects displayed in **Publication IV** and in Tampuu et al. (2021).

The SAR image pixel at the plot 6 contained signal from both the hollow and the hummock micro sites. As the DInSAR correlated better to the levelling measurements from the hummock plot, it could be that the signal in the pixel was dominated by the hummocks relative to hollows. Alternatively, the reason could simply be that the smaller amplitude of change at the hummock plot was intrinsically closer to what C-band DInSAR is capable of recording. DInSAR was not able to correctly solve deformations approaching the height of ambiguity neither at the hollow nor at the hummock nanotope. The share of hummocks and ridges versus hollows varies in different parts of a bog and between bogs (Couwenberg & Joosten 2005), affecting consequently the SAR pixels.

4.6. Problem of phase ambiguity in C-band InSAR

In **Publication IV** bog breathing was studied in Umbusi bog and Laukasoo bog in regard to the wavelength and the repeat cycle of the C-band Sentinel-1 mission. We recorded the range of the bog breathing in the growing period 2016 to be 6.9–14.7 cm at undisturbed and 8.0–11.6 at disturbed plots. That is considerably larger than what we measured with DInSAR 35 km away in climatically similar conditions in the Endla mire complex in **Publication I**. The interseasonal elevation changes are ought to be even larger than intraseasonal changes as the WT data from the bogs in the Endla mire complex let us presume (subsection 3.1.1). The results from Umbusi and Laukasoo bogs align with what was previously known of the phenomenon of bog breathing. In the literature review by Fritz (2006) surface oscillations of 2.6–11 cm were reported from 11 study plots (9 studies) in natural bogs and 0.7–13 cm from 14 plots (12 studies) in disturbed peatlands. Howie and Hebda (2018) recorded a multiyear average surface oscillation of 11.7 cm at natural raised bog plots and 9.1 cm at disturbed plots. Glaser et al. (2004) observed many occasions of deformations exceeding 10 cm or even 20 cm within 4 hours at a raised bog plot. Notwithstanding these large deformation values the InSAR studies from northern peatlands have often shared the underlying belief that peatland surface oscillations stay in the range comfortable for C-band being often only a few millimeters (e.g. Zhou et al. 2010, Marshall et al. 2022). Characteristic to the studies has also been the absence of ground truth data for validation (Cigna & Sowter 2017; Alshammari et al. 2018).

Table 6: Literature review of InSAR surface deformation studies in northern bogs. The range of recorded InSAR displacements along the radar line-of-sight (LOS) direction (assessed from the InSAR time series if presented) and the status of ground levelling data for validation are displayed. The last column (Remark) shows whether the authors have recorded problems or expressed concern over the reliability of the results regarding unwrapping (UW) or the ambiguity problem. The following bog types are differentiated: raised bog (R), blanket bog (B), fen (F), any peatland (P) and degraded (afforested drainage affected) blanket bog (DB).

Publication	Mission	Method	Study period	Bog type	Range (cm)	Ground truth	Remark
1. Zhou et al. 2010	Envisat	StaMPS	2003–2006	R	2.2	–	Disagreement between orbits
2. Zhou 2013 ^{Phd}	Envisat ALOS	SBAS	2002–2007	B	1.0	–	UW error
			2006–2010	B	1.5	–	
3. Cigna et al. 2014	ERS-1/2	ISBAS	1993–2000	B,F	–	–	
4. Cigna and Sowter 2017	ERS-1/2	ISBAS	1992–2000	P	–	–	
				B	5.5	–	
5. Alshammari et al. 2018	ERS-1/2 Sentinel-1	ISBAS	1992–2000 2015–2016	DB	–	+	Underestimation
				DB	–	(+)	Underestimation
6. Fiaschi et al. 2019	Sentinel-1	PS-InSAR	2015–2018	R	2.0	–	
				B	5.5	–	
7. Alshammari et al. 2020	Sentinel-1	ISBAS	2015–2016	B	1.7	–	
8. Bradley et al. 2022	Sentinel-1	APSYS	2015–2019	B	1.2	–	
9. Marshall et al. 2022	Sentinel-1	APSYS	2017–2019	B	2.5	+	Underestimation
10. Tampuu et al. 2020 ^I	Sentinel-1	DInSAR	2018	R	2.0*	–	Raising concern
11. Tampuu et al. 2021	Sentinel-1	DInSAR	2016	R	2.3	+	Underestimation
12. Tampuu et al. 202Xb ^{IV} _{<i>u</i>_{LOS}}	Sentinel-1	DInSAR	2016	R	3.1	+	Underestimation
13. Tampuu et al. 202Xa ^V _{<i>u</i>_{LOS}}	Sentinel-1	DS (EMI)	2016	R	1.7	+	Underestimation
		DInSAR	2016	R	2.4	+	Underestimation

I, IV, V Denoted are Publication I, Publication IV and Publication V included in this dissertation
{*u*{LOS}} *u*_{LOS} results (radar line of sight (LOS) projected to vertical direction) have been converted back to LOS for comparability

* An outlier excluded (3.0 cm with the outlier included)

^{Phd} PhD dissertation

(+) Limited levelling data

There have been all together 13 InSAR deformation phase studies conducted in permafrost-free northern bogs to my best knowledge (Table 6). Permafrost peatlands are intrinsically different from bogs (Moore 2002; Tarnocai & Stolbovoy 2006) and therefore are out of the scope of this dissertation. Only one of the studies has employed L-Band (satellite ALOS), the rest have relied on the C-band radar missions. All of the studies except ours where we used conventional DInSAR have employed the time-series approaches. One study relied on persistent scatterers (PS) and employed the Stanford Method for Persistent Scatterers (StaMPS) (Hooper et al. 2004; Hooper et al. 2007). The rest relied on distributed scatterers (DS) using Small Baseline Subset (SBAS) (Berardino et al. 2002) or Advanced Pixel System Intermittent Small Baseline Subset (APSYS) technique formerly known as Intermittent Small Baseline Subset (ISBAS) (Sowter et al. 2013). In one of our studies a hybrid PS/DS algorithm with DS phases being estimated with the EMI algorithm (Ansari et al. 2018) was used which is a DS approach distinct from approaches building on the SBAS technique. All the studies have recorded modest deformation ranges. Only few have raised concern or recorded a problem. All the research backed by the ground truth, however, have confirmed underestimation.

Absence of ground levelling measurements for validation of InSAR results is also common in the permafrost region (Iwahana et al. 2021) where a similar question of reliability arises. For example, the foundations laying C-band InSAR study by L. Liu et al. (2010) measured displacements of 1–4 cm in tundra at the Arctic coast during the thawing season but Iwahana et al. (2021) recorded in situ 5.8–14.3 cm in the Arctic inland, both on the North Slope, Alaska. The climatic conditions of the two regions are, however, distinctively different (L. Liu et al. 2010). In permafrost peatlands in northern Sweden, De la Barreda-Bautista et al. (2022) measured the maximum subsidence of 25 cm by the multispectral and true colour RGB derived Unmanned Aerial Vehicle (UAV) captured digital elevation models (DEMs) while InSAR detected the maximum of 1.5 cm.

Based on our findings the optimism towards the ability of C-band to obtain accurate deformation magnitudes over peatlands can be retained to at least some extent because there are ecotopes where the change in 6 days (Sentinel-1 revisit cycle) is in a range suitable for the C-band. Thus, in those less dynamic sites both the DS time-series and the 6-day baseline DInSAR indeed often contained accurate information about the deformation magnitude, though accessible only through the shortest temporal baselines. Marshall et al. (2022) also showed that dependant on the time period and the type of peatland or an area in the peatland chosen, the deformation range can stay in the unambiguous range. Though, without the detailed ancillary information it is difficult to decide where the InSAR estimates are reliable. For example we did not expect to see such large in situ deformations in the severely drainage affected zone with compacted peat close to the ditch. We would have not been surprised to see signs of irreversible compaction instead (Price & Schlotzhauer 1999; Holden et al. 2004). The capacity of peat to swell and shrink is reduced when the peat is degraded and loses elasticity (Howie & Hebda 2018).

Even if the estimates of magnitudes of peatland surface deformations in C-band are inaccurate, other characteristics of the deformation signal (e.g. direction of motion, timing of seasonal peaks and droughts and their relative amplitudes in comparison to other ecotopes) have been found to be still meaningful and thus helpful in characterising ecological conditions (Alshammari et al. 2020; Bradley et al. 2022; Marshall et al. 2022). Also, methods to cope with unwrapping errors have been proposed (Zhou 2013; Esch et al. 2019; Yunjun et al. 2019). These benefit from the phase closure method exploiting triplets of interferograms. In time domain, unwrapping errors break the consistency of triplets of interferometric phases (Biggs et al. 2007).

A promising solution to the ambiguity problem could be longer wavelength L-band (24 cm) sensors as suggested by Zhou et al. (2010), Zhou (2013) and Marshall et al. (2022). The future L-band missions will allow increased penetration through the forest cover (Wei & Sandwell 2010; Mohammadimanesh et al. 2018a; Umarhadi et al. 2021b) at bog margins and fitting relative surface changes in one phase cycle (Hoyt et al. 2020; Marshall et al. 2022). The planned launch date of the NASA-ISRO SAR (NISAR) Mission, a joint project between the United States and India, is in 2023 (NASA JPL 2022) and the estimated launch date of Radar Observing System for Europe at L-band (ROSE-L) in 2028 (Davidson & Furnell 2021).

5. CONCLUSIONS

This dissertation demonstrated how Sentinel-1 C-band InSAR phase measurements and coherence, considering the intrinsic limitations posed by the wavelength and the revisit cycle of the sensor, could improve understanding of bog surface dynamics and monitoring of peat extraction. Based on the results it can be concluded:

(1) The long term InSAR coherence could be used as aid to understanding of hydrologic conditions in the raised bog but it is not suitable for direct surface moisture retrieval (**Publications I and II**).

During dry periods long temporal baseline InSAR coherence (γ) is responsive to water table (WT) change in the open bog. The second degree polynomial regression model described the relationship in the drought year of 2018 with RMSE 0.047 (calculated for the dimensionless γ ; p -value < 0.001). In wet conditions the relationship does not exist. Estimation of soil moisture directly from γ is not achievable due to other contributors to the coherence. Nevertheless, coherence could help to derive information about the WT conditions and dynamics in dry summers or in disturbed sites. Long temporal baseline γ could be used in discrimination of the open bog from the wooded bog and bog pools (p -value < 0.05). The retention of coherence over a baseline of up to 6 months is intrinsic to only some ecotopes in the open. The pixels of higher (≥ 0.5) and lower (≥ 0.2) mean coherence, corresponding respectively to the upper and lower 10th percentile of the open bog pixels, were concentrated to different parts of the bog. That suggests usefulness of γ in distinguishing between ecotopes and characterization of seasonal hydrological conditions.

(2) The short term InSAR coherence can be used to monitor peat extraction considering intrinsic limitation of the 6-day repeat cycle. Coherence response is quantifiable and can be used in differentiation between active and abandoned peat production blocks, discrimination of partially harvested blocks and potentially in monitoring of peat extraction intensity (**Publication III**).

Short temporal baseline (6-day) coherence can detect surface altering works in peat production sites, making it possible to distinguish between actively used peat production blocks and the blocks fallen out of use (p -value < 0.001). The VV polarisation channel median γ was 0.19 in the production blocks during the production season while being 0.60 in the open bog and 0.58 in the abandoned cutaway bog (the last two used as a proxy for undisturbed peat production blocks). In VH polarisation γ was 0.17, 0.38 and 0.39, respectively. However, distinguishing the stages of the peat production cycle (milling, turning, harvesting) or discrimination between individual circles is not possible. The demonstration of how to identify the blocks where peat production has been carried out only on a partial spatial extent was provided using γ median and standard deviation. The demonstration of the potential for monitoring peat extraction intensity using γ dispersion was provided. A monitoring technique allowing distinguishing between active and abandoned peat production areas and discrimination between sites according to the intensity

of use would promote efficient resource use and benefit climate mitigation. The method proposed is transferable to other kinds of wide-area open-pit mining such as oil sands. The coherence in the peatland (open bog, abandoned cutaway bog and peat production area), differently from other land cover types, is little affected by rain. Only heavy rain on one of the acquisition dates while the other date is dry can cause decorrelation (**Publications I–III**). In the context of monitoring of peat extraction, the ways how to discriminate between the rainfall and the works caused decorrelation are: 1) inclusion of multiple orbital geometries, 2) comparison with undisturbed reference areas, 3) inclusion of backscatter intensity.

(3) The ambiguity problem makes C-band phase measurements in raised bogs unreliable. The C-band InSAR could be applicable in less dynamic bog areas if such areas were not that difficult to identify without place-specific in situ levelling measurements (**Publications I, IV and V**).

Long temporal baseline conventional Differential InSAR (DInSAR) and Distributed Scatterer (DS) InSAR time-series approach over the open bog displayed temporal and spatial consistency even though they underestimated the real surface changes. Despite a serious underestimation by the DS time series compared to the levelling data the correlation was high (r_s 0.76, p -value 0.004) because the deformation estimates between two consecutive acquisitions were mostly accurate (**Publication V**). That means the DS time series indeed contain the useful signal but surface changes in the magnitude close to the height of ambiguity of the sensor (~ 2.77 cm for Sentinel-1 (S1)) cause serious problems. Among all the InSAR approaches tested in this dissertation the 6-day temporal baseline (S1 revisit cycle) DInSAR was the most accurate method with r_s 0.93 (p -value < 0.001) between the ground levelling and the InSAR deformation at a natural hummock plot, while also underestimating near the height of ambiguity (**Publication IV**). Both approaches contained unwrapping errors that would have gone undetected if we had not had ground truth for validation (**Publication IV and V**). The literature analysis also shows the ground truth has always confirmed the underestimation or an unwrapping error by the C-band. InSAR phase measurements could be applicable to areas characterised by smaller and slower surface oscillations like in disturbed peatlands. However, we recorded the in situ surface changes larger than the height of ambiguity of S1 occurring during just 1-day periods at the severe drainage affected plots. The only nanotopes that constantly exhibited surface changes in any 6-day period smaller than the height of ambiguity were the hummocks in the natural bog. Using the C-band InSAR needs thus the prior assumption that the range of deformations lies in the detectable range. Without ground truth data it is extremely difficult to assess whether or not the assumption is justified.

The results of this dissertation provide new findings regarding implementation of C-band InSAR in monitoring of natural bogs and peat production with InSAR coherence. Measuring bog breathing directly with InSAR phase could be a promising opportunity but the ambiguity problem makes C-band InSAR unreliable. Probably, a solution could be the planned longer wavelength L-band missions.

REFERENCES

- Alshammari, L., Boyd, D.S., Sowter, A., Marshall, C., Andersen, R., Gilbert, P., ... Large, D.J. (2020) Use of Surface Motion Characteristics Determined by InSAR to Assess Peatland Condition. *Journal of Geophysical Research: Biogeosciences*, 125(1), e2018JG004953.
- Alshammari, L., Large, D., Boyd, D., Sowter, A., Anderson, R., Andersen, R., Marsh, S. (2018) Long-Term Peatland Condition Assessment via Surface Motion Monitoring Using the ISBAS DInSAR Technique over the Flow Country, Scotland. *Remote Sensing*, 10(7), 1103.
- Amani, M., Poncos, V., Brisco, B., Foroughnia, F., DeLancey, E.R., Ranjbar, S. (2021) InSAR Coherence Analysis for Wetlands in Alberta, Canada Using Time-Series Sentinel-1 Data. *Remote Sensing*, 13(16), 3315.
- Ansari, H., De Zan, F., Bamler, R. (2018) Efficient Phase Estimation for Interferogram Stacks. *IEEE Transactions on Geoscience and Remote Sensing*, 56(7), 4109–4125.
- Askne, J.I.H., Dammert, P., Ulander, L., Smith, G. (1997) C-band repeat-pass interferometric SAR observations of the forest. *IEEE Transactions on Geoscience and Remote Sensing*, 35(1), 25–35.
- Askne, J.I.H., Santoro, M., Smith, G., Fransson, J. (2003) Multitemporal repeat-pass SAR interferometry of boreal forests. *IEEE Transactions on Geoscience and Remote Sensing*, 41(7), 1540–1550.
- Asmuß, T., Bechtold, M., Tiemeyer, B. (2019) On the Potential of Sentinel-1 for High Resolution Monitoring of Water Table Dynamics in Grasslands on Organic Soils. *Remote Sensing*, 11(14), 1659.
- Bamler, R., Hartl, P. (1998) Synthetic aperture radar interferometry. *Inverse Problems*, 14(4), R1–R54.
- Barrett, B., Whelan, P., Dwyer, E. (2013) Detecting changes in surface soil moisture content using differential SAR interferometry. *International Journal of Remote Sensing*, 34(20), 7091–7112.
- Bauer-Marschallinger, B., Cao, S., Navacchi, C., Freeman, V., Reuß, F., Geudtner, D., ... Wagner, W. (2021) The normalised Sentinel-1 Global Backscatter Model, mapping Earth's land surface with C-band microwaves. *Scientific Data*, 8(1), 277.
- Beamish, D. (2013) Gamma ray attenuation in the soils of Northern Ireland, with special reference to peat. *Journal of Environmental Radioactivity*, 115, 13–27.
- Bechtold, M., De Lannoy, G.J.M., Reichle, R.H., Roose, D., Balliston, N., Burdun, I., ... Zarov, E.A. (2020) Improved groundwater table and L-band brightness temperature estimates for Northern Hemisphere peatlands using new model physics and SMOS observations in a global data assimilation framework. *Remote Sensing of Environment*, 246, 111805.
- Bechtold, M., Schlaffer, S., Tiemeyer, B., De Lannoy, G. (2018) Inferring Water Table Depth Dynamics from ENVISAT-ASAR C-Band Backscatter over a Range of Peatlands from Deeply-Drained to Natural Conditions. *Remote Sensing*, 10(4), 536.
- Beheim, E. (2006) The Effect of Peat Land Drainage and Afforestation on Runoff Dynamics. In: Krecek, J., Haigh, M. (eds.), *Environmental Role of Wetlands in Headwaters*. Springer. Dordrecht, Netherlands. pp. 59–75.
- Bekaert, D.P.S., Walters, R.J., Wright, T.J., Hooper, A.J., Parker, D.J. (2015) Statistical comparison of InSAR tropospheric correction techniques. *Remote Sensing of Environment*, 170, 40–47.

- Benjamini, Y., Hochberg, Y. (1995) Controlling the False Discovery Rate: A Practical and Powerful Approach to Multiple Testing. *Journal of the Royal Statistical Society: Series B (Methodological)*, 57(1), 289–300.
- Berardino, P., Fornaro, G., Lanari, R., Sansosti, E. (2002) A new algorithm for surface deformation monitoring based on small baseline differential SAR interferograms. *IEEE Transactions on Geoscience and Remote Sensing*, 40(11), 2375–2383.
- Beyer, C., Höper, H. (2015) Greenhouse gas exchange of rewetted bog peat extraction sites and a *Sphagnum* cultivation site in northwest Germany. *Biogeosciences*, 12(7), 2101–2117.
- Biggs, J., Wright, T., Lu, Z., Parsons, B. (2007) Multi-interferogram method for measuring interseismic deformation: Denali Fault, Alaska. *Geophysical Journal International*, 170(3), 1165–1179.
- Biggs, J., Wright, T.J. (2020) How satellite InSAR has grown from opportunistic science to routine monitoring over the last decade. *Nature Communications*, 11(1), 3863.
- Bourbigot, M., Johnsen, H., Piantanida, R., Hajduch, G., Poullaou, J. (2016) Sentinel-1 Product Definition. Issue 2.7, S1-RS-MDA-52-7440. https://sentinel.esa.int/web/sentinel/user-guides/sentinel-1-sar/document-library/-/asset_publisher/1dO7RF5fJMbd/content/sentinel-1-product-definition. Accessed: 16.01.2022.
- Bourgeau-Chavez, L.L., Endres, S., Powell, R., Battaglia, M., Benscoter, B., Turetsky, M., ... Banda, E. (2017) Mapping boreal peatland ecosystem types from multitemporal radar and optical satellite imagery. *Canadian Journal of Forest Research*, 47(4), 545–559.
- Bourgeau-Chavez, L.L., Endres, S., Graham, J., Hribljan, J., Chimner, R., Lillieskov, E.A., Battaglia, M. (2018) Mapping Peatlands in Boreal and Tropical Ecoregions. In: Liang, S. (ed.), *Comprehensive Remote Sensing*. Vol. 6. Elsevier. Oxford, UK. 24–44.
- Bourgeau-Chavez, L.L., Leblon, B., Charbonneau, F., Buckley, J.R. (2013) Evaluation of polarimetric Radarsat-2 SAR data for development of soil moisture retrieval algorithms over a chronosequence of black spruce boreal forests. *Remote Sensing of Environment*, 132, 71–85.
- Bousbih, S., Zribi, M., Lili-Chabaane, Z., Baghdadi, N., El Hajj, M., Gao, Q., Mougenot, B. (2017) Potential of Sentinel-1 Radar Data for the Assessment of Soil and Cereal Cover Parameters. *Sensors*, 17(11), 2617.
- Bradley, A.V., Andersen, R., Marshall, C., Sowter, A., Large, D.J. (2022) Identification of typical ecohydrological behaviours using InSAR allows landscape-scale mapping of peatland condition. *Earth Surface Dynamics*, 10(2), 261–277.
- Brandyk, T.J., Dodd, V.A., Grace, P.M. (1986) Steady State Infiltration and Capillary Rise for a Range of Irish Peat Soils. *Irish Journal of Agricultural Research*, 25(1), 133–147.
- Braun, A. (2021) Retrieval of digital elevation models from Sentinel-1 radar data – open applications, techniques, and limitations. *Open Geosciences*, 13(1), 532–569.
- Braun, A., Veci, L. (2021) TOPS Interferometry Tutorial. European Space Agency (ESA). https://step.esa.int/docs/tutorials/S1TBX%20TOPSAR%20Interferometry%20with%20Sentinel-1%20Tutorial_v2.pdf. Accessed: 07.02.2022.
- Brisco, B., Ahern, F., Murnaghan, K., White, L., Canisus, F., Lancaster, P. (2017) Seasonal Change in Wetland Coherence as an Aid to Wetland Monitoring. *Remote Sensing*, 9(2), 158.
- Burdun, I. (2020) *Improving groundwater table monitoring for Northern Hemisphere peatlands using optical and thermal satellite data*. PhD dissertation. University of Tartu. Tartu, Estonia.

- Burdun, I., Sagris, V., Mander, Ü. (2019) Relationships between field-measured hydrometeorological variables and satellite-based land surface temperature in a hemiboreal raised bog. *International Journal of Applied Earth Observation and Geoinformation*, 74, 295–301.
- Chambers, J.M., Cleveland, W.S., Kleiner, B., Tukey, P.A. (2018) *Graphical Methods for Data Analysis*. CRC Press. Boca Raton, US.
- Chasmer, L., Cobbaert, D., Mahoney, C., Millard, K., Peters, D., Devito, K., ... Niemann, O. (2020a) Remote Sensing of Boreal Wetlands 1: Data Use for Policy and Management. *Remote Sensing*, 12(8), 1320.
- Chasmer, L., Mahoney, C., Millard, K., Nelson, K., Peters, D., Merchant, M., ... Cobbaert, D. (2020b) Remote Sensing of Boreal Wetlands 2: Methods for Evaluating Boreal Wetland Ecosystem State and Drivers of Change. *Remote Sensing*, 12(8), 1321.
- Cigna, F., Sowter, A. (2017) The relationship between intermittent coherence and precision of ISBAS InSAR ground motion velocities: ERS-1/2 case studies in the UK. *Remote Sensing of Environment*, 202, 177–198.
- Cigna, F., Sowter, A., Jordan, C.J., Rawlins, B.G. (2014) Intermittent Small Baseline Subset (ISBAS) monitoring of land covers unfavourable for conventional C-band InSAR: proof-of-concept for peatland environments in North Wales, UK. In: *SAR Image Analysis, Modeling, and Techniques XIV*. Proceedings of SPIE. Vol. 9243. International Society for Optics and Photonics. 924305, pp. 1–6.
- Cleary, J., Roulet, N.T., Moore, T.R. (2005) Greenhouse Gas Emissions from Canadian Peat Extraction, 1990–2000: A Life-cycle Analysis. *AMBIO: A Journal of the Human Environment*, 34(6), 456–461.
- Clymo, R.S., Pearce, D.M.E., Conrad, R. (1995) Methane and Carbon Dioxide Production in, Transport through, and Efflux from a Peatland. *Philosophical Transactions: Physical Sciences and Engineering*, 351(1696), 249–259.
- Clymo, R.S., Turunen, J., Tolonen, K. (1998) Carbon Accumulation in Peatland. *Oikos*, 81(2), 368–388.
- Conroy, F., Bruna, M., Hanssen, R.F. (2021) Machine Learning And Data Fusion For InSAR Over Distributed Scatterers. In: *ESA Fringe 2021 – 11th International Workshop on Advances in the Science and Applications of SAR Interferometry*. 31 May–4 June 2021. Frascati, Italy. <https://fringe.esa.int/agenda/>.
- Corr, D.G., Rodriguez, A.F. (1999) Change detection using interferometric SAR data. In: *SAR Image Analysis, Modeling, and Techniques II*. Proceedings of SPIE. Vol. 3869. International Society for Optics and Photonics. pp. 127–138.
- Couwenberg, J., Joosten, H. (2005) Self-Organization in Raised Bog Patterning: The Origin of Microtope Zonation and Mesotope Diversity. *Journal of Ecology*, 93(6), 1238–1248.
- Crosetto, M., Monserrat, O., Cuevas-González, M., Devanthéry, N., Crippa, B. (2016) Persistent Scatterer Interferometry: A review. *ISPRS Journal of Photogrammetry and Remote Sensing*, 115, 78–89.
- Czapiewski, S., Szumińska, D. (2022) An Overview of Remote Sensing Data Applications in Peatland Research Based on Works from the Period 2010–2021. *Land*, 11(1), 24.
- Dahdal, B. (2011) *The use of interferometric spaceborne radar and GIS to measure ground subsidence in peat soils in Indonesia*. PhD dissertation. University of Leicester. Leicester, UK.
- Davidson, M.W.J., Furnell, R. (2021) ROSE-L: Copernicus L-Band Sar Mission. In: *2021 IEEE International Geoscience and Remote Sensing Symposium IGARSS*. IEEE. pp. 872–873.

- De la Barreda-Bautista, B., Boyd, D.S., Ledger, M., Siewert, M.B., Chandler, C., Bradley, A.V., ... Sjögersten, S. (2022) Towards a Monitoring Approach for Understanding Permafrost Degradation and Linked Subsidence in Arctic Peatlands. *Remote Sensing*, 14(3), 444.
- De Vroey, M., Radoux, J., Defourny, P. (2021) Grassland Mowing Detection Using Sentinel-1 Time Series: Potential and Limitations. *Remote Sensing*, 13(3), 348.
- De Zan, F., Gomba, G. (2018) Vegetation and soil moisture inversion from SAR closure phases: First experiments and results. *Remote Sensing of Environment*, 217, 562–572.
- De Zan, F., Parizzi, A., Prats-Iraola, P., López-Dekker, P. (2014) A SAR Interferometric Model for Soil Moisture. *IEEE Transactions on Geoscience and Remote Sensing*, 52(1), 418–425.
- Dise, N.B. (2009) Peatland Response to Global Change. *Science*, 326(5954), 810–811.
- Drösler, M., Freibauer, A., Christensen, T.R., Friborg, T. (2008) Observations and Status of Peatland Greenhouse Gas Emissions in Europe. In: Dolman, A.J., Valentini, R., Freibauer, A. (eds.), *The Continental-Scale Greenhouse Gas Balance of Europe*. Springer. New York, US. pp. 243–261.
- Eesti Turbaliit (2022) Kaevandamine. <http://www.turbaliit.ee/kaevandamine/>. Accessed: 14.01.2022.
- ESA (2022) Sentinel Application Platform SNAP. European Space Agency (ESA). <http://step.esa.int/main/toolboxes/snap/>. Accessed: 18.01.2022.
- Esch, C., Köhler, J., Gutjahr, K., Schuh, W.-D. (2019) On the Analysis of the Phase Unwrapping Process in a D-InSAR Stack with Special Focus on the Estimation of a Motion Model. *Remote Sensing*, 11(19), 2295.
- Estonian Environment Agency (2022a) Soo aastaraamatud. <https://www.ilmateenistus.ee/siseveed/aastaraamatud-ja-bulletaan/soo-aastaraamatud/>. Accessed: 14.01.2022.
- Estonian Environment Agency (2022b) Weather, Observation data, Daily data. <http://www.ilmateenistus.ee/ilm/ilmavaatlused/vaatlusandmed/oopaevaandmed/?lang=en>. Accessed: 15.01.2022.
- Estonian Land Board (2021) Geoportal, Estonian Topographic Database. https://geoportaal.maaamet.ee/index.php?lang_id=2&page_id=618. Updated: 04.11.2021.
- Ferretti, A., Monti-Guarnieri, A., Prati, C., Rocca, F. (2007) *InSAR Principles: Guidelines for SAR Interferometry Processing and Interpretation*. ESA Publications. Noordwijk, Netherlands.
- Ferretti, A., Prati, C., Rocca, F. (2001) Permanent scatterers in SAR interferometry. *IEEE Transactions on Geoscience and Remote Sensing*, 39(1), 8–20.
- Fiaschi, S., Holohan, E.P., Sheehy, M., Floris, M. (2019) PS-InSAR Analysis of Sentinel-1 Data for Detecting Ground Motion in Temperate Oceanic Climate Zones: A Case Study in the Republic of Ireland. *Remote Sensing*, 11(3), 348.
- Fielding, E.J. (2018) SAR Interferometry for Earthquake Studies. NASA Jet Propulsion Laboratory (JPL). <https://trs.jpl.nasa.gov/handle/2014/49629>. Accessed: 14.01.2022.
- Foster, J., Brooks, B., Cherubini, T., Shacat, C., Businger, S., Werner, C.L. (2006) Mitigating atmospheric noise for InSAR using a high resolution weather model. *Geophysical Research Letters*, 33(16).
- Fritz, C. (2006) *Surface oscillation in peatlands: How variable and important is it?* Master's thesis. University of Waikato. Hamilton, New Zealand.
- Fritz, C., Campbell, D.I., Schipper, L.A. (2008) Oscillating peat surface levels in a resiated peatland, New Zealand—magnitude and spatiotemporal variability. *Hydrological Processes*, 22(17), 3264–3274.

- Frolking, S., Talbot, J., Jones, M.C., Treat, C.C., Kauffman, J.B., Tuittila, E.-S., Roulet, N. (2011) Peatlands in the Earth's 21st century climate system. *Environmental Reviews*, 19, 371–396.
- Geudtner, D., Miranda, N., Navas-Traver, I., Vega, F.C., Prats, P., Yague-Martinez, N., ... Barat, I. (2018) Sentinel-1A/B SAR and InSAR Performance. In: *EUSAR 2018; 12th European Conference on Synthetic Aperture Radar*. VDE. pp. 641–645.
- Gewin, V. (2020) How peat could protect the planet. *Nature*, 578(7794), 204–209.
- Glaser, P.H., Chanton, J.P., Morin, P., Rosenberry, D.O., Siegel, D.I., Ruud, O., ... Reeve, A.S. (2004) Surface Deformations as Indicators of Deep Ebullition Fluxes in a Large Northern Peatland. *Global Biogeochemical Cycles*, 18(1), GB1003.
- Goldstein, R.M., Werner, C.L. (1998) Radar interferogram filtering for geophysical applications. *Geophysical Research Letters*, 25(21), 4035–4038.
- Goldstein, R.M., Zebker, H.A., Werner, C.L. (1988) Satellite radar interferometry: Two-dimensional phase unwrapping. *Radio Science*, 23(4), 713–720.
- Gong, W., Thiele, A., Hinz, S., Meyer, F.J., Hooper, A., Agram, P.S. (2016) Comparison of Small Baseline Interferometric SAR Processors for Estimating Ground Deformation. *Remote Sensing*, 8(4), 330.
- Gorham, E. (1991) Northern Peatlands: Role in the Carbon Cycle and Probable Responses to Climatic Warming. *Ecological Applications*, 1(2), 182–195.
- Graf, M., Bérubé, V., Rochefort, L. (2012) Restoration of peatlands after peat extraction: Impacts, restoration goals, and techniques. In: Vitt, D., Bhatti, J. (eds.), *Restoration and reclamation of boreal ecosystems: Attaining sustainable development*. Cambridge University Press. Cambridge, UK. pp. 259–280.
- Harris, L.I., Richardson, K., Bona, K.A., Davidson, S.J., Finkelstein, S.A., Garneau, M., ... Ray, J.C. (2022) The essential carbon service provided by northern peatlands. *Frontiers in Ecology and the Environment*, 20(4), 222–230.
- Hart, A. (2001) Mann-Whitney test is not just a test of medians: Differences in spread can be important. *British Medical Journal*, 323(7309), 391–393.
- Hersbach, H., Bell, B., Berrisford, P., Biavati, G., Horányi, A., Muñoz Sabater, J., ... Thépaut, J.-N. (2022) ERA5 hourly data on pressure levels from 1979 to present. Copernicus Climate Change Service (C3S) Climate Data Store (CDS). <https://doi.org/10.24381/cds.bd0915c6>. Accessed: 24.01.2022.
- Heuff, F.M.G., Hanssen, R.F. (2020) Insar Phase Reduction Using the Remove-Compute-Restore Method. In: *2020 IEEE International Geoscience and Remote Sensing Symposium IGARSS*. IEEE. pp. 786–789.
- Ho Tong Minh, D., Hanssen, R., Rocca, F. (2020) Radar Interferometry: 20 Years of Development in Time Series Techniques and Future Perspectives. *Remote Sensing*, 12(9), 1364.
- Holden, J., Burt, T.P. (2003) Hydrological Studies on Blanket Peat: The Significance of the Acrotelm-Catotelm Model. *Journal of Ecology*, 91(1), 86–102.
- Holden, J., Chapman, P.J., Labadz, J.C. (2004) Artificial drainage of peatlands: Hydrological and hydrochemical process and wetland restoration. *Progress in Physical Geography: Earth and Environment*, 28(1), 95–123.
- Hooper, A., Segall, P., Zebker, H. (2007) Persistent scatterer interferometric synthetic aperture radar for crustal deformation analysis, with application to Volcán Alcedo, Galápagos. *Journal of Geophysical Research: Solid Earth*, 112(B7), B07407.

- Hooper, A., Zebker, H., Segall, P., Kampes, B. (2004) A new method for measuring deformation on volcanoes and other natural terrains using InSAR persistent scatterers. *Geophysical Research Letters*, 31(23), L23611.
- Howie, S.A., Hebda, R.J. (2018) Bog surface oscillation (mire breathing): A useful measure in raised bog restoration. *Hydrological Processes*, 32(11), 1518–1530.
- Hoyt, A.M., Chaussard, E., Seppäläinen, S.S., Harvey, C.F. (2020) Widespread subsidence and carbon emissions across Southeast Asian peatlands. *Nature Geoscience*, 13(6), 435–440.
- Hu, J., Li, Z.W., Ding, X.L., Zhu, J.J., Zhang, L., Sun, Q. (2014) Resolving three-dimensional surface displacements from InSAR measurements: A review. *Earth-Science Reviews*, 133, 1–17.
- Huang, Y., Ciais, P., Luo, Y., Zhu, D., Wang, Y., Qiu, C., ... Qu, L. (2021) Tradeoff of CO₂ and CH₄ emissions from global peatlands under water-table drawdown. *Nature Climate Change*, 11(7), 618–622.
- Hugelius, G., Loisel, J., Chadburn, S., Jackson, R.B., Jones, M., MacDonald, G., ... Yu, Z. (2020) Large stocks of peatland carbon and nitrogen are vulnerable to permafrost thaw. *Proceedings of the National Academy of Sciences*, 117(34), 20438–20446.
- Ingram, H.a.P. (1982) Size and shape in raised mire ecosystems: A geophysical model. *Nature*, 297(5864), 300–303.
- Iwahana, G., Busey, R.C., Saito, K. (2021) Seasonal and Interannual Ground-Surface Displacement in Intact and Disturbed Tundra along the Dalton Highway on the North Slope, Alaska. *Land*, 10(1), 22.
- Jiang, M., Li, Z.W., Ding, X.L., Zhu, J.J., Feng, G.C. (2011) Modeling minimum and maximum detectable deformation gradients of interferometric SAR measurements. *International Journal of Applied Earth Observation and Geoinformation*, 13(5), 766–777.
- Jones, K., Lanthier, Y., van der Voet, P., van Valkengoed, E., Taylor, D., Fernández-Prieto, D. (2009) Monitoring and assessment of wetlands using Earth Observation: The GlobWetland project. *Journal of Environmental Management*, 90(7), 2154–2169.
- Joosten, H., Clarke, D. (2002) *Wise Use of Mires and Peatlands – Background Principles including a Framework for Decision-Making*. International Mire Conservation Group and International Peat Society. Saarijärvi, Finland.
- Karl, J.W., Maurer, B.A. (2010) Multivariate correlations between imagery and field measurements across scales: Comparing pixel aggregation and image segmentation. *Landscape Ecology*, 25(4), 591–605.
- Kasischke, E.S., Bourgeau-Chavez, L.L., Rober, A.R., Wyatt, K.H., Waddington, J.M., Turetsky, M.R. (2009) Effects of soil moisture and water depth on ERS SAR backscatter measurements from an Alaskan wetland complex. *Remote Sensing of Environment*, 113(9), 1868–1873.
- Kellner, E. (2001) Surface energy fluxes and control of evapotranspiration from a Swedish *Sphagnum* mire. *Agricultural and Forest Meteorology*, 110(2), 101–123.
- Kellner, E., Halldin, S. (2002) Water budget and surface-layer water storage in a *Sphagnum* bog in central Sweden. *Hydrological Processes*, 16(1), 87–103.
- Kellner, E., Lundin, L.-C. (2001) Calibration of Time Domain Reflectometry for Water Content in Peat Soil. *Hydrology Research*, 32(4-5), 315–332.
- Kim, J.-W., Lu, Z., Gutenberg, L., Zhu, Z. (2017) Characterizing hydrologic changes of the Great Dismal Swamp using SAR/InSAR. *Remote Sensing of Environment*, 198, 187–202.

- Kim, S.-W., Wdowinski, S., Amelung, F., Dixon, T.H., Won, J.-S. (2013) Interferometric Coherence Analysis of the Everglades Wetlands, South Florida. *IEEE Transactions on Geoscience and Remote Sensing*, 51(12), 5210–5224.
- Kont, A., Endjärv, E., Jaagus, J., Lode, E., Orviku, K., Ratas, U., . . . Tonisson, H. (2007) Impact of climate change on Estonian coastal and inland wetlands – a summary with new wetlands. *Boreal Environment Research*, 12, 653–671.
- Krüger, J.P., Leifeld, J., Glatzel, S., Szidat, S., Alewell, C. (2015) Biogeochemical indicators of peatland degradation – a case study of a temperate bog in northern Germany. *Biogeosciences*, 12(10), 2861–2871.
- Laine, J., Vasander, H., Sallantausta, T. (1995) Ecological effects of peatland drainage for forestry. *Environmental Reviews*, 3(3-4), 286–303.
- Lees, K., Quaife, T., Artz, R., Khomik, M., Clark, J. (2018) Potential for using remote sensing to estimate carbon fluxes across northern peatlands – A review. *Science of The Total Environment*, 615, 857–874.
- Leifeld, J., Menichetti, L. (2018) The underappreciated potential of peatlands in global climate change mitigation strategies. *Nature Communications*, 9(1), 1–7.
- Leifeld, J., Wüst-Galley, C., Page, S. (2019) Intact and managed peatland soils as a source and sink of GHGs from 1850 to 2100. *Nature Climate Change*, 9(12), 945–947.
- Li, J., Chen, W. (2005) A rule-based method for mapping Canada’s wetlands using optical, radar and DEM data. *International Journal of Remote Sensing*, 26(22), 5051–5069.
- Liang, S., Jiang, B., He, T., Zhu, X. (2020) Chapter 18: Soil moisture contents. In: Liang, S., Wang, J. (eds.), *Advanced Remote Sensing (Second Edition): Terrestrial Information Extraction and Applications*. Academic Press. Cambridge, US. pp. 685–711.
- Limpens, J., Berendse, F., Blodau, C., Canadell, J.G., Freeman, C., Holden, J., . . . Schaepman-Strub, G. (2008) Peatlands and the carbon cycle: From local processes to global implications – a synthesis. *Biogeosciences*, 5(5), 1475–1491.
- Lindholm, T., Markkula, I. (1984) Moisture conditions in hummocks and hollows in virgin and drained sites on the raised bog Laaviosuo, southern Finland. *Annales Botanici Fennici*, 21(3), 241–255.
- Liu, J.G., Mason, P.J. (2009) *Introduction to Interferometric Synthetic Aperture Radar Techniques. In: Liu, J.G., Mason, P.J. (eds.), *Essential image processing and GIS for remote sensing*. John Wiley & Sons. Chichester, UK. pp. 121–134.
- Liu, L., Zhang, T., Wahr, J. (2010) InSAR measurements of surface deformation over permafrost on the North Slope of Alaska. *Journal of Geophysical Research: Earth Surface*, 115(F3), 1–14.
- Lober, F., Holtgrave, A.-K., Schwieder, M., Pause, M., Vogt, J., Gocht, A., Erasmi, S. (2021) Mowing event detection in permanent grasslands: Systematic evaluation of input features from Sentinel-1, Sentinel-2, and Landsat 8 time series. *Remote Sensing of Environment*, 267, 112751.
- Mahdavi, S., Salehi, B., Granger, J., Amani, M., Brisco, B., Huang, W. (2018) Remote sensing for wetland classification: A comprehensive review. *GIScience & Remote Sensing*, 55(5), 623–658.
- Mann, H.B., Whitney, D.R. (1947) On a Test of Whether one of Two Random Variables is Stochastically Larger than the Other. *The Annals of Mathematical Statistics*, 18(1), 50–60.
- Marshall, C., Sterk, H.P., Gilbert, P.J., Andersen, R., Bradley, A.V., Sowter, A., . . . Large, D.J. (2022) Multiscale Variability and the Comparison of Ground and Satellite Radar

- Based Measures of Peatland Surface Motion for Peatland Monitoring. *Remote Sensing*, 14(2), 336.
- Massonnet, D., Feigl, K.L. (1998) Radar interferometry and its application to changes in the Earth's surface. *Reviews of Geophysics*, 36(4), 441–500.
- MathWorks (2022) MATLAB. <https://mathworks.com/products/matlab.html>. Accessed: 19.01.2022.
- McDonald, J.H. (2014) *Handbook of biological statistics*. Sparky House Publishing. Baltimore, US.
- Melton, J.R., Chan, E., Millard, K., Fortier, M., Winton, R.S., Martín-López, J.M., ... Verchot, L.V. (2022) A map of global peatland extent created using machine learning (Peat-ML). *Geoscientific Model Development Discussions*, 15, 4709–4738.
- Merchant, M.A., Adams, J.R., Berg, A.A., Baltzer, J.L., Quinton, W.L., Chasmer, L.E. (2017) Contributions of C-Band SAR Data and Polarimetric Decompositions to Subarctic Boreal Peatland Mapping. *IEEE Journal of Selected Topics in Applied Earth Observations and Remote Sensing*, 10(4), 1467–1482.
- Microsoft Corporation (2022) Microsoft Excel. <https://www.microsoft.com/en-ww/microsoft-365/excel>. Accessed: 25.01.2022.
- Millard, K. (2016) *Development of methods to map and monitor peatland ecosystems and hydrologic conditions using Radarsat-2 Synthetic Aperture Radar*. PhD dissertation. Carleton University. Ottawa, Canada.
- Millard, K., Kirby, P., Nandlall, S., Behnamian, A., Banks, S., Pacini, F. (2020) Using growing-season time series coherence for improved peatland mapping: Comparing the contributions of Sentinel-1 and RADARSAT-2 coherence in full and partial time series. *Remote Sensing*, 12(15), 2465.
- Millard, K., Richardson, M. (2018) Quantifying the relative contributions of vegetation and soil moisture conditions to polarimetric C-Band SAR response in a temperate peatland. *Remote Sensing of Environment*, 206, 123–138.
- Milodowski, D.T., Hancock, S., Silvestri, S., Mudd, S.M. (2020) Linking life and landscape with remote sensing. In: *Developments in Earth Surface Processes*. Vol. 23. Elsevier. pp. 129–182.
- Minasny, B., Berglund, Ö., Connolly, J., Hedley, C., de Vries, F., Gimona, A., ... Widyatmanti, W. (2019) Digital mapping of peatlands – A critical review. *Earth-Science Reviews*, 196, 102870.
- Mirmazloumi, S.M., Moghimi, A., Ranjgar, B., Mohseni, F., Ghorbanian, A., Ahmadi, S.A., ... Brisco, B. (2021) Status and Trends of Wetland Studies in Canada Using Remote Sensing Technology with a Focus on Wetland Classification: A Bibliographic Analysis. *Remote Sensing*, 13(20), 4025.
- Mohammadimanesh, F., Salehi, B., Mahdianpari, M., Brisco, B., Motagh, M. (2018a) Multi-temporal, multi-frequency, and multi-polarization coherence and SAR backscatter analysis of wetlands. *ISPRS Journal of Photogrammetry and Remote Sensing*, 142, 78–93.
- Mohammadimanesh, F., Salehi, B., Mahdianpari, M., Motagh, M., Brisco, B. (2018b) An efficient feature optimization for wetland mapping by synergistic use of SAR intensity, interferometry, and polarimetry data. *International journal of applied earth observation and geoinformation*, 73, 450–462.
- Montanarella, L., Jones, R.J.A., Hiederer, R. (2006) The distribution of peatland in Europe. *Mires and Peat*, 1, 1–10.

- Monti-Guarnieri, A., Manzoni, M., Giudici, D., Recchia, A., Tebaldini, S. (2020) Vegetated Target Decorrelation in SAR and Interferometry: Models, Simulation, and Performance Evaluation. *Remote Sensing*, 12(16), 2545.
- Moore, P.D. (2002) The future of cool temperate bogs. *Environmental Conservation*, 29(1), 3–20.
- Moore, P.D., Bellamy, D.J. (1974) *Peatlands*. Elek Science. London, UK.
- Moreira, A., Prats-Iraola, P., Younis, M., Krieger, G., Hajnsek, I., Papathanassiou, K.P. (2013) A tutorial on synthetic aperture radar. *IEEE Geoscience and Remote Sensing Magazine*, 1(1), 6–43.
- Morton, P.A., Heinemeyer, A. (2019) Bog breathing: The extent of peat shrinkage and expansion on blanket bogs in relation to water table, heather management and dominant vegetation and its implications for carbon stock assessments. *Wetlands Ecology and Management*, 27(4), 467–482.
- Mustamo, P., Maljanen, M., Hyvärinen, M., Ronkanen, A.-K., Kløve, B. (2016) Respiration and emissions of methane and nitrous oxide from a boreal peatland complex comprising different land-use types. 21, 405–426.
- NASA JPL (2022) NASA-ISRO SAR Mission (NISAR), Quick Facts. NASA Jet Propulsion Laboratory (JPL). <https://nisar.jpl.nasa.gov/mission/quick-facts/>. Accessed: 20.02.2022.
- Nichols, J.E., Peteet, D.M. (2019) Rapid expansion of northern peatlands and doubled estimate of carbon storage. *Nature Geoscience*, 12(11), 917–921.
- Nolan, M., Fatland, D. (2003) Penetration depth as a DInSAR observable and proxy for soil moisture. *IEEE Transactions on Geoscience and Remote Sensing*, 41(3), 532–537.
- Novellino, A., Cigna, F., Brahmi, M., Sowter, A., Bateson, L., Marsh, S. (2017) Assessing the Feasibility of a National InSAR Ground Deformation Map of Great Britain with Sentinel-1. *Geosciences*, 7(2), 19.
- Ojanen, P., Minkkinen, K., Alm, J., Penttilä, T. (2010) Soil–atmosphere CO₂, CH₄ and N₂O fluxes in boreal forestry-drained peatlands. *Forest Ecology and Management*, 260(3), 411–421.
- Osmanoğlu, B., Sunar, F., Wdowinski, S., Cabral-Cano, E. (2016) Time series analysis of InSAR data: Methods and trends. *ISPRS Journal of Photogrammetry and Remote Sensing*, 115, 90–102.
- Paal, J. (2004) "Loodusdirektiivi" elupaigatüüpide käsiraamat. Digimap. Tallinn, Estonia.
- Paal, J., Jürjendal, I., Kull, A. (2016) Impact of drainage on vegetation of transitional mires in Estonia. *Mires and Peat*, 18, 1–19.
- Paal, J., Leibak, E. (2011) *Estonian mires: inventory of habitats*. Regio. Tartu, Estonia.
- Päivänen, J., Hännell, B. (2012) *Peatland Ecology and Forestry – a Sound Approach*. Vol. 3. University of Helsinki Department of Forest Sciences Publications. Helsinki, Finland.
- Pakere, I., Blumberga, D. (2017) Energy Efficiency Indicators in Peat Extraction Industry – A Case Study. *Energy Procedia*, 113, 143–150.
- Pampaloni, P., Paloscia, S., Macelloni, G., Sigismondi, S. (1997) The potential of C- and L-band SAR in assessing vegetation biomass: ERS-1 & JERS-1 experiments. In: *Third ERS Symposium on Space at the service of our Environment*. Vol. 414. European Space Agency (ESA). Florence, Italy. pp. 1729–1733.
- Pandit, A., Sawant, S., Mohite, J., Pappula, S. (2022) Sentinel-1-derived coherence time-series for crop monitoring in Indian agriculture region. *Geocarto International*, (just-accepted), 1–21.

- Pepe, A., Calò, F. (2017) A Review of Interferometric Synthetic Aperture RADAR (InSAR) Multi-Track Approaches for the Retrieval of Earth's Surface Displacements. *Applied Sciences*, 7(12), 1264.
- Pepe, A., Lanari, R. (2006) On the Extension of the Minimum Cost Flow Algorithm for Phase Unwrapping of Multitemporal Differential SAR Interferograms. *IEEE Transactions on Geoscience and Remote Sensing*, 44(9), 2374–2383.
- Perissin, D. (2019) SARPROZ Manual. <https://www.sarproz.com/software-manual/>. Accessed: 19.01.2022.
- Perissin, D. (2022) SARPROZ: The SAR PROcessing tool by periZ. <https://www.sarproz.com/>. Accessed: 19.01.2022.
- Poggio, L., Lassauce, A., Gimona, A. (2019) Modelling the extent of northern peat soil and its uncertainty with Sentinel: Scotland as example of highly cloudy region. *Geoderma*, 346, 63–74.
- Pouliot, R., Rochefort, L., Karofeld, E. (2011) Initiation of microtopography in revegetated cutover peatlands. *Applied Vegetation Science*, 14(2), 158–171.
- Prats-Iraola, P., Rodriguez-Cassola, M., De Zan, F., Scheiber, R., López-Dekker, P., Barat, I., Geudtner, D. (2015) Role of the Orbital Tube in Interferometric Spaceborne SAR Missions. *IEEE Geoscience and Remote Sensing Letters*, 12(7), 1486–1490.
- Preiss, M., Gray, D., Stacy, N. (2006) Detecting scene changes using synthetic aperture Radar interferometry. *IEEE Transactions on Geoscience and Remote Sensing*, 44(8), 2041–2054.
- Price, J.S., Heathwaite, A., Baird, A. (2003) Hydrological processes in abandoned and restored peatlands: An overview of management approaches. *Wetlands Ecology and Management*, 11(1), 65–83.
- Price, J.S., Schlotzhauer, S.M. (1999) Importance of shrinkage and compression in determining water storage changes in peat: The case of a mined peatland. *Hydrological Processes*, 13(16), 2591–2601.
- Python Software Foundation (2022) Python. <https://www.python.org/>. Accessed: 19.01.2022.
- R Core Team (2022) R: The R Project for Statistical Computing. <https://www.r-project.org/>. Accessed: 19.01.2022.
- R Documentation (2022) Boxplot: Box Plots. <https://www.rdocumentation.org/packages/graphics/versions/3.6.1/topics/boxplot>. Accessed: 08.02.2022.
- Ramsey, III E., Lu, Z., Ragoonwala, A., Rykhus, R. (2006) Multiple Baseline Radar Interferometry Applied to Coastal Land Cover Classification and Change Analyses. *GIScience & Remote Sensing*, 43(4), 283–309.
- Rosen, P., Hensley, S., Joughin, I., Li, F., Madsen, S., Rodriguez, E., Goldstein, R. (2000) Synthetic aperture radar interferometry. *Proceedings of the IEEE*, 88(3), 333–382.
- Roulet, N.T. (1991) Surface Level and Water Table Fluctuations in a Subarctic Fen. *Arctic and Alpine Research*, 23(3), 303.
- Rudant, J.-P., Bedidi, A., Calonne, R., Massonnet, D., Netti, G., Tarchi, D. (1997) Laboratory experiments for the interpretation of phase shift in SAR interferograms. In: *The Proceedings of the 'Fringe 96' Workshop on ERS SAR Interferometry (Zurich, 30 Sept. - 2 Oct. 1996)*. ESA Publications Division, ESTEC. Noordwijk, Netherlands.
- Sadeghi, M., Babaeian, E., Tuller, M., Jones, S.B. (2017) The optical trapezoid model: A novel approach to remote sensing of soil moisture applied to Sentinel-2 and Landsat-8 observations. *Remote Sensing of Environment*, 198, 52–68.

- Salm, J.-O., Maddison, M., Tammik, S., Soosaar, K., Truu, J., Mander, Ü. (2012) Emissions of CO₂, CH₄ and N₂O from undisturbed, drained and mined peatlands in Estonia. *Hydrobiologia*, 692(1), 41–55.
- Santoro, M., Askne, J.I.H., Smith, G., Fransson, J.E.S. (2002) Stem volume retrieval in boreal forests from ERS-1/2 interferometry. *Remote Sensing of Environment*, 81(1), 19–35.
- Schouwenaars, J.M. (1993) Hydrological differences between bogs and bog-relicts and consequences for bog restoration. In: Best, E.P.H., Bakker, J.P. (eds.), *Netherlands-Wetlands*. Vol. 88. Springer. Dordrecht, Netherlands. pp. 217–224.
- Schuldt, B., Buras, A., Arend, M., Vitasse, Y., Beierkuhnlein, C., Damm, A., ... Kahmen, A. (2020) A first assessment of the impact of the extreme 2018 summer drought on Central European forests. *Basic and Applied Ecology*, 45, 86–103.
- Scott, C.P., Lohman, R.B., Jordan, T.E. (2017) InSAR constraints on soil moisture evolution after the March 2015 extreme precipitation event in Chile. *Scientific Reports*, 7(1), 4903.
- Shapiro, S.S., Wilk, M.B. (1965) An Analysis of Variance Test for Normality (Complete Samples). *Biometrika*, 52(3/4), 591–611.
- Silvola, J., Alm, J., Ahlholm, U., Nykanen, H., Martikainen, P.J. (1996) CO₂ Fluxes from Peat in Boreal Mires under Varying Temperature and Moisture Conditions. *Journal of Ecology*, 84(2), 219–228.
- Sowter, A., Bateson, L., Strange, P., Ambrose, K., Syafiudin, M.F. (2013) DInSAR estimation of land motion using intermittent coherence with application to the South Derbyshire and Leicestershire coalfields. *Remote Sensing Letters*, 4(10), 979–987.
- Spearman, C. (1987) The Proof and Measurement of Association between Two Things. *The American Journal of Psychology*, 100(3/4), 441–471.
- Strack, M., Price, J.S. (2009) Moisture controls on carbon dioxide dynamics of peat-*Sphagnum* monoliths. *Ecohydrology*, 2(1), 34–41.
- Sundh, I., Nilsson, M., Mikkilä, C., Granberg, G., Svensson, B.H. (2000) Fluxes of Methane and Carbon Dioxide on Peat-Mining Areas in Sweden. *Ambio*, 29(8), 499–503.
- Tamm, T. (2018) *Use of local statistics in remote sensing of grasslands and forests*. PhD dissertation. University of Tartu. Tartu, Estonia.
- Tamm, T., Zalite, K., Voormansik, K., Talgre, L. (2016) Relating Sentinel-1 Interferometric Coherence to Mowing Events on Grasslands. *Remote Sensing*, 8(10), 802.
- Tampuu, T., De Zan, F., Shau, R., Praks, J., Kohv, M., Kull, A. (2022) Reliability of Sentinel-1 InSAR distributed scatterer (DS) time series to estimate the temporal vertical movement of ombrotrophic bog surface. In: *EGU General Assembly 2022 (EGU22)*. 23–27 May 2022. Vienna, Austria. <https://doi.org/10.5194/egusphere-egu22-2387>.
- Tampuu, T., De Zan, F., Shau, R., Praks, J., Kohv, M., Kull, A. (202Xa) Can Bog Breathing Be Measured by Synthetic Aperture Radar Interferometry. In: *2022 IEEE International Geoscience and Remote Sensing Symposium IGARSS*. IEEE. (Accepted).
- Tampuu, T., Praks, J., De Zan, F., Kohv, M., Kull, A. (2021) Towards assessment of bog breathing with Sentinel-1 Differential InSAR. In: *Proceedings of the 16th International Peatland Congress 2021*. pp. 472–478.
- Tampuu, T., Praks, J., De Zan, F., Kohv, M., Kull, A. (202Xb) Could bog breathing be measured by Synthetic Aperture Radar? – The relationship between differential interferometric phase and ground measurements. *Mires and Peat*, (Submitted).

- Tampuu, T., Praks, J., Uiboupin, R., Kull, A. (2020) Long Term Interferometric Temporal Coherence and DInSAR Phase in Northern Peatlands. *Remote Sensing*, 12(10), 1566.
- Tarnocai, C., Stolbovoy, V. (2006) Chapter 2: Northern Peatlands their characteristics, development and sensitivity to climate change. In: Martini, I.P., Martínez Cortizas, A., Chesworth, W. (eds.), *Developments in Earth Surface Processes*. Vol. 9. Elsevier. Amsterdam, Netherlands. pp. 17–51.
- Thiel, C.J., Thiel, C., Schmullius, C.C. (2009) Operational Large-Area Forest Monitoring in Siberia Using ALOS PALSAR Summer Intensities and Winter Coherence. *IEEE Transactions on Geoscience and Remote Sensing*, 47(12), 3993–4000.
- Tissari, J.M., Yli-Tuomi, T., Raunemaa, T.M., Tiitta, P.T., Nuutinen, J.P., Willman, P.K., ... Jokiniemi, J.K. (2006) Fine particle emissions from milled peat production. *Boreal Environment Research*, 11, 283–293.
- Torbick, N., Persson, A., Olefeldt, D., Frohling, S., Salas, W., Hagen, S., ... Li, C. (2012) High Resolution Mapping of Peatland Hydroperiod at a High-Latitude Swedish Mire. *Remote Sensing*, 4(7), 1974–1994.
- Torres, R., Snoeij, P., Geudtner, D., Bibby, D., Davidson, M., Attema, E., ... Brown, M., et al. (2012) GMES Sentinel-1 mission. *Remote sensing of environment*, 120, 9–24.
- Touzi, R., Lopes, A., Bruniquel, J., Vachon, P.W. (1999) Coherence estimation for SAR imagery. *IEEE Transactions on Geoscience and Remote Sensing*, 37, 135–149.
- Tsyganskaya, V., Martinis, S., Marzahn, P., Ludwig, R. (2018) SAR-based detection of flooded vegetation – a review of characteristics and approaches. *International Journal of Remote Sensing*, 39(8), 2255–2293.
- Tukey, J.W. (1977) *Exploratory data analysis*. Addison-Wesley Publishing Company. Reading, US.
- Turetsky, M.R., Benscoter, B., Page, S., Rein, G., Van Der Werf, G.R., Watts, A. (2015) Global vulnerability of peatlands to fire and carbon loss. *Nature Geoscience*, 8(1), 11–14.
- Ulaby, F.T., Dubois, P.C., van Zyl, J. (1996) Radar mapping of surface soil moisture. *Journal of Hydrology*, 184(1), 57–84.
- Umarhadi, D.A., Avtar, R., Widyatmanti, W., Johnson, B.A., Yunus, A.P., Khedher, K.M., Singh, G. (2021a) Use of multifrequency (C-band and L-band) SAR data to monitor peat subsidence based on time-series SBAS InSAR technique. *Land Degradation & Development*, 32(16), 4779–4794.
- Umarhadi, D.A., Widyatmanti, W., Kumar, P., Yunus, A.P., Khedher, K.M., Kharrazi, A., Avtar, R. (2021b) Tropical peat subsidence rates are related to decadal LULC changes: Insights from InSAR analysis. *Science of The Total Environment*, 816, 1–16.
- Veber, G. (2021) *Greenhouse gas fluxes in natural and drained peatlands: spatial and temporal dynamics*. PhD dissertation. University of Tartu. Tartu, Estonia.
- Waddington, J.M., Plach, J., Cagampan, J.P., Luchese, M., Strack, M. (2009) Reducing the Carbon Footprint of Canadian Peat Extraction and Restoration. *AMBIO: A Journal of the Human Environment*, 38(4), 194–200.
- Wagner, W., Blöschl, G., Pampaloni, P., Calvet, J.-C., Bizzarri, B., Wigneron, J.-P., Kerr, Y. (2007) Operational readiness of microwave remote sensing of soil moisture for hydrologic applications. *Hydrology Research*, 38(1), 1–20.
- Webley, P.W., Wadge, G., James, I.N. (2004) Determining radio wave delay by non-hydrostatic atmospheric modelling of water vapour over mountains. *Physics and Chemistry of the Earth, Parts A/B/C*, 29(2), 139–148.

- Webster, K.L., Bhatti, J.S., Thompson, D.K., Nelson, S.A., Shaw, C.H., Bona, K.A., ... Kurz, W.A. (2018) Spatially-integrated estimates of net ecosystem exchange and methane fluxes from Canadian peatlands. *Carbon Balance and Management*, 13(1), 16.
- Wegmüller, U., Werner, C. (1997) Retrieval of vegetation parameters with SAR interferometry. *IEEE Transactions on Geoscience and Remote Sensing*, 35(1), 18–24.
- Wei, M., Sandwell, D.T. (2010) Decorrelation of L-Band and C-Band Interferometry Over Vegetated Areas in California. *IEEE Transactions on Geoscience and Remote Sensing*, 48(7), 2942–2952.
- Weydahl, D. (2001) Analysis of ERS Tandem SAR coherence from glaciers, valleys, and fjord ice on Svalbard. *IEEE Transactions on Geoscience and Remote Sensing*, 39(9), 2029–2039.
- Witze, A. (2020) The Arctic is burning like never before—and that’s bad news for climate change. *Nature*, 585(7825), 336–338.
- Xu, J., Morris, P.J., Liu, J., Holden, J. (2018) PEATMAP: Refining estimates of global peatland distribution based on a meta-analysis. *Catena*, 160, 134–140.
- Yagüe-Martínez, N., Prats-Iraola, P., González, F.R., Brcic, R., Shau, R., Geudtner, D., ... Bamler, R. (2016) Interferometric Processing of Sentinel-1 TOPS Data. *IEEE Transactions on Geoscience and Remote Sensing*, 54(4), 2220–2234.
- Yu, Z.C. (2012) Northern peatland carbon stocks and dynamics: a review. *Biogeosciences*, 9(10), 4071–4085.
- Yunjun, Z., Fattahi, H., Amelung, F. (2019) Small baseline InSAR time series analysis: Unwrapping error correction and noise reduction. *Computers & Geosciences*, 133, 104331.
- Zebker, H., Villasenor, J. (1992) Decorrelation in interferometric radar echoes. *IEEE Transactions on Geoscience and Remote Sensing*, 30(5), 950–959.
- Zhang, M., Li, Z., Tian, B., Zhou, J., Zeng, J. (2015) A method for monitoring hydrological conditions beneath herbaceous wetlands using multi-temporal ALOS PALSAR coherence data. *Remote Sensing Letters*, 6(8), 618–627.
- Zhou, Z. (2013) *The applications of InSAR time series analysis for monitoring long-term surface change in peatlands*. PhD dissertation. University of Glasgow. Glasgow, UK.
- Zhou, Z., Li, Z., Waldron, S., Tanaka, A. (2019) InSAR Time Series Analysis of L-Band Data for Understanding Tropical Peatland Degradation and Restoration. *Remote Sensing*, 11(21), 2592.
- Zhou, Z., Waldron, S., Li, Z. (2010) Integration of PS-InSAR and GPS for monitoring seasonal and long-term peatland surface fluctuations. In: *Proceedings of the Remote Sensing and Photogrammetry Society Conference Remote Sensing and the Carbon Cycle*. Vol. 1. 5 May 2010. London, UK. pp. 1–4.
- Zwieback, S., Berg, A.A. (2019) Fine-Scale SAR Soil Moisture Estimation in the Subarctic Tundra. *IEEE Transactions on Geoscience and Remote Sensing*, 57(7), 4898–4912.
- Zwieback, S., Hensley, S., Hajnsek, I. (2015a) A Polarimetric First-Order Model of Soil Moisture Effects on the DInSAR Coherence. *Remote Sensing*, 7(6), 7571–7596.
- Zwieback, S., Hensley, S., Hajnsek, I. (2015b) Assessment of soil moisture effects on L-band radar interferometry. *Remote Sensing of Environment*, 164, 77–89.
- Zwieback, S., Hensley, S., Hajnsek, I. (2017) Soil Moisture Estimation Using Differential Radar Interferometry: Toward Separating Soil Moisture and Displacements. *IEEE Transactions on Geoscience and Remote Sensing*, 55(9), 5069–5083.

SUMMARY

Peatlands are significant in regard to climate change because peatlands may switch from being a net carbon sink to an emitter of greenhouse gases. The delicate carbon balance in peatlands is controlled by the peatland water table (WT). Peatland soils contain globally nearly as much carbon as a half of what is currently in the atmosphere whereas a major fraction of peatlands is located in mid- and high latitudes of the Northern Hemisphere. Continuous monitoring over large or inaccessible peatland areas is only feasible by remote sensing instruments. Synthetic Aperture Radar (SAR) is an active microwave remote sensing system which has potential for global peatland monitoring because it can penetrate through clouds, covers simultaneously a vast area at high spatial resolution and has a short revisit cycle. In principal, SAR could be able to measure soil moisture even directly due to the sensitivity of the backscattered signal to the target's water content.

Interferometric SAR (InSAR) is an emerging technique to measure surface height changes utilising the difference in the path length that the signal travels between the SAR acquisitions of the same target from the same orbital position at different times. A co-product of InSAR processing is the coherence image, describing the similarity of the spatial patterns in the images. InSAR phase becomes relevant in measuring the peatland WT via the phenomenon known as bog breathing. Owing to elastic properties of the peat in acrotelm, the peat mass expands and contracts in response to its water content causing the bog surface rise and subside following the WT. Only a few studies have estimated bog surface deformations with InSAR phase in northern peatlands whereas the ground levelling data for validation has been absent in most cases.

The objective of the dissertation is testing Sentinel-1 C-band (Conventional Wavelength Band, ~ 5.6 cm) InSAR applicability in the bog environment to improve monitoring of peatlands. All the results were validated with the ground truth data. Specifically, I studied:

- 1) coherence response to the water table in raised bogs (**Publications I and II**),
- 2) coherence response to peat surface alteration caused by the milled peat production (**Publication III**),
- 3) reliability of bog surface displacement estimates based on InSAR phase (**Publications IV and V**).

The results of my studies show that the long term InSAR coherence could be used as a mean to better understand hydrologic conditions in the raised bog but it is not suitable for direct surface moisture retrieval. Coherence was responsive to the peatland WT only in drought conditions (**Publications I and II**).

The short term InSAR coherence can be used to monitor peat extraction considering the intrinsic limitation by the sensor's 6-day repeat cycle and the nature of the process of peat extraction. Coherence response can be quantified and used in differentiation between active and abandoned peat production blocks, discrimination of partially harvested blocks and potentially in monitoring of peat extraction intensity (**Publication III**).

The long temporal baseline conventional Differential InSAR (DInSAR) and the Distributed Scatterer (DS) InSAR time-series approach over the open bog displayed temporal and spatial consistency despite underestimation of surface displacements compared to the levelling data. However, the DS time series and the short temporal baseline conventional DInSAR did contain useful deformation signal but surface changes in the magnitude near the displacement height of ambiguity of the sensor (~ 2.77 cm for Sentinel-1) caused problems. The unwrapping errors would have gone undetected if we had not had ground truth for validation. The C-band InSAR could be applicable in less dynamic bog areas. Therefore, the ambiguity problem makes C-band phase measurements in raised bogs unreliable if significant vertical displacements are present in a short time (**Publications I, IV and V**).

The results of this dissertation provide new findings regarding implementation of C-band InSAR in monitoring of natural bogs and peat production sites with InSAR coherence, considering the intrinsic limitations posed by the wavelength and the revisit cycle of the sensor. Measuring bog breathing directly with InSAR phase could be a promising opportunity but the ambiguity problem makes C-band InSAR unreliable. The planned longer wavelength L-band (Long Wavelength Band, ~ 24 cm) missions might provide solution.

SUMMARY IN ESTONIAN

Interferomeetriline tehisavaradar kui vahend turbaalade pinna dünaamika jälgimiseks

Turvas on aegade jooksul liigniisketes keskkonnatingimustes akumulunud osaliselt lagunenuid taimejäänustest ja huumusest koosnev mullahorisont. Turbasse on üle maailma seotud süsinikukogus, mis võrdub peaaegu poolega sellest, mis on hetkel atmosfääris. Soode õrna ja keerukat süsinikuringet kontrollib soo veetase. Veetaseme alanemisel võivad sood muutuda süsiniku sidujast kasvahoonegaaside emiteerijaks. Seetõttu on soode kaitse ja taastamine kliimuutuse leevendamise seisukohast väga tähtis. Ulatuslike ja raskesti ligipääsetavate soode seisundit on võimalik operatiivselt hinnata vaid kaugseire meetoditel.

Tehisavaradar (SAR) on aktiivne kaugseiresüsteem, mis töötab mikrolainealas. SARI olulisimaiks omadusteks on, et ta näeb läbi pilvkatte, on vahetult tundlik seiratud objekti niiskussisaldusele ja suudab mõningal määral läbistada taimkattet. Satelliidile monteeritud SAR instrument suudab korraga katta suure maa-ala. Käesolevas doktoritöös on kasutatud radarsatelliidi Sentinel-1 andmeid. Sentinel-1 missioon koosneb kahest samal sünkroniseeritud orbiidil tiirlevast identsest satelliidist – Sentinel-1A ja Sentinel-1B – mida koos käsitletakse kui Sentinel-1, sest satelliitide identsuse ja jagatud orbiidi tõttu tekib olukord, kus tegemist on justkui ühesama sensoriga, mis teostab mõõtmisi lihtsalt kaks korda lühema aja tagant. Sentinel-1 ülesvõtte katab korraga peaaegu terve Eesti. Sensoril on hea ruumiline lahutus – resolutsioon 20 m – ja tihe ajaline samm – kumbki instrument jõuab täpselt samale kohale orbiidil tagasi iga 12 päeva tagant, A ja B instrumente kombineerides on ajasamm vaid 6 päeva.

SAR interferomeetria (InSAR) on meetod, mis kasutab radarisignaali poolt läbitava teekonna pikkuste erinevust kahe radari ülesvõtte vahel. Kui radaripildid on tehtud täpselt samast asukohast orbiidil aga eri aegadel, siis hakkab signaali poolt läbitud teekonna pikkuste vahe väga täpselt näitama kahe pildi vahele jääva ajaperioodi jooksul toimunud maapinna kõrgusmuutus ja meetodit nimetatakse kitsamalt diferentsiaalseks InSAR-iks (DInSAR). Interferomeetrilise töötluse tulemuseks on InSAR faasipilt, mida nimetatakse interferogrammiks, kus teekonna pikkuste erinevus on mõõdetud kui kahe sensorisse tagasi jõudnud signaali laine faaside vahe. See tähendab, et faasierinevused interferogrammil on pakitud tsükklitesse, mis vastavad poolele radarisignaali lainepikkusele. Sentinel-1 lainepikkus on 5,6 cm ja seega faasitsükli pikkus on $\sim 2,77$ cm. Interferogrammi arvutamise kaasproduktiks on koherentsuse pilt, mis kirjeldab interferogrammi moodustavate kahe SAR-ülesvõtte lokaalsete faasimustrite sarnasust läbi aja.

Minu doktoritöö eesmärk oli kombata InSAR-meetodi piire sellises interferomeetria jaoks keerulises keskkonnas nagu raba ja kasutada saadud tulemusi soode kaugseire edendamiseks. Töö käigus uurisin: 1) raba veetaseme mõju koherentsusele, 2) freesturba tootmisega kaasnevate turba pinna muutuste mõju koherentsusele, 3) InSAR meetodi usaldusväärsust raba pinna kõrguse muutuse hindamisel. Raba veetaseme mõju InSAR koherentsusele uuriti Endla soostiku

looduslähedases või looduslikus seisundis rabade näitel (**Publikatsioonid I ja II**), turba tootmise seiramise võimalusi InSAR koherentsuse abil Sangla, Soosaare ja Tassi freesturba tootmisalade näitel (**Publikatsioon III**) ja hooajalise raba pinna kõrgusmuutuste mõõtmise usaldusväärsust InSAR faasi abil Umbusi ja Laukasoo rabade näitel (**Publikatsioon IV ja V**).

Töö tulemusel leiti, et koherentsus peegeldab raba veetaseme kõrgusmuutusi, seda aga vaid põuastel suvedel. Raba veetase on läbi kapillaartõusu seotud raba pinnaniiskusega, mida SAR tuvastab. Märkades ilmastikuoludes koherentsuse ja veetaseme vahel suhet ei esine, sest raba pinna niiskussisaldus ei sõltu kapillaartõusust, vaid sademete hulgast. See tähendab, et raba pinna niiskussisalduse hindamine otse koherentsusest ei ole teostatav, sest tegurid, nagu taimestik, sademed ja muud muutused raba pinnal, mõjutavad koherentsusest rohkem kui kapillaartõusust tingitud pinnaniiskust. Koherentsuse abil on aga võimalik hankida täiendavat teavet raba veetaseme käigu ja kõrguse kohta kuival suvel või kuivendusest mõjutatud rabades. Koherentsus võimaldab raba ökotopide eristamist ja on abiks nende hüdroloogiliste tingimuste kirjeldamisel (**Publikatsioonid I ja II**).

Koherentsus võimaldab tuvastada, kui soopinna füüsiline struktuuri muutub. See lubab detekteerida freesturba tootmisega seonduvaid töid, mis omakorda teeb võimalikuks aktiivselt kasutatavate ja kasutusest välja langenud tootmisalade eristamise. Üksikuid tootmistsükleid ja turba kaevandamise mahtusid InSAR tehnoloogia ja Sentinel-1 kuuapäevane ajaline lahusus ei võimalda. Küll aga demonstreeris töö, kuidas koherentsuse mediaanväärtuste dispersiooni abil oleks võimalik hinnata turba kaevandamise intensiivsust, samuti tuvastada turbatootmisplokke, kus turvast on toodetud vaid osal ploki pindalast. Erinevalt teistest maakatte tüüpidest, mõjutab vihm turbaaladel (lageraba, jääksoo ja aktiivne turbatootmisala) InSAR koherentsust tavaliselt vaid vähesel määral. Tugev vihmasedu võib aga põhjustada koherentsuse kukkumise sama madalale kui tootmisväljakul tehtavad tööd. Kui kasutada paralleelselt erinevatelt orbiitidelt pärit koherentsuse aegridu, radarisignaali tagasihajumise intensiivsust või võrdluseks alasid, kus teadaolevalt turba tootmisega seonduvaid töid ei teostata, saab vihmast põhjustatud häiringud siiski tuvastada ja analüüsist kõrvaldada. Töös on visandatud seiremetoodika, mis võimaldab eristada aktiivseid turbatootmisalasid mahajäetud aladest ja jälgida turba tootmise intensiivsust, edendamaks tõhusamat ressursikasutust ja panustamaks kliimale kriisi leevendamisesse. Seiremetoodika on ülekantav ka muudele suurepinnalistele pealmaakaevandustele, nagu suure keskkonnamõjuga naftaliivad (**Publikatsioon III**).

Konventsionaalne DinSAR (**Publikatsioon I**) ja hajutatud tagasipeegeldajatel põhinev Distributed Scatterer (DS) InSAR aegridade meetod (**Publikatsioon V**) andsid küll ajaliselt ja ruumiliselt sisemiselt kooskõlalised tulemused, kuid alahindasid võrreldes maapealsete nivelleerimisandmetega oluliselt tegelikke pinna kõrgusmuutusi. Alahindamise põhjustas InSARi suutmatus õigesti hinnata muutusi, mis suuruselt lähenevad faastsükli pikkusele (poolele signaali lainepikkusest, mis on satelliidi Sentinel-1, mida meie kasutasime, puhul $\sim 2,77$ cm). Vaatamata sellele, et DS-aegread, mis mõõdavad kõrguse muutust ühest kokkuleppelisest alguskuupäevast, alahindasid võrreldes nivelleerimisandmetega raba pinna kõi-

kumiste ulatust, oli radari ja maapealsete võrdlusandmete korrelatsioon kõrge. Põhjuseks oli, et suhtelised kõrgusmuutused kahe järjestikuse radaripildi vahel olid enamasti täpsed. See tähendab, et DS-aegread ikkagi sisaldavad kasulikku signaali.

Kõige täpsemaks InSAR tehnikaks osutus minimaalse võimaliku, 6-päevase, ajalise sammuga konventsionaalne DInSAR (**Publikatsioon IV**). Kõrgusmuutused, mis lähenesid faasitsükli pikkusele, olid aga siingi alahinnatud. See tähendab, et ükski selle töö käigus rabas katsetatud InSAR meetod ei suutnud faasi korrektselt lahti pakkida. Vead oleksid jäänud avastamata, kui meil poleks võrdluseks olnud maapealseid kõrgusandmeid. Kõiki seni rabas teostatud uuringuid hõlmav kirjanduse analüüs näitas samuti, et maapealsete võrdlusandmete olemasolul on alati kinnitust leidnud, et C-laineala InSAR alahindab kõrgusmuutust või tuvastati faasi lahtipakkimisel viga. InSAR meetod võiks olla sobilik rabades, mida iseloomustavad väiksemad ja aeglasemalt toimuvad pinna deformatsioonid, nt nagu kuivendusest tugevalt häiritud alad. Ometi jäädvustasin isegi tugevalt kuivendatud kraavilähedasesest mõõtepunktist mitmel korral kõrgusmuutuseid, mis üheainsa päeva jooksul ületasid Sentinel-1 faasitsükli ulatuse. Ainus nonotoop, kus muutused olid mistahes 6-päeva pikkuse perioodi jooksul (vastab Sentinel-1 A ja B kombineeritud korduskülastustsüklile) alati faasitsüklilist väiksemad, oli looduslik rabamätas. C-laineala (~5,6 cm) InSAR on lagerabas kasutatav, aga usaldusväärse faasimõõtmise eelduseks on, et rabapinna deformatsioonide ulatus jääb tuvastatavasse vahemikku, milleks on pool sensori lainepikkust. Ilma detailsete maapealsete kõrgusandmeteta on aga äärmiselt raske hinnata, kas selline eeldus on õigustatud või mitte (**Publikatsioon IV**). Tõenäoliselt võiksid lahendust pakuda lähitulevikku planeeritud pikalainelised (L-laineala; ~24 cm) radarsatelliidi missioonid.

Doktoritöö toob esile kolm valdkonda, kus interferomeetrilised tehisavaradar-satelliidilt teostatavad mõõtmised suudavad oluliselt edendada soode seiret. C-laineala InSAR koherentsust saab kasutada turba kaevandamise jälgimiseks, siinjuures arvesse võttes SAR-ist ja turba kaevandamise protsessist tulenevaid olemuslikke piiranguid. Koherentsustest on kasu ka soode hüdroloogiliste tingimuste uurimisel, kuid see ei sobi rabapinna niiskuse otseseks mõõtmiseks. InSAR kõrgusmõõtmised rabas tavapärasel C-lainealal küll sisaldavad kasulikku deformatsioonisignaali aga ei ole usaldusväärsed, sest raba pind kõigub sageli C-laineala sensori jaoks ebamugavalt suures ulatus. Tõenäoliselt lahendust pakuvad siin lähituleviku pikalainelised L-laineala radarsatelliidi missioonid, millel on tänu palju pikemale lainepikkusele võimekus mõõta oluliselt suuremaid suhtelisi kõrguserinevusi.

ACKNOWLEDGEMENTS

I am truly grateful to all of you who have been part of the journey through my PhD project. Foremost, I deeply appreciate my supervisors Dr. **Ain Kull** from the University of Tartu, Dr. **Jaan Praks** from Aalto University and Dr. **Rivo Uiboupin** from Tallinn University of Technology who despite being ever busy found always time to discuss my questions, ideas or problems whenever I called, emailed or appeared in office. Thank you so much for your never failing enthusiasm and care. Also, *grazie mille*, Dr. **Francesco De Zan** from German Aerospace Center (DLR) who made it possible for me to gain international experience, understand advanced methods of InSAR and gather the broad and fragmented content of my research into a comprehensive whole. Many thanks to Dr. **Robert Shau** and Dr. **Alessandro Parizzi** from DLR and Dr. **Kaupo Voormansik** and Dr. **Tanel Tamm** from KappaZeta Ltd for InSAR time-series processing and Dr. **Marko Kohv** from the University of Tartu for providing in situ peatland surface levelling measurements. Sincere thanks also to representatives of AS Kraves and AS Elva E.P.T., the peat production companies, who allowed us to study their production sites while providing all the relevant data.

Thank you so much, Dr. **Alexander Kmoch** and Dr. **Anto Aasa** from the University of Tartu and Dr. **Karsten Kretschmer** from DLR, for your invaluable advice and hands in help when I was learning the programming languages R and Python. Many thanks to **Kalle Tihemets** and my friend Dr. **Kristjan Oopkaup** who always helped out with any general software related question or issues. Also, I would like to thank Datel AS and Dr. **Juhan-Peep Ernits** from Tallinn University of Technology for providing computing capacity and the Sarproz team for an excellent software for InSAR processing which comes with extremely flexible student licensing.

My colleagues and friends from the University of Tartu and DLR, I am very grateful to you as you made my PhD journey truly enjoyable. And my family – my parents and my brother with his family – you have always been here with me wherever I may have been or whatever I may have been doing, all my love!

My PhD research was funded by the Republic of Estonia and the European Union from the European Regional Development Fund. My stay at DLR was made possible by the national scholarship program Kristjan Jaak which is funded and managed by Archimedes Foundation in collaboration with the Ministry of Education and Research (Estonia).

PUBLICATIONS

CURRICULUM VITAE

Name Tauri Tampuu
Date of birth 08.06.1986
Address Department of Geography, Institute of Ecology and Earth Sciences, University of Tartu, Vanemuise 46, 51014 Tartu, Estonia
E-mail tauri.tampuu@ut.ee

Education

2018–2022 University of Tartu, PhD student in physical geography
2009–2011 University of Tartu, MSc student in environmental technology
2005–2009 University of Tartu, BSc in environmental technology
2002–2005 Gymnasium of Miina Härma
1993–2002 Lycée Descartes de Tartu

Institutions and positions

2014–2016 University of Tartu, Institute of Ecology and Earth Sciences, specialist of environmental technology (1,00)
2012–2013 University of Tartu, Institute of Ecology and Earth Sciences, specialist of environmental technology (1,00)
2011 University of Tartu, Institute of Ecology and Earth Sciences, specialist of environmental economics (0,60)

Scholarships and awards

2022 Dora Plus short study visits support for oral presentation at EGU General Assembly (EGU2022)
2021 Research prize for the promotion of the real-time economy by the Ministry of Economic Affairs and Communications, I prize for a research article
2020–2021 Kristjan Jaak scholarship for study periods abroad for conducting research in German Aerospace Center (DLR)
2019 Dora Plus short study visits support for oral presentation at Nordic Remote Sensing Conference 2019 (NoRSC'19)
2018–2022 Smart specialisation scholarships for PhD students

Supplementary education

2022 Artificial Intelligence for Non-IT Students, winter school/credit course, ENLIGHT, online/Tartu, Estonia
2020 Optical and SAR Copernicus Data for Land Applications, credit course, European Space Agency (ESA), Tartu, Estonia
2019 5th Advanced Course on Radar Polarimetry 2019, European Space Agency (ESA-ESRIN), Frascati, Italy

- 2017 Echoes in Space: Introduction to Radar Remote Sensing, European Space Agency (ESA), online course
- 2016 Introduction to Programming, credit online course, University of Tartu
- 2015 Basics of Programming, credit online course, University of Tartu

Publications

- Tampuu, T., De Zan, F., Shau, R., Praks, J., Kohv, M., Kull, A. (202X) Can Bog Breathing Be Measured by Synthetic Aperture Radar Interferometry. In: *2022 IEEE International Geoscience and Remote Sensing Symposium IGARSS*. IEEE. (Accepted).
- Tampuu, T., Praks, J., De Zan, F., Kohv, M., Kull, A. (202X) Could bog breathing be measured by Synthetic Aperture Radar? – The relationship between differential interferometric phase and ground measurements. *Mires and Peat*. (Submitted).
- Veber, G., Paal, J., Läänelaid, A., Sohar, K., Tampuu, T., Salm, J-O., Maddison, M., Teemusk, A., Mander, Ü., Kull, A. (202X) Simple vegetation and soil parameters determine greenhouse gas fluxes along drainage gradient in peatlands. (Submitted).
- Tampuu, T., De Zan, F., Shau, R., Praks, J., Kohv, M., Kull, A. (2022) Reliability of Sentinel-1 InSAR distributed scatterer (DS) time series to estimate the temporal vertical movement of ombrotrophic bog surface. *EGU General Assembly 2022*. <https://doi.org/10.5194/egusphere-egu22-2387>.
- Tampuu, T., Praks, J., De Zan, F., Kohv, M., Kull, A. (2021) Towards assessment of bog breathing with Sentinel-1 Differential InSAR. In: *Proceedings of the 16th International Peatland Congress 2021*. Publicon PCO. Tartu, Estonia. pp. 472–478.
- Tampuu, T., Praks, J., Kull, A., Uiboupin, R., Tamm, T., Voormansik, K. (2021) Detecting peat extraction related activity with multi-temporal Sentinel-1 InSAR coherence time series. *International Journal of Applied Earth Observation and Geoinformation*, 98, 102309.
- Tampuu, T., Praks, J., Kull, A. (2020) InSAR Coherence for Monitoring Water Table Fluctuations in Northern Peatlands. In: *2020 IEEE International Geoscience and Remote Sensing Symposium IGARSS*. pp. 4738–4741.
- Tampuu, T., Praks, J., Uiboupin, R., Kull, A. (2020) Long term interferometric temporal coherence and DInSAR phase in Northern Peatlands. *Remote Sensing*, 12(10), 1566.
- Gauk, M., Roose, A., Kull, A., Tampuu, T. (2014) Tartu eeslinnaasumite energiatarbe olelusringi analüüs [A life-cycle analysis on energy consumption of new residential settlements in the urban fringe of Tartu]. In: Järvet, A. (ed.), *Eesti Geograafia Seltsi aastaraamat*. OÜ Vali Press. Tallinn, Estonia. pp. 102–123.

ELULOOKIRJELDUS

Nimi Tauri Tampuu
Sünniaeg 08.06.1986
Aadress Geograafia osakond, ökoloogia ja maateaduste instituut, Tartu
Ülikool, Vanemuise 46, 51014 Tartu, Eesti
E-mail tauri.tampuu@ut.ee

Haridustee

2018–2022 Tartu Ülikool, doktoriõpe, loodusgeograafia
2009–2011 Tartu Ülikool, MSc õpe, keskkonnatehnoloogia
2005–2009 Tartu Ülikool, BSc õpe, keskkonnatehnoloogia
2002–2005 Miina Härma Gümnaasium
1993–2002 Tartu Descartes'i Lütseum

Töökohad ja ametid

2014–2016 Tartu Ülikool, Loodus- ja täppisteaduste valdkond, ökoloogia ja
maateaduste instituut, keskkonnatehnoloogia (1,00)
2012–2013 Tartu Ülikool, Loodus- ja täppisteaduste valdkond, ökoloogia ja
maateaduste instituut, keskkonnatehnoloogia (1,00)
2011 Tartu Ülikool, Loodus- ja tehnoloogiateaduskond, ökoloogia- ja
maateaduste instituut, keskkonnaökonomika spetsialist (0,60)

Stipendiumid

2022 Dora Plus lühiajalise õpirände stipendium suuliseks ettekandeks
konverentsil EGU General Assembly (EGU2022)
2021 MKMi reaalajamajanduse edendamise teaduspreemia, I koht
teadusartiklite kategoorias
2020–2021 Kristjan Jaagu välisõpingute stipendium teadustöökS Saksa
lennundus- ja kosmosekeskuses (DLR)
2019 Dora Plus lühiajalise õpirände stipendium suuliseks ettekan-
deks konverentsil *Nordic Remote Sensing Conference 2019*
(*NoRSC'19*)
2018–2022 Nutika spetsialiseerumise doktorandistipendium

Täiendõpe

2022 Artificial Intelligence for Non-IT Students, talvekool/akrediteeri-
tud kursus, ENLIGHT, e-kursus/Tartu, Eesti
2020 Optical and SAR Copernicus Data for Land Applications, akredi-
teeritud kursus, Euroopa Kosmoseagentuur (ESA), Tartu, Eesti
2019 5th Advanced Course on Radar Polarimetry 2019, European Space
Agency (ESA-ESRIN), Frascati, Italy

- 2017 Echoes in Space: Introduction to Radar Remote Sensing, Euroopa Kosmoseagentuur (ESA), e-kursus
- 2016 Programmeerimise alused, Tartu Ülikool, akrediteeritud e-kursus
- 2015 Programmeerimisest maälähedaselt, Tartu Ülikool, akrediteeritud e-kursus

Publikatsioonid

- Tampuu, T., De Zan, F., Shau, R., Praks, J., Kohv, M., Kull, A. (202X) Can Bog Breathing Be Measured by Synthetic Aperture Radar Interferometry. In: *2022 IEEE International Geoscience and Remote Sensing Symposium IGARSS*. IEEE. (Accepted).
- Tampuu, T., Praks, J., De Zan, F., Kohv, M., Kull, A. (202X) Could bog breathing be measured by Synthetic Aperture Radar? – The relationship between differential interferometric phase and ground measurements. *Mires and Peat*. (Submitted).
- Veber, G., Paal, J., Läänelaid, A., Sohar, K., Tampuu, T., Salm, J-O., Maddison, M., Teemusk, A., Mander, Ü., Kull, A. (202X) Simple vegetation and soil parameters determine greenhouse gas fluxes along drainage gradient in peatlands. (Submitted).
- Tampuu, T., De Zan, F., Shau, R., Praks, J., Kohv, M., Kull, A. (2022) Reliability of Sentinel-1 InSAR distributed scatterer (DS) time series to estimate the temporal vertical movement of ombrotrophic bog surface. *EGU General Assembly 2022*. <https://doi.org/10.5194/egusphere-egu22-2387>.
- Tampuu, T., Praks, J., De Zan, F., Kohv, M., Kull, A. (2021) Towards assessment of bog breathing with Sentinel-1 Differential InSAR. In: *Proceedings of the 16th International Peatland Congress 2021*. Publicon PCO. Tartu, Estonia. pp. 472–478.
- Tampuu, T., Praks, J., Kull, A., Uiboupin, R., Tamm, T., Voormansik, K. (2021) Detecting peat extraction related activity with multi-temporal Sentinel-1 InSAR coherence time series. *International Journal of Applied Earth Observation and Geoinformation*, 98, 102309.
- Tampuu, T., Praks, J., Kull, A. (2020) Insar Coherence for Monitoring Water Table Fluctuations in Northern Peatlands. In: *2020 IEEE International Geoscience and Remote Sensing Symposium IGARSS*. pp. 4738–4741.
- Tampuu, T., Praks, J., Uiboupin, R., Kull, A. (2020) Long term interferometric temporal coherence and DInSAR phase in Northern Peatlands. *Remote Sensing*, 12(10), 1566.
- Gauk, M., Roose, A., Kull, A., Tampuu, T. (2014) Tartu eeslinnaasumite energiatarbe olelusringi analüüs [A life-cycle analysis on energy consumption of new residential settlements in the urban fringe of Tartu]. In: Järvet, A. (ed.), *Eesti Geograafia Seltsi aastaraamat*. OÜ Vali Press. Tallinn, Estonia. pp. 102–123.

DISSERTATIONES GEOGRAPHICAE UNIVERSITATIS TARTUENSIS

1. **Вийви Руссак.** Солнечная радиация в Тыравере. Тарту, 1991.
2. **Urmas Peterson.** Studies on Reflectance Factor Dynamics of Forest Communities in Estonia. Tartu, 1993.
3. **Ülo Suursaar.** Soome lahe avaosa ja Eesti rannikumere vee kvaliteedi analüüs. Tartu, 1993.
4. **Kiira Aaviksoo.** Application of Markov Models in Investigation of Vegetation and Land Use Dynamics in Estonian Mire Landscapes. Tartu, 1993.
5. **Kjell Wepling.** On the assessment of feasible liming strategies for acid sulphate waters in Finland. Tartu, 1997.
6. **Hannes Palang.** Landscape changes in Estonia: the past and the future. Tartu, 1998.
7. **Eiki Berg.** Estonia's northeastern periphery in politics: socio-economic and ethnic dimensions. Tartu, 1999.
8. **Valdo Kuusemets.** Nitrogen and phosphorus transformation in riparian buffer zones of agricultural landscapes in Estonia. Tartu, 1999.
9. **Kalev Sepp.** The methodology and applications of agricultural landscape monitoring in Estonia. Tartu, 1999.
10. **Rein Ahas.** Spatial and temporal variability of phenological phases in Estonia. Tartu, 1999.
11. **Эрки Таммиксаар.** Географические аспекты творчества Карла Бэра в 1830–1840 гг. Тарту, 2000.
12. **Garri Raagmaa.** Regional identity and public leaders in regional economic development. Tartu, 2000.
13. **Tiit Tammaru.** Linnastumine ja linnade kasv Eestis nõukogude aastatel. Tartu, 2001.
14. **Tõnu Muring.** Wastewater treatment wetlands in Estonia: efficiency and landscape analysis. Tartu, 2001.
15. **Ain Kull.** Impact of weather and climatic fluctuations on nutrient flows in rural catchments. Tartu, 2001.
16. **Robert Szava-Kovats.** Assessment of stream sediment contamination by median sum of weighted residuals regression. Tartu, 2001.
17. **Heno Sarv.** Indigenous Europeans east of Moscow. Population and Migration Patterns of the Largest Finno-Ugrian Peoples in Russia from the 18th to the 20th Centuries. Tartu, 2002.
18. **Mart Külvik.** Ecological networks in Estonia — concepts and applications. Tartu, 2002.
19. **Arvo Järvet.** Influence of hydrological factors and human impact on the ecological state of shallow Lake Võrtsjärv in Estonia. Tartu, 2004.
20. **Katrin Pajuste.** Deposition and transformation of air pollutants in coniferous forests. Tartu, 2004.

21. **Helen Sooväli.** *Saaremaa waltz*. Landscape imagery of Saaremaa Island in the 20th century. Tartu, 2004.
22. **Antti Roose.** Optimisation of environmental monitoring network by integrated modelling strategy with geographic information system — an Estonian case. Tartu, 2005.
23. **Anto Aasa.** Changes in phenological time series in Estonia and Central and Eastern Europe 1951–1998. Relationships with air temperature and atmospheric circulation. Tartu, 2005.
24. **Anneli Palo.** Relationships between landscape factors and vegetation site types: case study from Saare county, Estonia. Tartu, 2005.
25. **Mait Sepp.** Influence of atmospheric circulation on environmental variables in Estonia. Tartu, 2005.
26. **Helen Alumäe.** Landscape preferences of local people: considerations for landscape planning in rural areas of Estonia. Tartu, 2006.
27. **Aarne Luud.** Evaluation of moose habitats and forest reclamation in Estonian oil shale mining areas. Tartu, 2006.
28. **Taavi Pae.** Formation of cultural traits in Estonia resulting from historical administrative division. Tartu, 2006.
29. **Anneli Kährik.** Socio-spatial residential segregation in post-socialist cities: the case of Tallinn, Estonia. Tartu, 2006.
30. **Dago Antov.** Road user perception towards road safety in Estonia. Tartu, 2006.
31. **Üllas Ehrlich.** Ecological economics as a tool for resource based nature conservation management in Estonia. Tartu, 2007.
32. **Evelyn Uuema.** Indicatory value of landscape metrics for river water quality and landscape pattern. Tartu, 2007.
33. **Raivo Aunap.** The applicability of gis data in detecting and representing changes in landscape: three case studies in Estonia. Tartu, 2007.
34. **Kai Treier.** Trends of air pollutants in precipitation at Estonian monitoring stations. Tartu, 2008.
35. **Kadri Leetmaa.** Residential suburbanisation in the Tallinn metropolitan area. Tartu, 2008.
36. **Mare Remm.** Geographic aspects of enterobiasis in Estonia. Tartu, 2009.
37. **Alar Teemusk.** Temperature and water regime, and runoff water quality of planted roofs. Tartu, 2009.
38. **Kai Kimmel.** Ecosystem services of Estonian wetlands. Tartu, 2009.
39. **Merje Lesta.** Evaluation of regulation functions of rural landscapes for the optimal siting of treatment wetlands and mitigation of greenhouse gas emissions. Tartu, 2009.
40. **Siiri Silm.** The seasonality of social phenomena in Estonia: the location of the population, alcohol consumption and births. Tartu, 2009.
41. **Ene Indermitte.** Exposure to fluorides in drinking water and dental fluorosis risk among the population of Estonia. Tartu, 2010.
42. **Kaido Soosaar.** Greenhouse gas fluxes in rural landscapes of Estonia. Tartu, 2010.

43. **Jaan Pärn.** Landscape factors in material transport from rural catchments in Estonia. Tartu, 2010.
44. **Triin Saue.** Simulated potato crop yield as an indicator of climate variability in Estonia. Tartu, 2011.
45. **Katrin Rosenvald.** Factors affecting EcM roots and rhizosphere in silver birch stands. Tartu, 2011.
46. **Ülle Marksoo.** Long-term unemployment and its regional disparities in Estonia. Tartu, 2011, 163 p.
47. **Hando Hain.** The role of voluntary certification in promoting sustainable natural resource use in transitional economies. Tartu, 2012, 180 p.
48. **Jüri-Ott Salm.** Emission of greenhouse gases CO₂, CH₄, and N₂O from Estonian transitional fens and ombrotrophic bogs: the impact of different land-use practices. Tartu, 2012, 125 p.
49. **Valentina Sagris.** Land Parcel Identification System conceptual model: development of geoinfo community conceptual model. Tartu, 2013, 161 p.
50. **Kristina Sohar.** Oak dendrochronology and climatic signal in Finland and the Baltic States. Tartu, 2013, 129 p.
51. **Riho Marja.** The relationships between farmland birds, land use and landscape structure in Northern Europe. Tartu, 2013, 134 p.
52. **Olle Järv.** Mobile phone based data in human travel behaviour studies: New insights from a longitudinal perspective. Tartu, 2013, 168 p.
53. **Sven-Erik Enno.** Thunderstorm and lightning climatology in the Baltic countries and in northern Europe. Tartu, 2014, 142 p.
54. **Kaupo Mändla.** Southern cyclones in northern Europe and their influence on climate variability. Tartu, 2014, 142 p.
55. **Riina Vaht.** The impact of oil shale mine water on hydrological pathways and regime in northeast Estonia. Tartu, 2014, 111 p.
56. **Jaanus Veemaa.** Reconsidering geography and power: policy ensembles, spatial knowledge, and the quest for consistent imagination. Tartu, 2014, 163 p.
57. **Kristi Anniste.** East-West migration in Europe: The case of Estonia after regaining independence. Tartu, 2014, 151 p.
58. **Piret Pungas-Kohv.** Between maintaining and sustaining heritage in landscape: The examples of Estonian mires and village swings. Tartu, 2015, 210 p.
59. **Mart Reimann.** Formation and assessment of landscape recreational values. Tartu, 2015, 127 p.
60. **Järvi Järveoja.** Fluxes of the greenhouse gases CO₂, CH₄ and N₂O from abandoned peat extraction areas: Impact of bioenergy crop cultivation and peatland restoration. Tartu, 2015, 171 p.
61. **Raili Torga.** The effects of elevated humidity, extreme weather conditions and clear-cut on greenhouse gas emissions in fast growing deciduous forests. Tartu, 2016, 128 p.
62. **Mari Nuga.** Soviet-era summerhouses On homes and planning in post-socialist suburbia. Tartu, 2016, 179 p.

63. **Age Poom.** Spatial aspects of the environmental load of consumption and mobility. Tartu, 2017, 141 p.
64. **Merle Muru.** GIS-based palaeogeographical reconstructions of the Baltic Sea shores in Estonia and adjoining areas during the Stone Age. Tartu, 2017, 132 p.
65. **Ülle Napa.** Heavy metals in Estonian coniferous forests. Tartu, 2017, 129 p.
66. **Liisi Jakobson.** Mutual effects of wind speed, air temperature and sea ice concentration in the Arctic and their teleconnections with climate variability in the eastern Baltic Sea region. Tartu, 2018, 118 p.
67. **Tanel Tamm.** Use of local statistics in remote sensing of grasslands and forests. Tartu, 2018, 106 p.
68. **Enel Pungas.** Differences in Migration Intentions by Ethnicity and Education: The Case of Estonia. Tartu, 2018, 142 p.
69. **Kadi Mägi.** Ethnic residential segregation and integration of the Russian-speaking population in Estonia. Tartu, 2018, 173 p.
70. **Kiira Mõisja.** Thematic accuracy and completeness of topographic maps. Tartu, 2018, 112 p.
71. **Kristiina Kukk.** Understanding the vicious circle of segregation: The role of leisure time activities. Tartu, 2019, 143 p.
72. **Kaie Kriiska.** Variation in annual carbon fluxes affecting the soil organic carbon pool and the dynamics of decomposition in hemiboreal coniferous forests. Tartu, 2019, 146 p.
73. **Pille Metspalu.** The changing role of the planner. Implications of creative pragmatism in Estonian spatial planning. Tartu, 2019, 128 p.
74. **Janika Raun.** Mobile positioning data for tourism destination studies and statistics. Tartu, 2020, 153 p.
75. **Birgit Viru.** Snow cover dynamics and its impact on greenhouse gas fluxes in drained peatlands in Estonia. Tartu, 2020, 123 p.
76. **Iuliia Burdun.** Improving groundwater table monitoring for Northern Hemisphere peatlands using optical and thermal satellite data. Tartu, 2020, 162 p.
77. **Ingmar Pastak.** Gentrification and displacement of long-term residents in post-industrial neighbourhoods of Tallinn. Tartu, 2021, 141 p.
78. **Veronika Mooses.** Towards a more comprehensive understanding of ethnic segregation: activity space and the vicious circle of segregation. Tartu, 2021, 161 p.
79. **Johanna Pirrus.** Contemporary Urban Policies and Planning Measures in Socialist-Era Large Housing Estates. Tartu, 2021, 142 p.
80. **Gert Veber.** Greenhouse gas fluxes in natural and drained peatlands: spatial and temporal dynamics. Tartu, 2021, 210 p.
81. **Anniki Puura.** Relationships between personal social networks and spatial mobility with mobile phone data. Tartu, 2021, 144 p.
82. **Alisa Krasnova.** Greenhouse gas fluxes in hemiboreal forest ecosystems. Tartu, 2022, 185 p.